
Electronic Thesis and Dissertation Repository

9-5-2018 2:00 PM

Electrospun collagen fibers for tissue regeneration applications

Ying Li

The University of Western Ontario

Supervisor

Wan, Wankei


The University of Western Ontario

Graduate Program in Biomedical Engineering

A thesis submitted in partial fulfillment of the requirements for the degree in Doctor of
Philosophy

© Ying Li 2018

Follow this and additional works at: <https://ir.lib.uwo.ca/etd>

 Part of the [Biology and Biomimetic Materials Commons](#), [Biomaterials Commons](#), [Biomedical Devices and Instrumentation Commons](#), and the [Mechanics of Materials Commons](#)

Recommended Citation

Li, Ying, "Electrospun collagen fibers for tissue regeneration applications" (2018). *Electronic Thesis and Dissertation Repository*. 5721.

<https://ir.lib.uwo.ca/etd/5721>

This Dissertation/Thesis is brought to you for free and open access by Scholarship@Western. It has been accepted for inclusion in Electronic Thesis and Dissertation Repository by an authorized administrator of Scholarship@Western. For more information, please contact wlsadmin@uwo.ca.

Abstract

Tissue engineering aims to regenerate damaged and deceased tissue by combining cells with scaffold made from an appropriate biomaterial and providing a conducive environment to guide cell growth and the formation or regeneration of new tissue or organ. While collagen, an important material of the extracellular matrix (ECM), is a natural choice as a scaffold biomaterial, the conducive environment can only be created by having the ability to control the geometry, organization, structural and mechanical properties of the scaffold. Moreover, degradability and degradation rate control of the scaffold has to be taken into consideration too. In this work, we aim at developing a scaffold that possess the geometry, organization, structural and mechanical properties of the ECM, that is also degradable with degradation rate control. We accomplish this through fabrication of scaffolds composed of collagen fibers with diameters of ~ 50 to 500 nm using electrospinning. These fibers can be organized and provide structural and mechanical support for the cells populating it. The versatile electrospinning setup not only allows mimicking the define architecture of the native ECM environment containing collagen fibers but, in the core-shell or porous structure, can also enable bioactive molecule encapsulation and their controlled release into the cell culture environment. Post fabrication processing for fiber stability via chemical or photochemical crosslinking as well as ion implantation resulted in fibers with controlled degradation rate and enhanced mechanical properties. Chemical structure characterization demonstrated close resemblance of fiber surface and native collagen. Favorable cell adhesion and proliferation demonstrated good cell compatibility using the human fetal lung (IMR-90) cells. By implementing the strategy developed in this thesis to construct scaffolds using electrospun collagen fiber that possess appropriate organization and properties to mimic the natural environment, scaffolds can be custom designed for specific tissue engineering applications with potentially improved outcome.

Keywords

Electrospinning, collagen, crosslinking, nanomechanics, cell compatibility, nanofiber, fiber organization

Acknowledgments

This thesis would not have been possible without the support and guidance of those around me.

I would first like to thank my supervisor Dr. Wan for his guidance and support over the years. He constantly challenged me with ideas and questions, pushed me to learn, to think and to work hard.

I would also like to thank Dr. Hutter, Dr. Goncharova and Mr. Hendriks for patiently explaining concepts and assisting me in performing AFM and ion implantation.

Specially, I would like to thank Dr. Hutter and Dr. deBruyn for guiding me and encouraging me with insightful talks over the years.

I would like to thank Dr. Hrymak for being one of my advisory committee members and providing me with valuable suggestions and critics.

I would like to thank Karen Nygard, Dr. Richard Gardiner, Dr. Saman Maleki and Dr. Rene Figueredo Pupofor teaching and assisting me with cell culture, cell staining and cell imaging work.

I would like to thank all the members of the lab group as it has been a pleasure to work with you all. Specifically, I would like to thank Dr. Jian Liu and Dr. Helium Mak for assisting me with many aspects of this project, setting up the equipment and building the components with me. Xinyi, Julie, Asha and Dawn for helping me both in the lab and in daily life.

Finally, I would like to thank my family and my friends for the unconditional support over the years.

Table of Contents

Abstract.....	i
Acknowledgments.....	ii
Table of Contents.....	iii
List of Tables.....	vii
List of Figures.....	viii
List of Appendices.....	xiv
List of Abbreviations.....	xv
1 Introduction.....	1
2 Background and Literature Review.....	4
2.1 Extracellular matrix structure and function.....	4
2.2 Cell – substrate interaction.....	5
2.3 Tissue Engineering.....	6
2.4 Cell compatibility of tissue engineering scaffold.....	7
2.5 Electrospinning.....	8
2.5.1 Setup and operating principles.....	8
2.5.2 Electrospinning conditions and parameters.....	9
2.6 Use of electrospun fibers in tissue engineering.....	14
2.6.1 Synthetic vs. natural polymers.....	15
2.7 Collagen.....	16
2.7.1 Structure and Function.....	16
2.7.2 Fibrillar collagens.....	17
2.7.3 Collagen stability.....	18
2.7.4 Collagen as a biomaterial for tissue engineering applications.....	18
2.8 Electrospinning collagen.....	18

2.8.1	Crosslinking of electrospun collagen fibers.....	19
2.9	Mechanical Testing Techniques	22
2.9.1	The overall scaffold mechanical property determination	22
2.9.2	Single fiber property determination	23
3	Materials and Methods.....	28
3.1	Materials	28
3.2	Isolation and purification of Type I collagen from rat tails	28
3.3	Collagen solution / shell solution.....	29
3.4	Core solution.....	29
3.5	Electrospinning	29
3.5.1	Humidity control.....	29
3.5.2	Solid random fibers.....	30
3.5.3	Aligned fibers.....	31
3.5.4	Core-shell fibers.....	31
3.6	Crosslinking	31
3.6.1	Genipin crosslinking	31
3.6.2	Green light and Rose Bengal crosslinking.....	32
3.6.3	Ion beam implantation	32
3.7	Characterization	32
3.7.1	Scanning electron microscopy (SEM)	32
3.7.2	Transmission electron microscopy (TEM)	32
3.7.3	X-ray photoelectron spectroscopy (XPS)	33
3.7.4	Fluorescence Microscopy	33
3.7.5	Imaging processing (ImageJ).....	33
3.8	Mechanical Testing.....	34
3.8.1	Sample preparation	34

3.8.2	Force volume measurement	35
3.8.3	Contact AFM force plots	35
3.8.4	Determination of the elastic modulus	37
3.8.5	Analytical models	39
3.9	Cell culture on electrospun collagen fibers.....	41
4	Results	43
4.1	Effect of humidity on fiber size and morphology.....	45
4.2	Other factors affecting fiber morphology and size	48
4.3	Fiber alignment to mimic tissue structure.....	52
4.4	Core-shell fiber fabrication.....	53
4.5	Effect of crosslinking on fiber size, morphology and stability.....	56
4.5.1	UV-riboflavin.....	56
4.5.2	Green light and Rose Bengal	58
4.5.3	Ion beam implantation	60
4.6	Mechanical properties of fibers	78
4.6.1	Vacuum dried electrospun collagen fibers.....	78
4.6.2	Green light crosslinking.....	81
4.6.3	Genipin crosslinked electrospun collagen fibers	83
4.6.4	Ion implantation	84
4.6.5	Change of solvent system	86
4.7	Cell compatibility of crosslinked collagen fibers	88
5	Discussion	95
5.1	Tissue engineering	95
5.2	Preparation of electrospun collagen fibers.....	96
5.2.1	Effect of humidity.....	96
5.2.2	Other parameters.....	99

5.3 Fiber alignment and 2D FFT.....	101
5.4 Core-shell fiber	102
5.5 Collagen fiber stabilization and aqueous stability	103
5.5.1 Change of chemical structure of ion implantation (XPS).....	106
5.6 Mechanical properties.....	109
5.7 Cell compatibility.....	113
6 Conclusion	116
7 Future work	117
Reference	119
Appendices.....	147
Curriculum Vitae	152

List of Tables

Table 4.1. Implantation conditions for three samples.....	61
Table 4.2. Average fiber diameter and standard deviation before and after ion treatment.....	62
Table 4.3. Amount of oxygen, nitrogen and carbon present.....	65
Table 5.1. Summary comparison of collagen Young's moduli	111

List of Figures

Figure 2.1. Electrospinning collectors used to collect aligned fibers: (a) parallel plates, (b) rotating drum, (c) rotating disc.	13
Figure 2.2. Schematic diagram illustrating collagen's hierarchical structure (Adapted from [23]).....	17
Figure 3.1. Humidity controlled chamber for electrospinning	30
Figure 3.2 AFM height image of fibers suspended over trenches with sufficient fractions of the support substrates allowing fiber height measurements and substrate mechanical testing.	35
Figure 3.3. Deflection of the cantilever vs. sample	36
Figure 3.4. AFM height image of fibers suspended over trenches with points that were selected to acquire force curves. (black points: points selected as being on fibers; blue points: points on the rigid substrate). Other measurement positions (red points) are not used in the analysis, but serve to verify the registration between the image and grid of force curves	38
Figure 3.5. Relative slopes of the force plots and the curve fit obtained from multiple points along the fiber	40
Figure 4.1 SEM images of electrospun collagen fibers spun with 25wt% collagen solution in relative humidity (RH) levels of (a) 20%, (b) 25%, (c) 30%, (d) 35%, (e) 40%, (f) 45%. Scale bar: 1 μ m.....	46
Figure 4.2. Plot of average fiber diameter as a function of relative humidity for a 25 wt% collagen solution (black squares with standar deviations indicated by error bars). Average fiber diameter and fiber size distribution can be further reduced by reducing the solution concentration (red circle).....	46
Figure 4.3. SEM images of electrospun collagen fibers spun with 5 wt% collagen solution in HFIP at relative humidity (RH) levels of (a) 25%, (b) 30%, (c) 35%, (d) 40%. Scale bar: 2 μ m.....	47

Figure 4.4. Plot of average fiber diameter as a function of relative humidity for a 5 wt% collagen solution in HFIP.	48
Figure 4.5. SEM images of electrospun collagen fibers spun with 20 wt% collagen solution at a flow rate of 0.1 mL/hr in relative humidity (RH) levels of (a) 20%, (b) 25%, (c) 30%, (d) 35%, (e) 40%, (f) 45%. Scale bar: 2 μ m.	49
Figure 4.6. SEM images of electrospun collagen fibers spun with 20 wt% collagen solution at a flow rate of 0.15 mL/hr in relative humidity (RH) levels of (a) 20%, (b) 25%, (c) 30%, (d) 35%, (e) 40%, (f) 45%. Scale bar: 2 μ m.	50
Figure 4.7. SEM micrograph of (a) beaded fibers with 15 wt% collagen solution and (b) electrospayed beads with 10 wt% collagen solution.	51
Figure 4.8. (a) random electrospun collagen fibers; (b) aligned electrospun collagen fibers; frequency plot of 2D FFT of (c) random fibers, (d) aligned fibers.	52
Figure 4.9. (a) SEM image of rat tympanic membrane; (b) SEM image of a two-layer electrospun structure of aligned fibers; (c) frequency FFT plot of fiber alignment for (a) and (b).	53
Figure 4.10. TEM images of coaxial electrospun PEG-collagen fibers. (a) and (b) core-shell structure with lighter shell indicating collagen and darker core indicating PEG with collagen; (c) and (d) hollow structure with collagen shell only.	55
Figure 4.11. (a) as spun collagen fibers; (b) fibers exposed to water and gelled into film.	56
Figure 4.12. (a) riboflavin encapsulated electrospun collagen fibers; (b) pieces of riboflavin encapsulated inside the fiber showing a larger fiber size; (c) fibers crosslinked in pure ethanol for 60 mins; (d)-(f) UV crosslinked fibers after immersed in water for one hour.	58
Figure 4.13. SEM micrographs of electrospun collagen fibers containing the photoinitiator Rose Bengal. (a) – (b) as-spun fibers, some of which show irregular shapes indicating encapsulation of Rose Bengal particles. (c) - (e) 24 hours water test for fibers crosslinked in pure ethanol for 22 hours. (f) – (i) 24 hours water test for fibers crosslinked in isopropanol for 22 hours.	59

Figure 4.14. SEM micrographs of Rose Bengal incorporated electrospun collagen fibers crosslinked in pure isopropanol for 22 hours and immersed in water for 7 days.	60
Figure 4.15. SEM micrographs of electrospun collagen scaffolds (a) as-spun, (b) ion implantation with 4×10^{15} ions/cm ² , 1×1 cm ² aperture and 200nA current, (c) ion implantation with 4×10^{15} ions/cm ² , 3×3 cm ² aperture and 900nA current, (d) ion implantation with 8×10^{15} ions/cm ² , 3×3 cm ² aperture and 900nA current; (e)-(h) histograms of fiber diameter distribution for samples in (a)-(d) with best-fit normal distributions.....	63
Figure 4.16. SEM micrographs of N ⁺ implanted eletrospun collagen fibers immersed in water for 7 days. (a) Implantation with 4×10^{15} ions/cm ² (b) implantation with 8×10^{15} ions/cm ²	64
Figure 4.17. Full XPS survey on freeze dried type I collagen.....	66
Figure 4.18. Full XPS survey spectrum on 4×10^{15} ions/cm ² N ⁺ implanted collagen film....	67
Figure 4.19. Full XPS survey spectrum of as spun collagen fibers	67
Figure 4.20. Full XPS survey spectrum of 4×10^{15} ions/cm ² N ⁺ ion implanted electrospun collagen fibers.....	68
Figure 4.21. Full XPS survey spectrum of 8×10^{15} ions/cm ² N ⁺ ion implanted electrospun collagen fibers.....	68
Figure 4.22. High resolution XPS of N 1s for collagen film	70
Figure 4.23. High resolution XPS of N 1s for collagen film implanted with 4×10^{15} ions/cm ² N ⁺	70
Figure 4.24. High resolution XPS of N 1s for as spun collagen fibers.....	71
Figure 4.25. High resolution XPS of N 1s for electrospun collagen fibers implanted with 4×10^{15} ions/cm ² N ⁺	71
Figure 4.26. High resolution XPS of N 1s for electrospun collagen fibers implanted with 8×10^{15} ions/cm ² N ⁺	72

Figure 4.27. High resolution XPS of C 1s for collagen film	73
Figure 4.28. High resolution XPS of C 1s for collagen film implanted with 4×10^{15} ions/cm ² N ⁺	73
Figure 4.29. High resolution XPS of C 1s for electrospun collagen fibers	74
Figure 4.30. High resolution XPS of C 1s for collagen fibers implanted with 4×10^{15} ions/cm ² N ⁺	74
Figure 4.31. High resolution XPS of C 1s for collagen fibers implanted with 8×10^{15} ions/cm ² N ⁺	75
Figure 4.32. High resolution XPS of O 1s for collagen film	76
Figure 4.33. High resolution XPS of O 1s for collagen film implanted with 4×10^{15} ions/cm ² N ⁺	76
Figure 4.34. High resolution XPS of O 1s for electrospun collagen fibers	77
Figure 4.35. High resolution XPS of O 1s for electrospun collagen fibers implanted with 4×10^{15} ions/cm ² N ⁺	77
Figure 4.36. High resolution XPS of O 1s for electrospun collagen fibers implanted with 8×10^{15} ions/cm ² N ⁺	78
Figure 4.37. SEM image of electrospun collagen type I fibers on trenched silicon wafers. The electrospun fibers are randomly oriented on the surface.	79
Figure 4.38. Plot of Young's modulus as a function of fiber diameter for as spun electrospun collagen fibers (half blue circles) and vacuum dried as spun fibers (black squares).....	79
Figure 4.39. Plot of Young's modulus of electrospun Rose Bengal incorporated collagen fibers	81
Figure 4.40. Plot of Young's modulus of collagen fibers incorporating photoinitiator (red triangles) and vacuum dried as spun fibers (black disks).	82

Figure 4.41. Plot of Young's modulus of Rose Bengal incorporated (red triangle) and green light crosslinked (blue triangle) collagen fibers.....	83
Figure 4.42. Plot of Young's modulus as a function of fiber diameter for genipin-crosslinked collagen fibers (purple circles) and as spun electrospun collagen fibers (black dots).....	84
Figure 4.43. Plots of Young's modulus as a function of fiber diameter for (a) nitrogen treatment with dosage of 4×10^{15} ions/cm ² ; (b) nitrogen treatment with dosage of 8×10^{15} ions/cm ² ; (c) overlay of the two ion implantation dosages; (d) comparison between ion implanted fibers and as spun collagen fibers.	85
Figure 4.44. Plots of Young's modulus of (a) collagen fibers spun with HFIP solvent system and implanted with different dosage of nitrogen ions; (b) electrospun collagen fibers prepared with HFIP and acetic acid and implanted with 4×10^{15} ions/cm ² nitrogen; (c) electrospun collagen fibers prepared with HFIP and acetic acid and implanted with 8×10^{15} ions/cm ² nitrogen.	87
Figure 4.45 Optical image (brightfield) of IMR-90 on culture plate after 24 hours seeding, initial seeding density: 20,000 cells / well.	89
Figure 4.46. SEM images of all crosslinked samples after 24 hours of cell seeding. (All have the scale bar of 20 μ m)	90
Figure 4.47. SEM images of filopodia extension on crosslinked electrospun collagen. (a) filopodia extended from the cell to reach to genipin crosslinked electrospun collagen fibers. (b) additional cells grow on the bottom of the fiber layer. (c) filopodia reach out, anchor and align with fiber direction. (d) filopodia extended and reached to entangle the fibers underneath the top layer.....	91
Figure 4.48. SEM images of filopodia extension on LED crosslinked electrospun collagen fibers. (a) long filopodia extension with length of more than 100 μ m. (b) filopodia extension and entanglements between cells.....	92
Figure 4.49. SEM images of crosslinked collagen samples after 1, 4 and 7 days of IMR90 culture. (All have the scale bar of 100 μ m)	93

Figure 4.50. Fluorescence images of IMR 90 cultured on aligned crosslinked electrospun collagen nanofiber; a: cell nucleus; b: filamentous actin; c: overlaid image	94
Figure 4.51. Fluorescence image of IMR 90 cultured on aligned vs. random collagen fibers.	94
Figure 5.1. Fibers sticking to collector and with each other	98
Figure 5.2 IMR 90 seeded on N ⁺ implanted aligned fibers for 24 hours.....	114

List of Appendices

Appendix A Rat tail collagen preparation procedure	147
Appendix B Deflection due to tension.....	148
Appendix C green light light distance and intensity chart	150
Appendix D Rose Bengal UV-Vis spectra in different solvent system	151

List of Abbreviations

AFM	Atomic force microscope
BM	Bioactive molecules
DCV	Direct current voltage
DHT	Dehydrothermal
ECM	Extracellular Matrix
FBS	foetal bovine sera
FFT	Fast Fourier transform
GA	Glutaraldehyde
GAGs	Glycosaminoglycans
HFIP	1,1,1,3,3,3 hexafluoro-2-propanol
PBS	phosphate-buffered saline
PCL	Polycaprolactone
PEG	Poly (ethylene glycol)
PEO	Polyethylene oxide
PGA	Poly (glycolic acid)
PLA	Poly (L-lactic acid)
PLCA	Poly (lactic acid-co-caprolactone)
PLGA	Poly (Lactic-co-glycolic acid)
PVA	Poly(vinyl alcohol)
RH	Relative humidity
RPMI	Roswell Park Memorial Institute
SEM	Scanning Electron Microscopy
TEM	Transmission Electron Microscopy
WD	Working distance
XPS	X-ray Photoelectron Spectroscopy

1 Introduction

The goal of tissue engineering is to assemble functional constructs to restore, maintain or improve damaged tissues [1]. Among the many requirements that are known for the process, scaffold is one of the critical components. Knowing that extracellular matrix (ECM) is the major component of the microenvironment of the cell and takes part in most cellular process and cell behaviors, it is desirable to create constructs that can replicate the structural, chemical, physical and mechanical aspects of the ECM for tissue repair [1]–[3]. Collagen, the most abundant protein which serves as the structural and mechanical support for the cells, is the optimal biomaterial to create a scaffold that mimic the native ECM [4]–[6].

As collagen is often presented as an organized 3D nanofibrous structure with fiber diameter between 50 to 500nm in many different tissues, electrospinning has been widely used to fabricate nanosized collagen fibers [7]–[10]. The versatility of the electrospinning process and setup allows collagen fibers with controlled size, structure, morphology and organization to be obtained [11]–[16].

The objective of the current research is to use electrospinning to fabricate collagen fibers, and to use them as building blocks to create a tissue regeneration environment that resembles the native ECM. As electrospun collagen fibers are not stable in aqueous solutions, they have to be stabilized. Chemical, photochemical and physical methods have been suggested for introducing exogenous crosslinks into the molecular structure of collagen-based materials to control their degradation rate and enhance their mechanical stabilities. The effects of different stabilization methods on fiber structure, morphology, and properties will be investigated and compared.

This thesis aims at developing a stabilized, cell compatible, electrospun collagen fibrous scaffold that replicate the structural, chemical, physical and mechanical aspects of the natural ECM for tissue engineering applications. The developed nanofibrous structure mimics the microanatomic and mechanical properties, and provide mechanical support for cell growth. When placed in an appropriate biochemical environment such as cell

culture media, such a system will provide signals to guide cell migration, proliferation and differentiation.

There are five main objectives of this work:

- 1) To fabricate 3D electrospun collagen fibrous scaffolds, and to optimize the processing parameters to obtain fibers with desirable and controllable fiber morphology, structure and diameter that mimics the microanatomic structure of the native tissue
- 2) To use coaxial electrospinning to demonstrate the possibility of incorporation of bioactive molecules (BM) for drug delivery applications.
- 3) To stabilize the scaffolds in aqueous environment using chemical, photochemical and physical methods while preserving the fibrous morphology
- 4) To characterize the effect of this stabilization in terms of aqueous stability, mechanical properties and chemical properties of the fibers
- 5) To evaluate the in-vitro cell compatibility of the stabilized electrospun collagen scaffold for tissue regeneration applications

This thesis is organized in the following way. Chapter 2 is a literature review which provides background on the major components of this thesis: the effect of the ECM on cellular behavior, tissue engineering principles, electrospinning, collagen as a biomaterial, collagen stabilization, nano mechanical testing, and cell compatibility of electrospun collagen fibers. Chapter 3 describes the materials and methods used in this thesis for scaffold fabrication, modification, and characterization. In Chapter 4, results of the work performed to address the objectives of this thesis are presented. These include: optimizing the parameters of the electrospinning process for fiber fabrication, emphasizing environmental effects on fiber morphology and diameter; the effect of electrospinning setup variation on fiber organization relative to native collagen fiber arrangement; the effect of crosslinking methods on fiber stabilization; the effect of stabilization on fiber diameter and mechanical properties; characterization of ion beam modified fibers using X-ray Photoelectron Spectroscopy (XPS). Finally, the in-vitro response of fetal lung fibroblast (IMR90) cells to the stabilized collagen fiber scaffold

will be presented in terms of the biological parameters including cell attachment and morphology. A comparison of the effect of fiber orientation cell behavior will also be included. Chapter 5 is a discussion of the results presented in Chapter 4, and their implications and relevance in tissue regeneration applications. Chapter 6, summarizes the work done, identifies the significance of the results, presents the conclusion. The final chapter, Chapter 7, suggests the future work which needs to be carried out.

2 Background and Literature Review

2.1 Extracellular matrix structure and function

In the human body, the natural environment of cells is composed of a collection of macromolecules secreted by support cells [3], [17], [18]. The non-cellular portion of tissues is termed the extracellular matrix (ECM) and serves to mechanically support cells in a three dimensional space while providing biochemical signals for cellular activity regulation [19]. The major components of the ECM include proteins, proteoglycans and glycosaminoglycans (GAGs) [20]. The ECM makes up a large majority of tissue volume, and also provides tissue with the unique geometric shape consisting primarily of protein fibers with diameters between 30 and 500 nm [21]. All the protein components are subject to degradation and modifications, and different components in the ECM are constantly being degraded, synthesized, secreted, organized, and modified by the cellular components [22]. Historically, the function of native ECM was only believed to be as a structural framework for tissues [23]. However, it is now understood that the ECM, through interactions with receptors on the cell surface, play an essential role in cellular activity and wound healing [24]. Cell-ECM interaction is responsible for pattern formation, morphogenesis, and phenotype acquisition and maintenance [22]. Wound healing, inflammation, formation of granulation tissues, and remodeling are all mediated by cell-ECM interaction during clot formation [22]. Cell adhesion, migration, growth, differentiation and apoptosis are all modulated by the transmission of signals between cell nucleus and the ECM. Growth factors and signaling molecules are proteins presented within the ECM, and ECM environment protects these proteins from premature degradation [22], [25].

The ECM has the ability to communicate with cells by sending signals across the cell membrane to soluble molecules in the cytoplasm and through direct connections with the cytoskeleton into the cell nucleus [22]. Thus ECM has the ability to alter cellular function while cells repair, remodel and regenerate the ECM at the same time. Due to this cell-ECM dynamic reciprocity, the cellular response to the ECM often results in changes to the state of the ECM. Thus, creating an ECM analogue that can replicate these physiological cell-ECM interactions is extremely important, but challenging. It was

suggested using natural polymers which constitute the native ECM may possess the properties required by cells for proper cellular responses [22].

2.2 Cell – substrate interaction

Cells receive chemical and physical signals from neighboring cells, the surrounding fluid and the extracellular matrix (ECM) [26]. Cells integrate these various stimuli and interpret them to generate appropriate cellular responses [26]–[30]. During directed migration, cells are guided by a combination of mechanical and chemical cues presented by neighboring cells and the surrounding extracellular matrix. One important class of signals that guide cell migration is topographic cues. Degree of tension [18], [31], [32], topography [26], [33], [34] and stiffness [17], [35], [36] of the substrate are important in cell morphology, signaling and proliferation. In particular, contact guidance in 3D is the phenomena by which the matrix provides directional cues to the cells and directs the motility response via anisotropy in the microenvironment [28].

Although the ECM in the human body is complex and tissue specific, its major components are polysaccharide chains and fibrous proteins, which have both structural and adhesive functions [37]. Collagen with diameter approximately 50-500nm is the major protein present in the ECM. It provides structural support to tissues and regulate cellular functions [3]. The micrometer scale architecture of these fibrous networks constrains spatially where cells can form adhesions and imparts complex mechanical characteristics to the ECM.

Previous works on collagen gels indicate that contact guidance promotes cell migration along the axis of collagen alignment [27], [28]. Work on fibroblasts and mammary epithelial cells shows that contact guidance cues arising from collagen alignment promote 3D cell migration along the axis of collagen alignment [28]. Londono et al. demonstrated that individual cells are contact guided by grooves [33], while Teixeira et al. demonstrated contact guidance of epithelial cells by well-defined micro- and nanostructured grooves [26].

Cells reside in or on a complex 3D ECM containing networks of fibers with diameters on the order of nanometers [38], [39]. These fiber networks vary in density and organization depending on the tissues [40]–[43]. It is desirable to examine the role of contact guidance in promoting 3D cell migration in both random and aligned fibrous scaffolds.

2.3 Tissue Engineering

Tissue engineering aims to develop functional constructs resembling the structure and function of native tissues to improve or replace damaged ones and to serve as an alternative to organ transplantation [44], [45]. In tissue engineering, cells are often seeded onto artificial structures capable of supporting 3D tissue formation. An optimal scaffold for tissue engineering applications should meet some basic requirements, such as biocompatibility, biodegradability, sterilizability, physical and chemical properties that correspond to those of native tissues [3]. It is desirable to have the scaffold mimic the mechanical and functional properties of the extracellular matrix (ECM) of the tissues to be generated. As the scaffold should possess the ability to support cell attachment as well as to facilitate nutrient transport throughout the assembly, it is essential to have a high surface area and an inter-connected 3D porous structure. Proper geometry, pore size, and scaffold architecture are all important factors that can significantly affect cellular behavior such as cell attachment, proliferation and differentiation [46].

It is well established that the ECM provides signals that control many cell activities such as differentiation, adhesion, migration, proliferation and apoptosis [19], [47]. These signals are orchestrated by the three-dimensional organization of the matrix, which provides both specific interactions and also structural clues. The creation of ECM-mimicking scaffolds that facilitate the generation of high levels of cellular complexity is the ultimate objective of tissue engineering.

An ideal tissue engineering scaffold should mimic the form and functionality of the native ECM to serve as a “synthetic ECM” [16], [22], [34]. It should replicate the structural, chemical, physical and mechanical aspects of the native ECM. Thus, a successful tissue engineering scaffold should:

- 1) Have an appropriate porosity that allows cell migration and penetration,
- 2) Have a high surface area to volume ratio and proper surface chemistry to promote cell adhesion, growth, migration and differentiation,
- 3) Be constructed from materials that are biocompatible and degradable with a degradation rate that closely resembles the rate of native tissue regeneration to promote proper tissue growth,
- 4) Be mechanically strong, to provide support and stimulate cell growth.

Because the dimensions of the building blocks of a tissue engineered scaffold should be on the same scale as those of natural ECM, 3D nanofibrous structures have great potential for producing scaffolds that resemble the fibrillary features of ECM.

Many studies have reported the fabrication of nanofibers using various techniques, such as electrospinning, self-assembly, phase separation, bacterial cellulose, templating, drawing, extraction, and vapor phase polymerization [3], [48]. Among these methods, electrospinning is a simple, inexpensive and versatile approach with the ability to generate nanosized fibers to form fibrous structure with random and organized arrangements, and has gained widespread interest as a potential scaffolding technique for tissue engineering applications [44], [49], [50].

2.4 Cell compatibility of tissue engineering scaffold

Fabricated scaffolds may interact with the host tissue cells, and these scaffolds should actively facilitate and regulate cell activities [24]. A scaffold should support cell attachment, growth and differentiation during both in vitro culture and in vivo implantation [2]. The biomaterials used to fabricate the scaffolds should be biocompatible with the host tissue. It should possess the correct structure, geometry, and mechanical properties and be compatible with the cell type that is present in the tissue that is being regenerated. The biomaterial used in the scaffold should cause minimal immune rejection and may include biological cues such as bioactive molecules and cell-adhesive ligands to enhance cell attachment. Growth-stimulating signals such as growth factors can also be encapsulated in the scaffold to speed up regeneration [3], [34], [45], [47], [49], [51], [52]. In such cases, the engineered scaffold may also serve as a delivery vehicle or reservoir

for the bioactive molecules. The scaffold surface provides the anchoring site for cell attachment, which is the initial stage for tissue regeneration, thus the surface properties of the scaffold should allow good cell adhesion [2], [45], [53]. Hence, surface modification of the biomaterials has become increasingly popular for enhancing cell adhesion [54]–[60].

2.5 Electrospinning

2.5.1 Setup and operating principles

Electrospinning is a notable fiber fabrication technique used to produce non-woven fibrous materials with fiber diameters in the order of a few nanometers to $> 1 \mu\text{m}$ [61]. A typical electrospinning setup consists of a conductive capillary which the solution to be electrospun is forced through, a high voltage source with positive or negative polarity, which applies electric charges into the liquid, and a ground collector [62]–[64]. Polymers are dissolved in a solvent at a concentration high enough for polymer chain entanglement to occur [49], [64]–[68]. Too low a concentration prevent fibers to form, while higher concentration results in a viscosity that is too high for the solution to be pulled out of the capillary. During the electrospinning process, a polymer solution is first forced through the spinneret and forms a droplet at the tip of the spinneret. The droplet is held in place by its surface tension. As an electric field is applied to the droplet, the droplet is first deformed into a conical shape termed a Taylor cone by the electrostatic force, which is in equilibrium with surface tension [69], [70]. Further increases in the applied voltage results in the electrostatic force overcoming the surface tension, and a jet of solution is ejected from the tip of the Taylor cone. The electric force stretches the polymer jet as it is drawn from the tip of the Taylor cone and attracted to the ground electrode. This stretching and drawing reduces the jet diameter. As the jet travels in the electric field, the solvent evaporates and the dry nanometer to micrometer-scale fibers are collected as a randomly oriented web on the collector [61], [71], [72]. The fibers produced via electrospinning have a nonwoven structure with interconnected pores and a large surface to volume ratio. These features give such fibrous scaffolds many biomedical and industrial applications such as filtration devices, membranes, protective clothing, and tissue engineering scaffolds [64], [73], [74]. Various materials and process parameters

can affect the final fiber properties and architecture [2], [3], [47], [61], [73], [75], [76]. The flexibility in tailoring scaffold properties such as fiber diameter, scaffold size, porosity, and fiber morphology, offers the possibility to design electrospun scaffolds that can meet the demands of numerous practical applications. In particular, the morphological resemblance of electrospun nanofibers to native ECM is the major factor driving the use of electrospun scaffolds for tissue engineering [3]. Moreover, the high surface area vs. volume ratio and interconnected pores of the scaffolds ensure desirable cell attachment and nutrients transport [3]. The stability of the fibers, which depends on the chemical structure, composition and processing procedure, can be further improved by post processing [2], [3], [19], [75], [77].

2.5.2 Electrospinning conditions and parameters

The ability for electrospinning to create tissue specific scaffolds arises from the adaptability of the process and the system control offered by a number of controllable processing parameters:

- 1) Polymer and solution properties such as polymer type, polymer molecular weight, polymer concentration, viscosity, conductivity, volatility and surface tension,
- 2) processing conditions such as electric field gradients, voltage, capillary diameters, distance from the capillary to the collector, solution flow rate,
- 3) environmental conditions such as temperature, humidity, air velocity and static electricity.

By adjusting these electrospinning parameters, most thermoplastic materials can be electrospun [48], [51]. Each of the parameters, individually or in conjunction with one another, can affect fiber diameter, morphology, and scaffold porosity [45], [78]. The effects of some of these variables on fiber diameter, diameter distribution and fiber morphology have been independently studied. The mechanical properties of the scaffold can be altered by the organization of the fibers, the types of the polymers used, and the size of the fiber constituents. Fiber orientation can also be controlled by changing the setup of the ground collector, for example by as using a rotating electrode[3], [12], [45]. After the scaffold has been produced, its mechanical properties and degradation

behaviors can be further modified by post-spinning processes such as annealing, stretching or crosslinking [50], [79]–[82].

Empirical observations and analytical models have been utilized to provide quantitative prediction of the size of fibers fabricated by the electrospinning process [50], [63]–[65], [67], [83]–[85]. Some general trends can be summarized as follow:

Concentration: At very low concentration, polymeric nano or micro particles will be obtained as a result of electrospinning [3], [68], [73], [86]. As the concentration increases, a mixture of beads and fibers will be formed. Further increase in concentration allows smooth nanofibers to form. At concentrations higher than the optimal concentration range, either fiber formation is prevented due to high viscosity, or micro-ribbon fibers form due to incomplete solvent evaporation [22], [48], [68], [87]–[89].

Molecular weight: Molecular weight affects the entanglement of polymer chains in solution, with longer chains being more entangled. More entanglement leads to an increase in solution viscosity [12], [22], [50], [73], [79], [88], [90]–[97]. Lowering the molecular weight results in the formation of beads. While increasing the molecular weight leads to chain entanglement and smooth fiber formation. Micro-ribbon fibers will be obtained if the molecular weight is too high.

Flow rate: Several studies have shown that lower flow rates result in smaller fiber diameter [64], [84], [98]. Higher flow rate results either in fibers with larger diameter or beaded fibers [64], [73], [78], [99]. Further increases in the flow rate created fibers which were not completely dried before reaching the collector.

Solution viscosity: It has been shown that continuous and smooth fibers cannot be formed at very low solution viscosity while too high of viscosity impedes jet formation. There is a limited range of viscosity over which electrospinning produces acceptable fibers [50], [67], [68], [85], [88], [92], [97], [100]–[103]. The solution viscosity is strongly correlated with molecular weight and polymer concentration, an increase in either concentration or molecular weight can increase the viscosity. On the other hand,

environmental parameters such as ambient temperature can also affect viscosity [65], [69], [88].

Surface tension: Surface tension is a function of solvent composition and is mainly affected by the choice of solvent [14], [19], [50], [53], [92], [102], [104], [105]. For a fixed polymer concentration, reducing surface tension by using a more volatile solvent can convert beaded fibers to smooth fibers [73].

Charge density and conductivity: The conductivity of the polymer solution is determined by the polymer and solvent used, as well as by the presence of ionic additives [50], [70], [83], [92], [106], [107]. The electrical conductivity can be tuned by adding ionic salts such as NaCl and KH_2PO_4 . Solutions with high conductivity have high surface charge density and under a given electric field, high conductivity results in an increase in the elongation force on the jet. As a result, the solution undergoes a greater tensile stretch and forms thinner fibers.

Voltage: For electrospinning, charged jets can only be ejected from the Taylor cone when the applied voltage is higher than a certain threshold. However, the effect of applied voltage on fiber diameter is a bit controversial. Reneker et al. demonstrated that there is not much effect of electric field on the diameter of electrospun polyethylene oxide (PEO) nanofibers [108]. While Bhardwaj et al. suggested a higher voltage causes greater stretching of the solution, thus thinner fibers, several groups have also suggested that higher voltages result in larger diameter or beaded fibers [50], [66], [84], [109].

Collector-tip distance: The influence of tip to collector distance on fiber morphology and diameter has been examined for various polymers [45], [49], [76], [109], [110]. It was found that a minimum distance is needed to provide sufficient time for the solvent to completely evaporate before the dry fibers reach the collector. On the other hand, beading is observed when the collector is placed too far from needle tip [49], [84], [111], [112].

Thompson et al. studied the effects of experimental parameters on nanofiber diameter based on a model of electrospinning [64]. Their model indicates which parameters have the greatest influence on the fiber diameters. Among the 13 materials and operating

parameters studied in the paper, they evaluated the parameters on a relative basis to determine a strong-moderate-minor rating for the influence on fiber diameter. The result showed that volumetric charge density, distance from nozzle to collector, initial jet radius, relaxation time, and viscosity are the five parameters having the most significant effect on the jet radius. Initial polymer concentration, solution density, electric potential, perturbation frequency, and solvent vapor pressure have moderate effects on the fiber diameters. While parameters such as relative humidity, surface tension, and vapor diffusivity have minor effects on the resulting jet radius. Although this study did not consider the effect of temperature directly, temperature does affect solution density, vapor diffusivity, viscosity, and relaxation time. Other potential factors such as solution pH, charge polarity and pressure were not included in their model. The 13 materials included in the study vary in structure and properties such as hydrophilicity, and the available experimental data included in the study are insufficient to fully validate the model results for most of the parameters. The electrospinning process is complex and it is difficult (or in some cases, impossible) to experimentally vary one parameter while all the others are kept constant. Varying one parameter at a time would give insight into the electrospinning process and suggest that to better control the process one must control the parameters which have the strongest effect. For each polymer type and solvent system, there is usually a relatively narrow set of experimental conditions that provide optimum results. Thus each polymer/solution system should be investigated independently to identify the effect of each parameter.

2.5.2.1 Fiber alignment

A stationary ground electrode collects the electrospun fibers in a random orientation. However, for many applications, it is essential to control the alignment of the fibers within the scaffolds. For example, the basic structure of tendon, ligament, dura mater, tympanic membrane and sciatic nerve bundles all consist of aligned collagen fibers [113]–[115]. The alignment is important as it defines the spatial arrangement that is significant for tissue function. It has also been reported that the arrangement of cells in controlled two- and three- dimensional architecture has beneficial effects on cell differentiation, proliferation and functional longevity [34].

To collect aligned fibers, several studies have examined different collector designs to control the orientation of electrospun fibers. There are currently three main types of collectors used to generate aligned fibers: parallel plates, rotating drums and rotating discs (Figure 2.1).

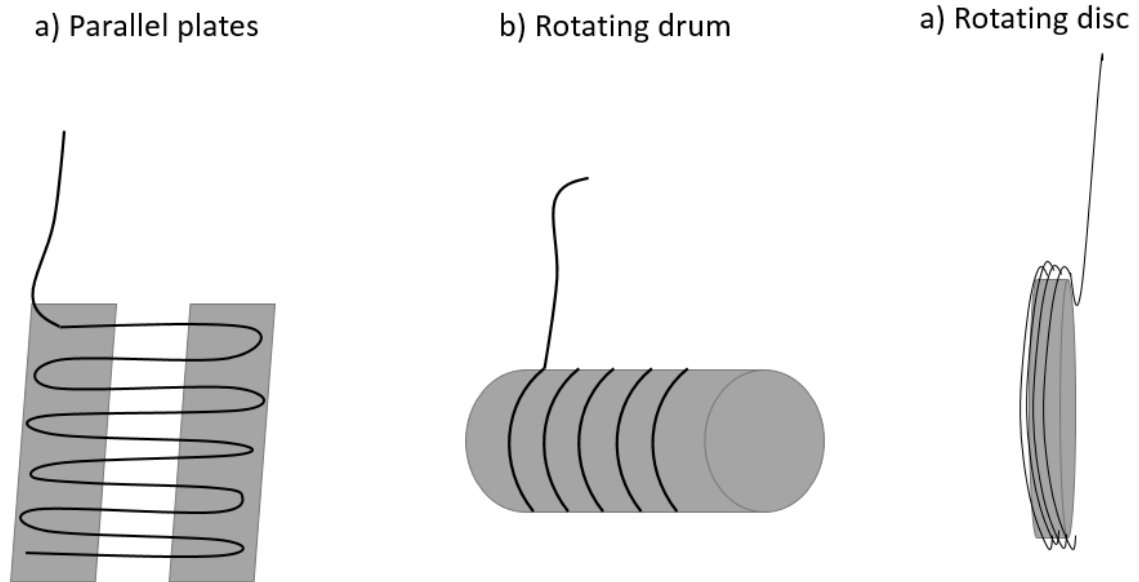


Figure 2.1. Electrospinning collectors used to collect aligned fibers: (a) parallel plates, (b) rotating drum, (c) rotating disc.

Parallel plates consist of two grounded conductive plates separated by a gap. Fibers are captured in the space between the plates in uniaxially aligned form. The mechanism of this alignment is explained by Li et al. when two conductive strips with an insulating gap are used, the electric field is altered, causing a different motion in fibers and causing them to align across the gap [116]. In contrast, when a continuous collector with no gap is used, the electrostatic forces have no preferential direction and cause random deposition of fibers. At the same time, repulsive electrostatic interactions between the deposited fibers impact the alignment. Continuous electrodes result in immediate discharge of fibers while electrodes with an insulating gap result in parallel deposition of fibers which remain highly charged after contacting the electrodes. The electrostatic repulsion of fibers with the same charge results in deposition of fibers with parallel alignment to reach the

lowest possible state of energy [116]. Rotating drum or disc collectors produce fiber alignment when the speed of rotation matches the fiber drawing rate.

2.5.2.1.1 Determination of fiber alignment (2D FFT)

Due to the importance of fiber and cell alignment in cell behavior and tissue engineering, it is essential to quantify and characterize the degree of alignment for a given scaffold. 2D fast Fourier transform (FFT) of images of the deposited fibers provides a reliable and relatively straightforward method of measuring the degree of fiber alignment in electrospun scaffolds. 2D FFT has been used widely in the literature as a standard method for measuring the degree of scaffold alignment [113], [117].

The 2D FFT function converts spatial information in an image into a mathematically defined frequency domain which maps the rate at which pixel intensities change. The FFT of an image containing randomly aligned fibers generates a frequency plot with the majority of white pixels concentrated symmetrically around the origin, and the FFT of an image containing aligned fibers will generate a frequency plot with peaks corresponding to the spacing of the fibers and the degree and direction of alignment [113], [117]–[119].

The spectra generated by a 2D FFT are not easy to read and therefore translating the spectra into a plot is more direct way representing the degree of alignment. A plot of nominal pixel intensity versus orientation can be generated by summing the pixel intensities along the radius for each angle of the circular projection (0 - 360°). Often, the summation of pixels is only carried out between 0 - 180° as the frequency plot is symmetric along the 180° line. The summation generates an easily read plot showing peaks at the angles along which most of the fibers are aligned. A high, narrow peak is indicative of a higher degree of uniform alignment, while a broader peak or the presence of a shoulder on the peak indicates that there may be more than one principal axis of alignment and the alignment of the fibers is less organized.

2.6 Use of electrospun fibers in tissue engineering

Electrospun fibrous scaffolds are particularly attractive for tissue regeneration and biomedical applications due to their high surface area for cell adhesion and

interconnected porous network for cell penetration and migration [53], [64], [120]. The fibrous structures can be electrospun into controlled organization with fiber alignment to mimic the natural ECM structure. Electrospun fibrous scaffolds based on synthetic polymers, natural polymers, synthetic/natural blends, have been successfully studied for regenerating cartilage, bone, bladder, skin and neural tissues [3], [45], [47], [49], [52], [121], [122].

The material choice for tissue engineering applications depends on the type of scaffold required, the nature of the tissues to be regenerated, and their time required for regeneration. The best material will fulfil the requirements of specific chemical, physical, and mechanical properties and degradation times required for the particular application.

2.6.1 Synthetic vs. natural polymers

Both synthetic and natural polymers can be used for producing 3D non-woven fibers via electrospinning. To date, more than 50 different polymers have been successfully electrospun [44], [49], [50], [63], [70], [84], [107], [108], [123], [124].

For tissue engineering applications, synthetic biodegradable polyesters such as polycaprolactone (PCL), poly(lactic acid) (PLA), poly(glycolic acid) (PGA), poly(Lactic-co-glycolic acid) (PLGA) and poly(lactic acid-co-caprolactone) (PLCL) are preferred materials used for electrospun fibers due to their good processability and stable mechanical properties [45]. Synthetic materials offer a versatile alternative to naturally derived biopolymers, their mechanical properties can be highly tailored and they are easy to synthesize and shape [47]. Many synthetic polymers already have established mechanical histories and are routinely used in medical implants, substantially increasing their applicability for regulatory approval [47].

While a synthetic polymer scaffold can mimic the structure of the native ECM, the ability to electrospin a naturally occurring protein such as collagen can provide cells with a recognizable, physiologically relevant platform from which to proliferate and ultimately remodel [22]. With collagen constituting the majority of the human body's structural ECM, electrospun collagen has been used in a number of tissue engineering applications

[7], [10], [12], [87], [125]–[129]. Other natural polymers such as fibrinogen, gelatin, silk, chitosan and elastin have been electrospun into nanofibers in the creation of bioactive ECM analogues in tissue engineering for their excellent bioactive properties [130]. However, natural biopolymers tend to display poor processability, which needs to be modified for better electrospinnability. For example, some of the natural polymers lost their stability during the electrospinning process due to the harsh solvent used and the high electric field [10], [13], [131]–[134]. As a result, these electrospun fibers need to be crosslinked in order for them to retain their fibrous form.

2.7 Collagen

2.7.1 Structure and Function

Collagen is one of the most abundant proteins in the human body and it fulfills a variety of mechanical functions [135]–[137]. It is present in skin, arteries, cartilage, bones, dentin and in most of the extracellular matrix in general [43]. Most types of collagen present in the human body are in the form of fibers and they are the major building blocks in load-bearing tissues. As fibrous tissues are much stronger along the fiber direction than perpendicular to it, their properties are anisotropic. These fibrils are assembled into a variety of more complex structures to provide different mechanical properties for the target tissues [138]. For example, elastic skin, soft cartilage, stiff bone and tendons are all constructed from a hierarchical assembly of collagen fibers. Hierarchical structuring has the advantage of allowing for optimization and mechanical adaptation at every structural level [139].

For example, every bone in our body will have a slightly different arrangement of the basic mineral collagen fibrils as the basic building blocks. As a consequence, the bending stiffness, fracture resistance and other mechanical properties of bone will differ from site to site due to the different local architecture [23].

The collagen fibrils have a thickness in the range from 50 to a few hundred nanometers and are assembled in a complex hierarchical way into macroscopic structures. At the lowest level, the collagen molecules are triple-helical protein chains with a length of about 300 nm. These collagen molecules are further assembled into microfibrils in which

the collagen molecules are arranged in a staggered, parallel manner. Neighboring molecules are shifted by about 67 nm inside the fibrils. The covalent crosslinking between the collagen molecules provides the mechanical properties of the fibrils [139]. The hierarchical structure of collagen is illustrated in Figure 2.2.

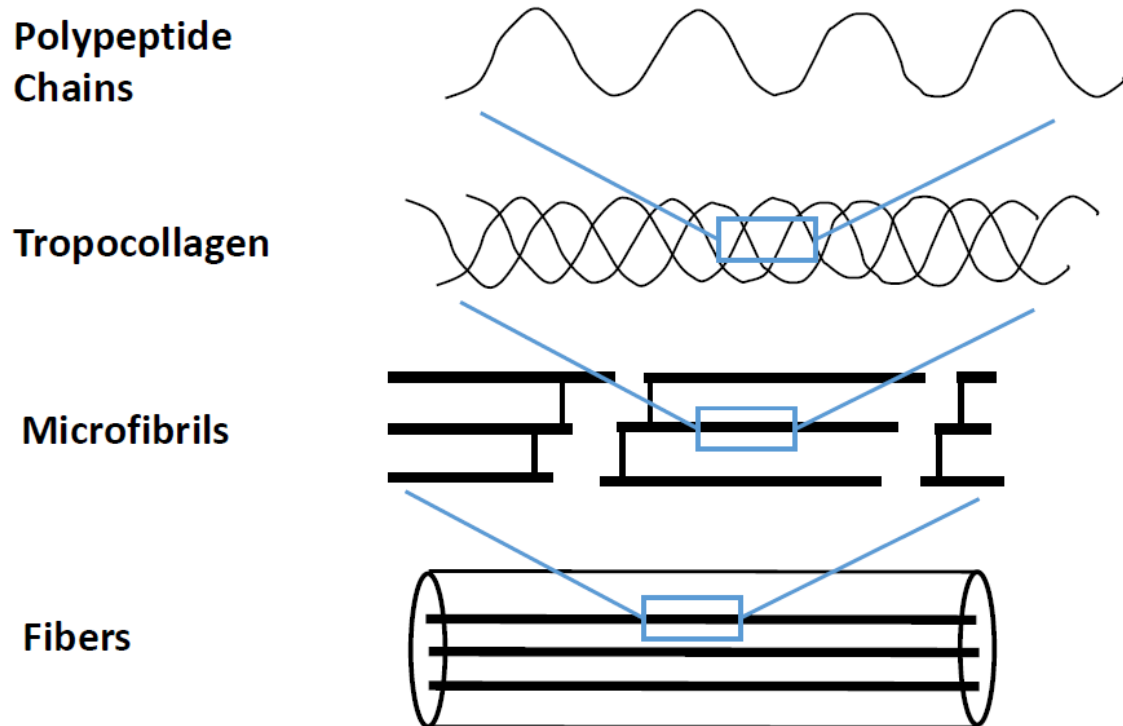


Figure 2.2. Schematic diagram illustrating collagen's hierarchical structure
(Adapted from [23])

2.7.2 Fibrillar collagens

There are 28 different proteins known as collagens found in human [23], [138]. They can be grouped into a number of subfamilies. From the biomechanical point of view, the fibrillar collagens are of the most interest [140]. These proteins are characterized by a repeating banding pattern called D-banding, which has a periodicity of 64-67 nm, depending on the tissue. Within the fibril, collagen molecules of length 300 nm and width 1.5nm are staggered with respect to their neighbors by multiples of D.

2.7.3 Collagen stability

It has long been known that stability of the collagen triple helix is related to the content of the amino acids proline and hydroxyproline, which together make up about 20% of the total amino acids in human fibrillary collagens [141]. This is a result of the cyclic nature of the side chains that restricts flexibility about the peptide bond. Prolyl hydroxylation provides further stabilization. The mechanism of triple-helix stabilization by prolyl hydroxylation has generated much controversy but a general consensus is emerging that this is due to two effects: (1) increased hydrogen bonding through hydration networks and (2) the electron-withdrawing effect of the hydroxyl group [142], [143].

2.7.4 Collagen as a biomaterial for tissue engineering applications

Aside from collagen's widespread presence in the body, its low cytotoxic responses, high water affinity, good cell compatibility, availability with different isolation methods from a variety of sources, and biodegradability make collagen an attractive biomaterial for tissue engineering applications [6], [22], [144]–[146]. The immunogenicity of the collagen is not insignificant and has been studied since the 1960s [147]. However, the clinical significance of such immunogenicity has been shown to be very low and is often considered to be negligible [147]. The possibility of synthesizing collagen-like peptides with the ability to self-assemble into nanofibrous structures permits the construction of well-characterized scaffolds for study of cell-matrix interactions and for applications in tissue repair [148].

2.8 Electrospinning collagen

In 2002, the electrospinning of collagen with the use of 1,1,1,3,3,3 hexafluoro-2-propanol (HFIP) as solvent was first reported [16]. Since then, numerous works on the electrospinning and characterization of collagen fibers have demonstrated that the electrospinning process has the potential to produce collagen fibers that closely mimic the structural and biological properties of the natural collagen ECM [7], [9], [22], [87], [91], [129], [136], [149]. Electrospun fibers of type I, II and III collagen dissolved in HFIP exhibited a linear relationship between polymer concentration and average fiber diameter [22]. Later, a more benign solvent, acetic acid, was used for electrospinning type I

collagen. Compared to HFIP, acetic acid is non-toxic and more economical, and can better maintain the ultrastructural integrity of the collagen [7], [150].

2.8.1 Crosslinking of electrospun collagen fibers

Recent studies have shown that collagen undergoes some conformation changes during electrospinning, and the electrospun collagen fibers does not retain its native structure [21], [136]. As a result, electrospun collagen lacks mechanical and structural stability upon hydration [7], [12], [16], [22], [129], [150]. In order to increase the stability of electrospun collagen, crosslinking is often needed. Crosslinking is essential to stabilize the electrospun fibers by targeting the intramolecular covalent bonds [134]. It is accomplished by the reaction of functional groups on the surface of the collagen fiber that can bridge and link to the adjacent functional groups to construct aqueous stable network [6]. This process is called crosslinking and can be used to tailor the rate of biodegradation, providing collagen networks which degrade at a specific rate into bioresorbable components such as amino acids.

A number of crosslinking methods have been shown to successfully improve the stability and mechanical properties of collagen-based scaffolds [136], [151], [152]. These methods can be categorized into chemical, physical, biophysical and photochemical crosslinking [131], [136], [153], [154].

Each crosslinking method has demonstrated a different degree of structural and mechanical stability, largely attributed to the different crosslinking mechanisms, concentration and reaction time.

Crosslinking with glutaraldehyde (GA) involves a heterogeneous crosslinking distribution that occurs only on the surface of the fibers, which leads to intermolecular crosslinks connecting distant collagen molecules [25]. The ability of GA to self-polymerize accounts for its effectiveness as a crosslinker.

Carbodiimide has been extensively used as an alternative to GA to introduce carboxyl group crosslinking. This approach is more cytocompatible as it doesn't introduce foreign crosslinking molecules, less resistant to proteolytic attack, and less susceptible to

calcification [25]. However, as crosslinking only occurs at “zero distance”, the resultant crosslinking is not as strong as those produced by other methods that can crosslink proximate collagen molecules.

Dehydrothermal (DHT) crosslinking is a physical crosslinking method performed at high temperature in high vacuum. Thermal energy was used to generate highly reactive groups from stable precursors to undergo chemical reactions [152], [153]. For collagen, thermal energy induces the formation of amide and ester crosslinks [155].

Chemical crosslinking using glutaraldehyde vapor has been investigated the most, but this method is cytotoxic and results in calcification in host tissues [156], [157]. Physical crosslinking achieved by heat, dehydrothermal treatment (DHT) have also been used, however, this method compromises the stability of collagen due to thermal degradation [153]. Although genipin crosslinking showed promising results with controlled fiber swelling [129], previous study found genipin crosslinked collagen scaffold did not support neutral stem/progenitor cell differentiation due to the presence of unreacted cytotoxic genipin [158].

2.8.1.1 Photochemical crosslinking

Photochemical crosslinking serves as an attractive alternative to the aforementioned crosslinking methods. Both ultraviolet light with riboflavin as photoinitiator and green light with Rose Bengal have been proposed to stabilize collagen-based materials and enhance their mechanical properties [159], [160].

Ultraviolet radiation is a crosslinking method that produces radicals in the form of unpaired electrons. Crosslinks are subsequently induced by bonding between these radicals. Photosensitizers such as cinnamate and riboflavin have also been used to promote UV crosslinking of collagen [25], [134], [151]. Although UV-riboflavin crosslinking has been used to treat keratoconus corneas, studies on collagen crosslinking with riboflavin have been associated with drawbacks, including cytotoxicity to keratocytes [161]. Long periods of irradiation have been shown to fragment and denature the collagen molecule [134]. In addition, the crosslinking occurs at the surface of the

scaffold, creating heterogeneous properties. The use of Rose Bengal excited by green light was suggested as an improved procedure. It has been used by ophthalmologists to detect corneal abrasions [162]. Photochemical crosslinking with Rose Bengal has been used by Chan et al. to improve the physiochemical properties of collagen gel for cartilage tissue engineering [159]. Their studies suggest that this crosslinking method thermally stabilizes collagen hydrogels and improves the mechanical properties. Later, the method was modified to stabilize the fibrous structure of electrospun collagen scaffolds [7]. With low concentration Rose Bengal, the fibrous morphology was well maintained with minimally toxicity [7].

The exact mechanisms of the binding and interaction between Rose Bengal and collagen remain to be elucidated. One possible explanation is that water and ethanol provide ground state oxygen that may react with Rose Bengal to produce reactive singlet oxygen which then oxidizes surrounding molecules [159], [162]–[166].

Nanofibrous scaffold made using laser irradiation photochemical crosslinking, scaffold nanofibrous architecture remained intact for at least 21 days, implying that cells cultured on these substrates will continuously experience topographical signals over prolonged time duration [7].

2.8.1.2 Physical crosslinking

An approach to enhance the aqueous stability of polymer systems without invoking the use of potentially cytotoxic chemicals is using physical crosslinking. This approach has been well established and well characterized in the case of poly(vinyl alcohol) hydrogels produced using a low temperature thermal cycling process [58], [79]. An associated approach is to induce internal structural rearrangement on the molecular level without the use of additional chemical agents, but instead based on kinetic energy and momentum transfer. One way to achieve this is via ion bombardment or ion implantation. When reactive ions are used, the chemically-induced structural rearrangement could lead not only to stability enhancement but also to additional biochemical benefits such as improved cell adhesion [55], [56].

Ion implantation is a well-established technique in the materials post-processing industry. Ionized atoms or molecules with well-defined energies or energy ranges are produced in an accelerator by heating a gas or using a strong electromagnetic field. These ions can be utilized in various ways to either modify or characterize materials. By carefully choosing the implantation parameters such as ion species, energy and dosage, it allows for the selective modification of tribological, chemical and physical properties of the material [57], [60], [79], [167]. For the treatment of polymers, control of the treatment process becomes more critical as excessive energy deposition could damage or denature the material [59], [79]. Broad-energy (non-monochromatic) ion beam implantation is often used because it provides a wider range of ion doping depths, thus distributing energy over a greater depth range and minimizing thermal damage [58]. Ion beam treatment can tailor both mechanical and chemical properties of polymer surfaces for specific applications [79]. By matching the scaffold properties to that of the native tissue, more normal and stable cell adhesion can be induced [35], [168]. Previous work in our lab determined the conditions to use ion beam treatment to modify the stability of collagen fibers prepared using electrospinning techniques [126].

2.9 Mechanical Testing Techniques

While the structural-function relationship between collagen fibrils and constituent tissues is still being resolved, it is understood that the properties and organizations of single fibrils determine the overall tissue properties [169]–[172]. The properties of a specific structure rely on the architecture at the microscopic level, the defined diameter and properties of the single fiber constituent the structure determine the macroscopic mechanical properties of the tissue. Thus, the single fibril provides the key to scaffold structures from the nanoscopic to macroscopic length scale. The overall mechanical properties of a fibrous scaffold are a function of the mechanical properties of individual fibers and the organization of the fibers within the scaffold [169]–[172].

2.9.1 The overall scaffold mechanical property determination

Planar biaxial mechanical testing allows determination of bulk mechanical properties by studying the two-dimensional stress-state of fiber mats [104], [171], [173], [174]. It was

found that the bulk mechanical response of the mats can be modulated by altering the fiber architectures[173]. Fiber alignment, fiber density and fiber intersection density can tailor scaffold mechanical behavior[171], [173].

Stress-strain response of electrospun fiber mats can also be conveniently determined using conventional tensile testers [42], [175]–[178]. There are plenty of papers in the literature but fiber diameter, fiber density, fiber orientation and alignment renders fiber mats with different mechanical properties[42], [175], [176].

Since the overall properties of the mats depend on the assemblies and properties of individual fibers, it is crucial to determine the properties of individual fibers that make up the scaffold [179]. Fiber mats with desired properties for particular applications can be obtained by assembling the fiber mats with controlled fiber material, fiber size, fiber alignment and fiber density.

2.9.2 Single fiber property determination

Conventional tensile tests can be used to determine the mechanical properties of individual polymer fibers with diameters larger than 10 μm [179]–[181]. As the fiber diameter decreases into the nanometer range, this technique is no longer applicable, as it becomes difficult to mount the single fiber without damage or slipping from the grip, and to maintain perfect alignment of the fiber with the loading direction to avoid unwanted bending moments [182]. Moreover, there are also claims that the mechanical properties of fibers deviate from those of the corresponding bulk material as the diameter decreases into submicron or nanometer range [74], [79], [170], [183]–[185]. To overcome these obstacles and determine the mechanical properties of single electrospun nanofibers, numerous mechanical characterization techniques have been proposed by different researchers based on tensile, stretching, resonance excitation and bending of fibers [61]. One of the most popular approaches makes use of the high 3-D spatial resolution and subnanonewton force sensitivity of the atomic force microscope (AFM)[8], [61], [81], [99], [125], [149], [172], [182], [186]–[200]. AFM-based methods have been used to perform three-point bending, nanoindentation, nanotensile and resonance contact based mechanical testing of nanofibers.

2.9.2.1 AFM based fiber mechanics determination

The AFM has nano to piconewton force sensitivity and can detect Ångstrom-scale deformations. The working principle of the AFM is based on the interaction between the AFM tip and the sample surface upon or near contact. The determination of the mechanical behavior is done by measuring the bending of fiber when it is contacted by the AFM tip, by indentation of the fiber by the tip, or by tensile testing.

The three-point bending test is the most common bending test. Fibers were fabricated and deposited onto a substrate covered with holes or grooves so that a section of the fiber was freely suspended. The ends of the fibers were either fixed onto the substrate surface by electrostatic force or glued to the substrate by ion deposition or other techniques. The fiber was bent by the AFM cantilever by applying a small deflection along its suspended length while force-versus-displacement data were collected. The fiber's mechanical properties, such as Young's modulus, bending modulus, and shear modulus, can be obtained using beam-bending theory. Materials such as conductive polymer nanofibers, biological materials, biodegradable polymers, and carbon nanotubes have been tested using the AFM-based three point bending setup [81], [182], [189], [190], [194], [197], [200], [201]. While in earlier AFM studies of the mechanical properties of nanofibers, elastic moduli were calculated from deflection measurements at a single point at the center of the suspended fibers, finding the precise center point of the fiber could be challenging. Considering the positional accuracy of the scanner, the scanner calibration, and the microscope controller stability, multipoints measurements were later performed to help achieve higher accuracy and smaller uncertainty based on all the measurements along the suspended fiber length [61], [79], [87], [185], [191], [202].

Three-point bending using the lateral force arm is an approach that first deposits fibers on trenched wafers, with the suspended portion perpendicular to the trench, then the AFM arm was used to manipulate the fiber to determine its mechanical properties. With the AFM operating in the lateral force mode, the AFM tip was used to bend the fiber parallel to the trench length [8], [149], [172], [199]. The stress-strain properties of the fibers could be obtained by placing the AFM tip next to the midpoint of the suspended fiber, then using the tip to stretch the fiber laterally. Images or videos of the manipulation were

collected to determine the fiber size and tip travel distance. The lateral force measured was converted into the stress exerted on the fiber to generate stress-strain curves. The mechanical properties of the fibers, including their elastic modulus and ultimate tensile strength, were determined using these curves. This method allows a large range of fiber displacement with the possibility of manipulating the fibers until fiber failure. However, this method required the test fibers to be oriented perpendicularly to the trench to provide an easy geometry for data analysis, thus errors in these measurements are larger than those of other nanomanipulation methods, such as the scanning mode AFM bending test [149].

AFM-based uniaxial tensile tests have been performed on polymer fibers such as polyethylene oxide (PEO) [186]. The fiber was first isolated and one end was attached to a movable optical microscope and the other to the piezoresistive AFM cantilever tip. The AFM tip was used to measure the force exerted on the fiber as it was stretched by moving the microscope stage. Compared to other tensile tests on polymer nanofibers, this method directly manipulates a single fiber and does not require the perfect alignment of the fiber to the loading direction [61], [179], [182], [196], [203], [204]. However, the resolution is limited by the displacement resolution of the microscope stage and the force resolution of the AFM. The force sensitivity is also limited by the combination of different parts of actuators and the spring constant of the cantilever [61].

AFM indentation uses the AFM cantilever tip to push and probe the curved surface of fibers to determine their elastic and elastic-plastic behavior. However, due to the difficulty of probing the curved surface of the fibers and inaccuracy due to the effect of underlying substrate, this method has not been widely adopted for use on polymeric fibers.

Wang et al. used an AFM tip in contact mode to indent electrospun silk fiber [188]. Since the diameter of the fiber was > 800 nm and the tip of the AFM cantilever was < 10 nm, indentation was performed under the assumption that the measurements were free of substrate effects. However, due to the uncertainty in the cantilever stiffness and tip geometry, the absolute value of the modulus could not be determined. Instead, a reference

sample of epoxy with predetermined elastic modulus was indented using the same probe and parameters, by comparing the contact area and loading curves of the AFM tip on the epoxy and the silk fibers, the elastic modulus of the silk fibers could be calculated [188]. Tan et al. studied the mechanical properties of poly(L-lactic acid) (PLA) nanofibers and used the Hertz model to analyze the force-indentation data. The model treated the fiber as a cylinder and the AFM tip as a sphere. The elastic modulus was found to vary with the fiber diameter, with higher values for smaller-diameter fibers [205]. Other studies used AFM indentation test to determine modulus of fibers or spatial variation of the fiber cross-sections [61], [206], [207]. In each study, various assumptions had to be made in order to calculate the modulus using contact mechanical models. For example, several studies assumed there was no change of Poisson's ratio, spring constant and tip geometry during the indentation test [61]. Additional assumptions such as comparative tip radius and indentation depth, tip geometry and relative curvature between the tip and fiber surface need to be made to ensure accuracy and applicability of each model.

2.9.2.2 Non-AFM based fiber mechanics determination

A number of commercial uniaxial tensile testers have been used for single fiber or multiple fiber mechanical testing. Fiber that can be tested with these instruments are limited to a fiber diameter larger than 300 nm with a force resolution of 50 nN [61], [100], [179], [180], [182], [196], [208], [209]. To perform a tensile test on a single fiber, the fiber has to be isolated and properly mounted to prevent it from slipping out or breaking at the grips. As the fiber size becomes so small that directly mounting the sample becomes difficult, a frame that holds aligned fibers could be used to partition and isolate a single fiber for testing. The isolated portions that contained single fibers were chosen and cut to include only the desired fiber for testing. Tan et al. performed tensile tests on electrospun polycaprolactone (PCL) fibers with diameters of the range of 300 – 900 nm. They found no apparent correlation between the Young's modulus and fiber diameter, while the tensile strength and yield stress were size dependent [179], [182]. Chew et al. also used a commercial nanotensile testing system for electrospun PCL nanofibers [196]. Only specimens within the gauge length of 20 mm were used for testing, while specimens that failed near the edge of the mount were discarded. The

results showed that the Young's modulus and tensile strength increased with reduced fiber size. Both strength and stiffness were at least twofold higher than those of bulk PCL. However, the mechanical properties were plotted against the average diameter of a group of fibers rather than individual fiber diameter.

Due to the difficulties in handling the fine fibers, the smallest fiber that could be handled by the system was around 1 μm . Misalignment between the sample axis and loading direction also resulted in an unwanted bending moment that led to premature sample failure [182], and stress-strain curves reported in some of the studies are rather noisy. The sample preparation, partition, fixation, and manipulation of a single fiber can be time consuming and challenging. To better measure the fiber size and mechanical properties, the AFM has been suggested for its better sensitivity and higher resolution [61].

The resonance behavior of polymer fibers can be used to determine their mechanical properties. Exposing fibers to external stimuli, such as electric fields or chemical vapor, can be used for fiber excitation, and the resonance frequency measured in the system can then be modeled to obtain the fiber elastic modulus [210]–[212]. Boussaad et al. measured the mechanical properties of a polymer wire ($\sim 7\mu\text{m}$) made from nitrocellulose/toluene sulfonamide formaldehyde resin [210]. The polymer wire was bridged across the two prongs of a microfabricated tuning fork. As the wire was formed by stretching it has a built-in mechanical stress. When the wire is exposed to organic vapors, the stress in the polymer wire diminishes, and the changes in the resonance can be detected by the tuning fork. Cuenot et al. measured the resonance frequencies of AFM cantilevers in contact with various nanomaterials to obtain their mechanical properties [211], [212]. The mechanical resonance frequency was measured by modulating the cantilever deflection with an oscillating electric field applied between the sample holder and AFM tip. The change in the resonance frequency when the AFM tip touched the fiber was used to calculate the Young's modulus of specimens such as polypyrrole nanotubes.

3 Materials and Methods

3.1 Materials

The following materials (Table 3.1) were purchased for electrospinning and crosslinking the collagen fibers

Materials	Supplier
Hexafluoroisopropanol (HFIP) (105228, 1,1,1,3,3,3-hexafluoroisopropanol)	Sigma Aldrich, Oakville, ON, Canada
Poly (ethylene glycol) (PEG) (309028, 10 kDa)	Sigma Aldrich, Oakville, ON, Canada
Genipin (MW = 226.23g/mol)	Challenge Bioproduct Co
Anhydrous Ethyl Alcohol	Commercial Alcohols, Brampton, ON, Canada
Glacial acetic acid	Caledon Labs, Georgetown, ON, Canada

3.2 Isolation and purification of Type I collagen from rat tails

Type I rat tail collagen was extracted and purified with methods established previously [62], [213]. A detailed extraction procedure is presented in Appendix A. In short, a frozen rat tails were thawed in 70% ethanol for at least 30 minutes, scapular and forceps were used to dissect that rat tail skin and expose the white collagen fibers. Collagen fibers was mechanically extracted from rat tail tendons, incubated in sterile 0.0175 M acetic acid for 7 days at 4 °C with mechanical stirring. Undissolved collagen fibers were removed by centrifugation at 10,000 g at 4 °C for eight hours. The collagen solution was kept frozen at -20 °C to be lyophilized for collagen powder.

3.3 Collagen solution / shell solution

5 wt% type I collagen in HFIP was prepared by adding 84.2 mg of type I collagen from rat tail to 1 mL of HFIP, and vortex at room temperature for approximately 2 hours to dissolve the solution.

25 wt% collagen in 40 v/v% acetic acid was prepared by adding 340 mg of type I collagen from rat tail to 1 mL of 40 v/v% acetic acid, and dissolve overnight.

3.4 Core solution

Bovine Serum Albumin (BSA) solutions with concentrations of 10 mg/mL were prepared as previously established [62]. The solution was prepared by dissolving 100 mg of BSA in 10 mL of double distilled water to obtain a concentration of 10 mg/mL. In order to provide stability and to prevent mixing during the electrospinning process, poly(ethylene glycol) (PEG), with molecular weight of 10 kDa, was dissolved into the BSA core solution to achieve a final concentration of 200 mg/mL.

3.5 Electrospinning

3.5.1 Humidity control

The control of humidity was achieved using a custom built split flow chamber (Figure 3.1). A dry nitrogen stream was split into two. One stream flowed through a water bath where it was saturated with water vapor and the other stream remained dry. Humidity was controlled by controlling the ratio of the blending of these two streams. Humidity and temperature levels were constantly monitored using a humidity and temperature monitor (OMEGA Engineering Inc). A humidity control within the range of 5 – 65 (± 5) % at a temperature of 21 ± 2 °C can be achieved with our system.

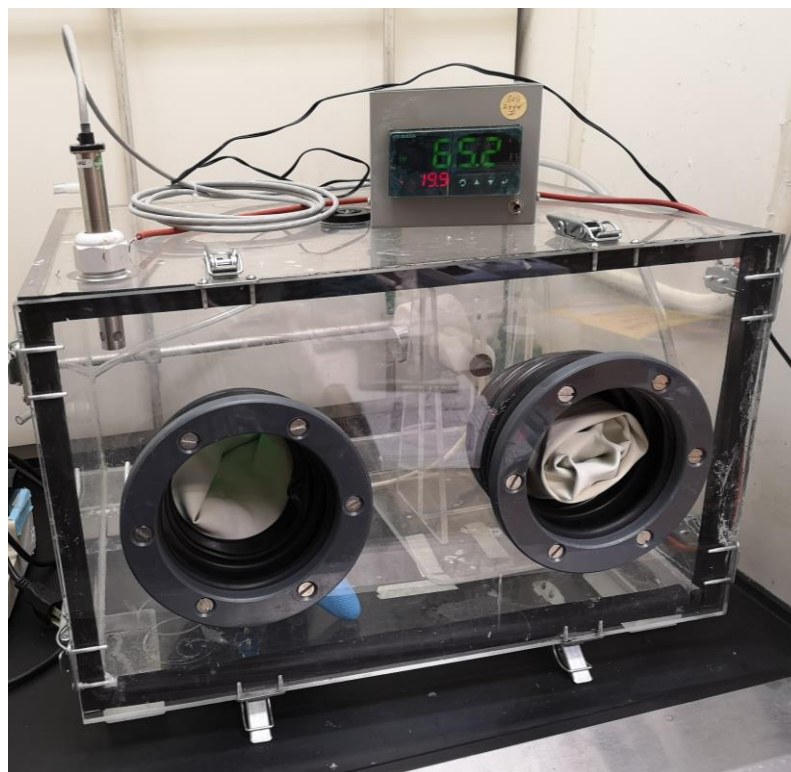


Figure 3.1. Humidity controlled chamber for electrospinning

3.5.2 Solid random fibers

5 wt% collagen in hexafluoroisopropanol (HFIP), 22wt% and 25wt% solution of collagen in 40v/v% glacial acetic acid (Caledon Labs, Georgetown, ON, Canada) were prepared for electrospinning. The solution was transferred into a 1 mL syringe, which was mounted on a syringe pump (Harvard Apparatus). The spinning solution was pushed through a blunt stainless steel needle (22G, Hamilton) at a constant flow rate of 0.15 mL/hr. A voltage of 20 kV was applied to the syringe needle relative to the grounded substrate placed at a distance of 20 cm from the needle tip. Collagen solution was electrospun at room temperature at controlled humidity ranging from 20 to 55%. Humidity level was recorded at the beginning and the end of each run using a humidity and temperature monitor (OMEGA Engineering Inc).

3.5.3 Aligned fibers

By replacing the stationary collector with a rotating mandrel, aligned fibers can be collected with a rotation speed of 7000 rpm and a mandrel diameter of 10 cm. Two layers aligned fibers can be obtained by placing one layer over the other orthogonally.

The mandrel was rotated by a variable speed DC motor which was powered by a 0 – 30 direct current voltage (DCV) source. The motor was capable of 10,000 rpm unloaded, but could only spin the mandrel at a maximum of 7000 rpm. To collect aligned fibers, the maximum rotation speed of 7000 rpm was used.

3.5.4 Core-shell fibers

With previously established procedure [62], core-shell polyethylene glycol (PEG)/collagen fibers can also be produced by using a core-shell needle. The dual syringe pump (Model 33, Harvard Apparatus), was used to control the flow rate of the core and shell solutions independently. The two solutions were fed concentrically into spinneret with the 20 gauge and 30 gauge needles for the outer and inner needles respectively. The shell solution (collagen) was pumped at 0.18 mL/hr and the core solution (PEG) was pumped at 0.06 mL/hr. The voltage source and electrode collector were the same as those used in electrospinning solid fibers.

3.6 Crosslinking

3.6.1 Genipin crosslinking

Genipin (Challenge Bio Products) crosslinking was performed in a solvent system consisting of ethanol and water. The concentration of genipin was 0.03 M in 3% water in ethanol and the reaction time was 3 days. Crosslinking was performed following procedures previously established [89], [129]. The electrospun collagen fibers were placed in vials containing 20ml of the crosslinking solution and placing the vials in a 37 °C shaker bath to speed up the crosslinking reaction. The lids of the vials were not screwed tightly allowing solution exposure to oxygen in the air. After the crosslinking period, all samples were stored in pure ethanol for further tests.

3.6.2 Green light and Rose Bengal crosslinking

For green light crosslinking, 25 wt% collagen solution in 40 v/v% acetic acid was prepared with 0.1 w/v% Rose Bengal. Electrospinning was carried out as described in Section 2.2. To distribute the Rose Bengal suspension evenly, the resulting collagen solution was vortexed before electrospinning.

To crosslink the fibers, electrospun collagen fibers were immersed in 99.5% isopropanol (anhydrous) or pure ethanol and irradiated with a light wavelength at 520nm, at an intensity of 7 mW/cm² for 22 hours. The UV-Vis spectra of Rose Bengal in water, isopropanol and ethanol are shown in Appendix D. The intensity of the light was measured with a light meter (LI-COR LI-190R). The light intensity is a function of distance and the relationship between light intensity and distance is shown in Appendix C. After crosslinking, the scaffolds were dried in vacuum overnight to remove isopropanol residue.

3.6.3 Ion beam implantation

Nitrogen (N⁺) ion beam was generated using the 1.7 MV tandetron accelerator. Fibers on silicon wafers were mounted on the sample holder with a 1 μm thick tantalum (Ta) foil placed 2mm in front of the samples. Ion beam treatment was performed with the samples placed vertically at room temperature in ultra-high vacuum (~ 10⁻⁸ torr). The beam current was around 100nA for a total dosage of 8 x 10¹⁵ ions/cm² and 4 x 10¹⁵ ions/cm².

3.7 Characterization

3.7.1 Scanning electron microscopy (SEM)

Fiber size and morphology were observed using a high-resolution scanning electron microscope (LEO 1540). The fibers were not sputter coated and were kept intact by using a low accelerating voltage of 1 kV.

3.7.2 Transmission electron microscopy (TEM)

A Philips CM 10 transmission electron microscope with a digital camera was used to obtain images of core-shell collagen fibers structure. Collagen core-shell fibers were

directly electrospun onto a copper TEM grid with 600 meshes. An accelerating voltage of 60 ~80kV was used to characterize the core-shell structure.

3.7.3 X-ray photoelectron spectroscopy (XPS)

The elemental chemical composition and chemical structure of the collagen sample surface was analyzed by an X-ray photoelectron spectroscopy (XPS) system from Kratos Axis Ultra. The 210 W Al-K α monochrome source tested the samples in the hybrid mode with 90° take-off angles. The pass energy of the survey scan was 160 eV and the high-resolution scan was 20 eV. Data analysis and multiplex fitting was performed by CasaXPS software.

3.7.4 Fluorescence Microscopy

A compound fluorescence: Imager Z1 with multichannel fluorescent imaging capability was used to obtain fluorescence images of the stained cells. Cell cytoskeleton and cell nuclei were imaged with AF 568 and DAPI channels respectively.

3.7.5 Imaging processing (ImageJ)

3.7.5.1 Fiber diameter

ImageJ was used to determine fiber diameter. The scale bar on the image was first measured in pixels and calibrated into actual length/pixel. Fiber diameters were then measured in pixels and converted into nanometers. For each sample, four images were acquired and 30 fibers were randomly selected for each image for measurement. To measure the fiber diameter, a line was drawn on the fiber perpendicular to its axis. The length of the line was automatically converted into micrometers by the software. The diameter distribution of a fiber mat was determined from 120 randomly chosen fibers on four SEM images captured randomly inside a 1 cm² area. The data was then statistically analyzed using Origin 8. The statistical significance of data sets were evaluated using a one-way analysis of variation (ANOVA) included in the software.

3.7.5.2 FFT analysis

ImageJ and Photoshop were used to carry out 2D FFT analysis of the aligned fibers. Photoshop was used to crop unnecessary data that may obscure the FFT analysis from the image (e.g. scale bar and imaging parameters). ImageJ was then used to generate the FFT frequency plot, and an oval-profile plug-in was used to sum the pixel intensities along the radius for angle of the projection (0 - 360°). This data was then imported into Origin 8 to construct a plot of intensity versus angle.

3.8 Mechanical Testing

3.8.1 Sample preparation

All fibers were deposited on custom-designed silicon substrates with various width and 2 μm depth. Trenches were fabricated by photolithography and reactive ion etching at the Western Nanofabrication Facility (London, Canada), using a custom-designed mask produced at the University of Alberta NanoFab facility (Edmonton, Canada).

Atomic force microscopy experiments were performed using a multimode AFM with a NanoscopeIIIa controller (Bruker). DNP-S10 silicon nitride cantilevers (Bruker) with nominal spring constants of 0.12 N/m were used for AFM imaging and mechanical testing. Actual spring constants were measured using installed software based on the thermal noise method. Measurements were performed at a temperature of approximately 32 °C at the sample position, and the humidity was kept at 35% by using a AtmosBag (Aldrich). The spring constant of each cantilever was checked periodically throughout the experiments.

Using a microscope (Olympus SZ-ST5) attached to the AFM optical head, the precise locations of suitable fibers suspended over gaps were identified. The targeted areas were then imaged in contact mode. The scanning position and size were adjusted to include the entire suspending portion and a sufficient fraction of the supported substrate of each target fiber to facilitate subsequent mechanical testing (Figure 3.2).

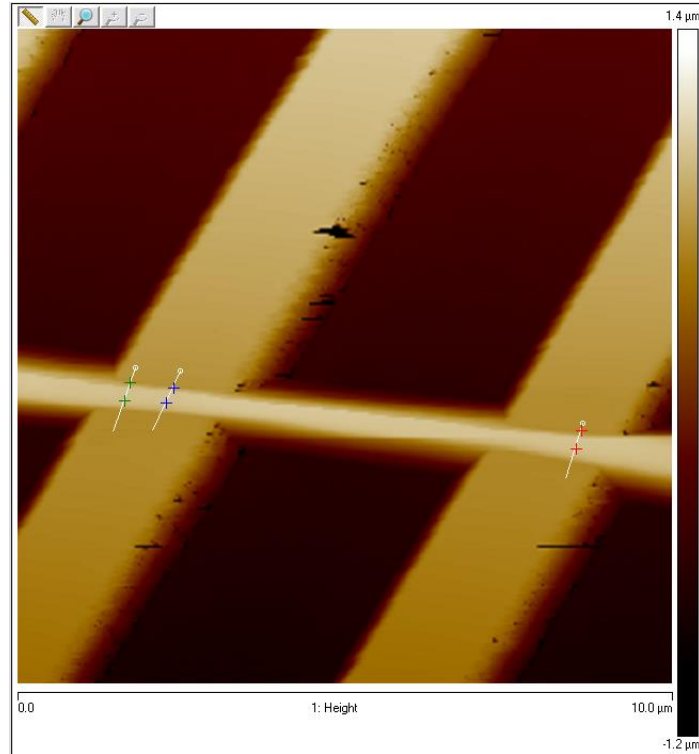


Figure 3.2 AFM height image of fibers suspended over trenches with sufficient fractions of the support substrates allowing fiber height measurements and substrate mechanical testing.

3.8.2 Force volume measurement

AFM force volume mode was used to perform the mechanical testing as previously established [79], [191], [193]. A force (F) was applied to the sample at multiple points along each suspended fiber as the piezo moved the sample upward toward the AFM tip. The deflection of the cantilever (Δy) as a result of the vertical displacement of the sample (Δz) was acquired to obtain force curves. The ramp size which is the vertical displacement of the piezo was set between 1 to 2 μm and the trigger threshold, which is the maximum deflection of the cantilever) was set to 150 – 200 nm for all fibers.

3.8.3 Contact AFM force plots

In contact AFM force plots, the horizontal axis demonstrates the vertical displacement of the probe relative to the sample, and the deflection of the cantilever is plotted on the vertical axis. An example of a force plot is shown in Figure 3.3.

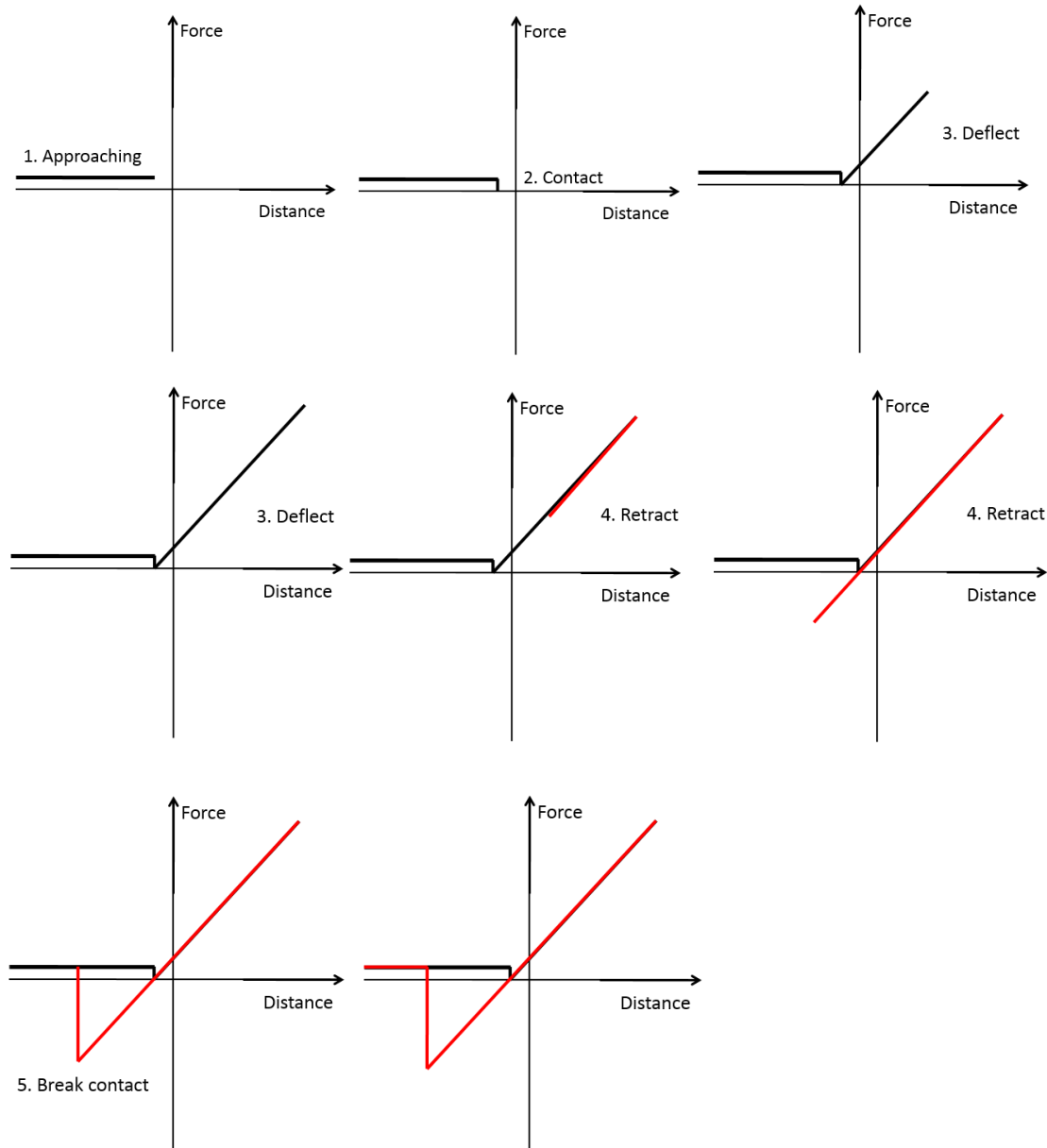


Figure 3.3. Deflection of the cantilever vs. sample

Each force plot provides significant information about sample-tip interactions. As the tip approaches the sample, it is attracted to the surface due to various forces such as electrostatic and / or surface tension. From the graph, direction of 1 indicates the piezo extends and the tip descends, however, there is no contact with the sample yet. As the tip is getting close to the surface, the tip is attracted to the sample by the forces near the surface, indicated by the dip shown in 2. As the contact between the tip and surface was established, further extension of the piezo results in the cantilever bending upward as its tip

presses into the surface. After the cantilever reaches the trigger threshold shown in 3, the piezo would retract and this causes relaxation of the cantilever until tip forces are in equilibrium with surface forces shown in 4. As piezo starts retracting the cantilever keeps bending downward due to the attractive force from the surface keeping the tip in contact with the sample surface. During retraction, when the tip eventually breaks free of the attractive forces on the surface, the cantilever rebounds sharply upward to its equilibrium position, this sudden movement is represented by 5. After which, the piezo continues retracting and while the tip remains in its equilibrium position as there is no further contact with the sample.

Force curves reveal useful information about the elasticity of the material the cantilever interacted with. Cantilever deflection for a given downward tip movement is an indication of the material's elasticity. For hard materials, the cantilever will experience larger deflections compared with softer samples.

3.8.4 Determination of the elastic modulus

Mechanical bending tests were performed as previously described [191], [193]. This technique is performed by measuring force curves on a grid of positions using force-volume mode. Each force curve records cantilever deflection versus the vertical sample displacement. Specific points on the contact image were selected for force curve collection. Approximately 900 points were selected to acquire force curves over an area containing the entire suspended portion of the fiber and parts of the rigid substrate (Figure 3.4). The force curves were acquired with ramp sizes of 0.8-1.4 μm at a ramp rate of 1.03 Hz. For each force curve, the maximum cantilever deflection was limited to 250 nm.

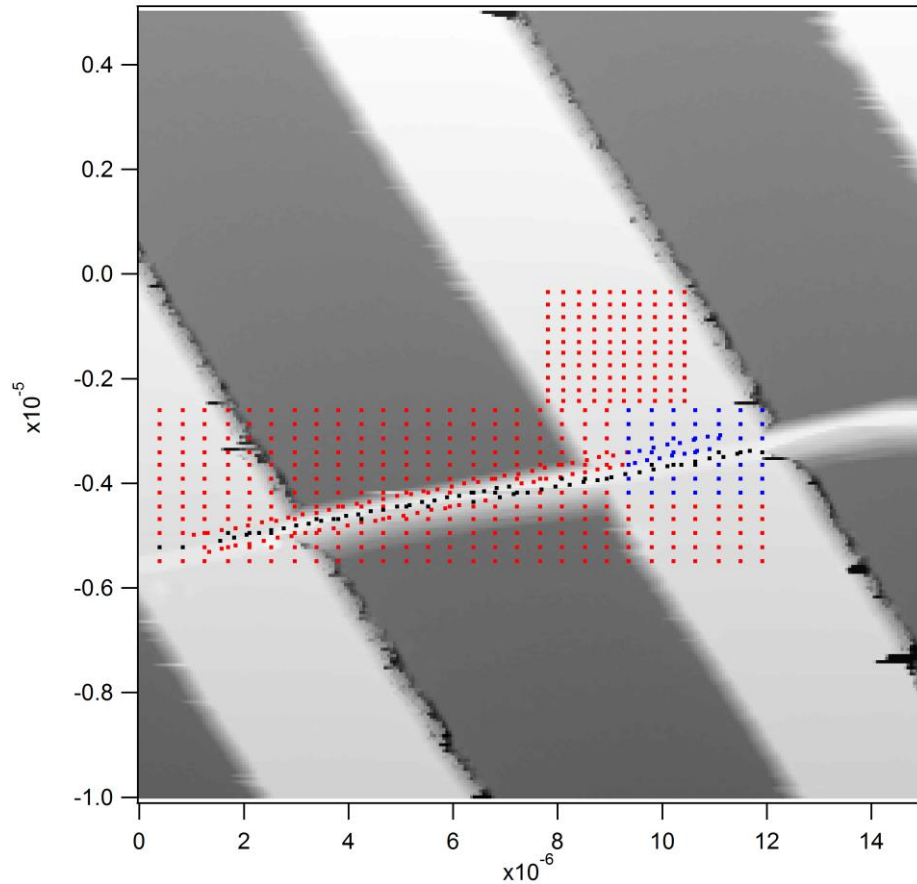


Figure 3.4. AFM height image of fibers suspended over trenches with points that were selected to acquire force curves. (black points: points selected as being on fibers; blue points: points on the rigid substrate). Other measurement positions (red points) are not used in the analysis, but serve to verify the registration between the image and grid of force curves

Fibers with diameters in the range of 60-300 nm and suspended lengths of 5.1-7.2 μm on trenched silicon substrates were chosen for AFM mechanical testing.

The diameter of a fiber was determined from the height profile of the AFM image on the supported portion of the fiber. The diameter was measured at three different locations along the supported segments, and the average and standard deviation were calculated.

3.8.5 Analytical models

3.8.5.1 Pure bending model

The simplest beam model, Euler-Bernoulli model, was used to analyze the experimental data. A fiber with suspended length L is subjected to an applied force F at a distance a from one of its ends. The deflection $\delta(a)$ of fiber is given by

$$\delta(a) = \frac{F}{3EI} \left[\frac{a(L-a)}{L} \right]^3 \quad (1)$$

where E is the Young's modulus of the fiber and I is the moment of inertia ($\frac{\pi d^4}{64}$ for a circular cross section).

The vertical sample displacement Δz must equal to the sum of the cantilever deflection Δy and fiber deflection $\delta(a)$. Since the force applied by the AFM cantilever tip is governed by $F = k \Delta y$, where k is the spring constant of the cantilever, equation (1) becomes

$$\Delta z = \Delta y \left[1 + \frac{k}{3EI} \left(\frac{a(L-a)}{L} \right)^3 \right]. \quad (2)$$

Therefore the slope of a force curve along a suspended fiber is expected to be

$$\frac{dy}{dz} = \left[1 + \frac{k}{3EI} \left(\frac{a(L-a)}{L} \right)^3 \right]^{-1}. \quad (3)$$

Young's modulus E of the fiber can be determined by fitting this equation to the force-curve slopes measured as a function of position a along the fiber.

Igor Pro (WaveMetrics) with custom analysis routines was used to analyze force data. Force curves on the fiber and the substrates were first identified (Figure 3.4). Because the deflection signal is initially uncalibrated, a histogram of the slopes on the rigid substrate or fiber supported by the rigid substrates was used to determine a calibration factor on the assumption that the cantilever deflection on the rigid substrate must equal to the piezo displacement after contact is achieved (i.e., $\frac{dy}{dz} = 1$). The slopes of the force curves along

the suspended fiber were calibrated using this factor and were plotted along the fiber as a function of position, as shown in Figure 3.5. The resulting curve was fit to Eq. 3 to determine Young's modulus E of the fiber. The agreement between the experimental data and the derived curve for a clamped-beam model demonstrates that the multi-point mechanical test with the Euler Bernoulli model is valid for the collagen fibers. It is also assumed that the fibers are firmly attached to the surface at the supporting substrate so that fiber displacement on the substrate can be neglected. If there is slippage of cantilever on the collagen fibers, the force-displacement curves would have sudden jumps and the slopes vs. displacement cannot be fitted with Euler-Bernoulli model. In this case, the particular fiber would not be considered for mechanical property determination. Similar observation was reported previously [193].

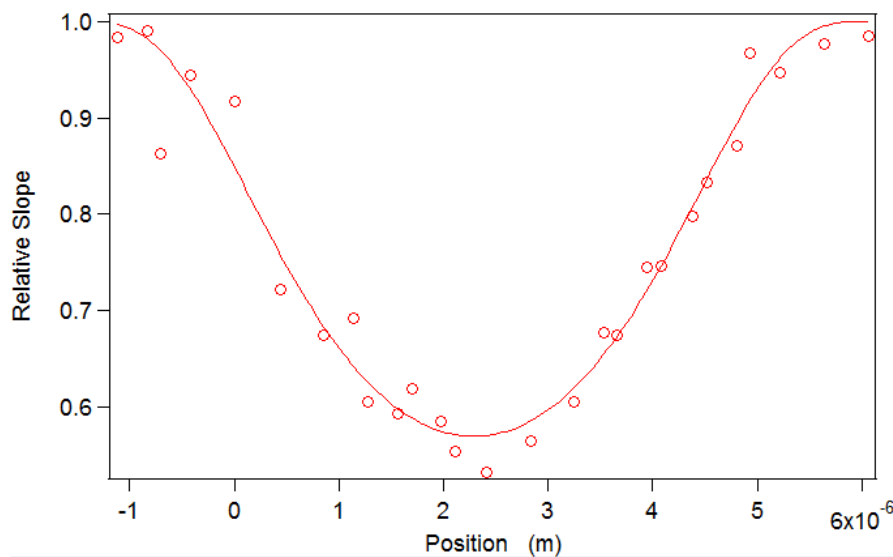


Figure 3.5. Relative slopes of the force plots and the curve fit obtained from multiple points along the fiber

3.8.5.2 Deflection due to Tension

For AFM three point bending tests, the deflection of the fiber is due to tensile, compressive and shear deformations. When the aspect ratio is much greater than one, shear stress is negligible in comparison to bending stress[193]. This is the assumption

used in the Euler- Bernoulli model and was adapted for use in most studies[81], [125], [182], [186], [197], [200], [209], [214], [215].

Heidelberg et al. showed that tensile stress due to elongation of a deformed fibers, has to be taken into account when the fiber displacement is comparable or larger than its radius[216]. The study demonstrated that in some cases an apparent increase in Young's modulus at small diameters (50nm – 100nm) was an artifact of models when the effects of fiber stretching was neglected.

Building on the Heidelberg model, the existence of an initial tension in the fibers and a tension due to the elongation of fibers were taken into account by Hudson et al. [191]. Hudson et al. considered the case in which a constant initial tension T_0 was applied to the fiber. It was found that for small diameters fibers under this condition, even in the small-deformation limit, axial tension due to both the applied force and a pre-existing strain has a significant effect on fiber deflection.

3.9 Cell culture on electrospun collagen fibers

IMR-90 human fetal lung fibroblasts were obtained from Center for Translational Cancer Research (London, ON). Fibroblasts were plated on T 25 cell culture flasks at a density of 4×10^5 cells. The cells were cultured in minimal medium containing growth media (RPMI 1640. 1x + 10% FBS (foetal bovine sera)). The cells were incubated at 37° in a humidified atmosphere of 5% CO_2 :air. For maintenance of cell cultures, the medium was changed every 72 hours. Fibroblasts were passaged between 24 to 26 times for this study. The following procedure is used to seed and culture fibroblasts on crosslinked electrospun collagen samples:

1. Immerse samples in 70% ethanol for 30 minutes for sterilization, and then leave the samples to air dry for 15 minutes
2. Remove the cell culture flask with fibroblasts from incubator and aspirate the growth media from the fibroblasts
3. Add 1ml of penicillin streptomycin (Pen Strep) into 100ml of growth media (RPMI 1640. 1x + 10% FBS (foetal bovine sera)) and gently stir and mix the solution

4. Open vacuum, use a glass pipette to aspirate the media out of the flask (tilt the flask so no cells are being touched by the pipette tip)
5. Use the 5ml plastic pipette to add 1mL of trypsin into the cell flask and gently stir to detach the cells from the bottom (wait for a minute or two for the cells to detach)
6. Use 10mL plastic pipette to add 10mL growth media (RPM1 1640. 1x + 10% FBS) to flush the cells into single detached cells
7. Use 10mL plastic pipette to transfer 9mL of cell solution into a centrifuge tube
8. Take 500 μ L of cell solution into 19.5mL of PBS to make a 40x dilute solution
9. Use Beckman Coulter Z1 Coulter particle counter to count the cells (two times, each count gives cell counts in 0.5mL of solution), calculate the cell count per mL
10. Disposed the counted cells into waste bottle
11. Dilute the cell solution accordingly using the growth media, place ~10000 cells/well into a 24 wells plate
12. Add cell solution containing ~10000 cells into each well containing

To apply the fluorescent label (staining) to the cells for confocal and fluorescence image, the following procedure was used:

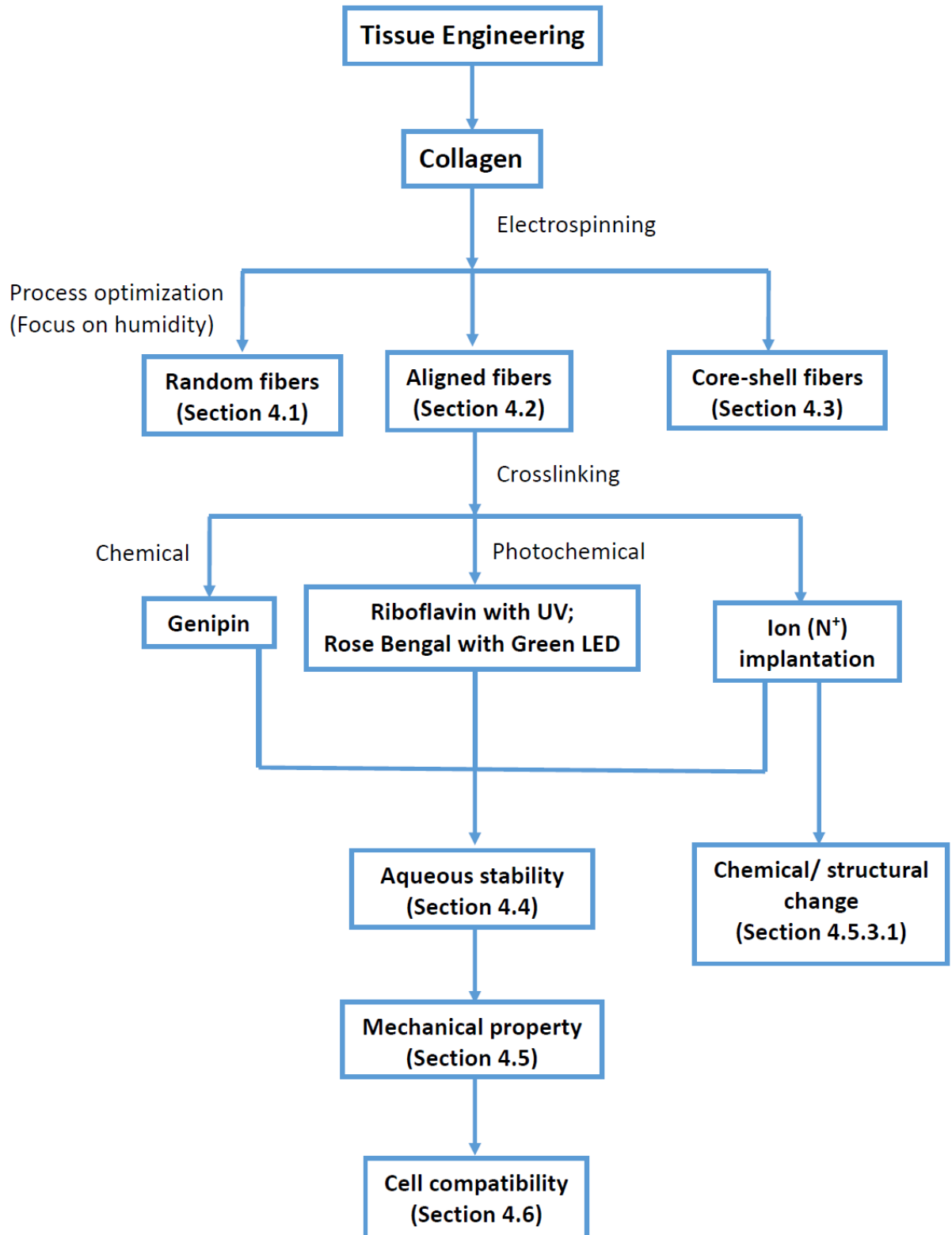
1. Fix the cells using 4 wt% of paraformaldehyde for 45 minutes.
2. Rinse in PBS three times with PBS (5 minutes each).
3. Wash the samples with 0.1wt% Triton X-100 in PBS for 10 minutes to permeabilize the cell membranes for fluorescent stain.
5. Rinse the samples in water for 1 minute
6. Rinse the samples in PBS twice (5 minutes each).
7. Apply Universal SNIPER Blocker for 10 minutes under aluminum foil
8. Dilute 1:100 Alexa 568 in antibody diluting solution, apply the antibody and incubate for 30 minutes in covered humidity chamber.
9. Rinse off excess antibody in PBS twice (5 minutes each).
10. Dilute DAPI 180 μ M stock solution into 1:300 solution and stain the samples in dark for 2 minutes.
11. Rinse the samples in PBS twice (5 minutes each)
12. Mount the samples with 1 drop of Pro-Long Gold Anti-Fade mounting media.

4 Results

This chapter starts with a fundamental study on the production and process optimization of collagen fibers using the electrospinning technique. The effects of humidity on fiber size and morphology attribute to the hydrophilic property of collagen and solvent systems are investigated (Section 4.1). To demonstrate the electrospun fibers can mimic the native tissue structure and morphology, aligned electrospun collagen fibers were produced and compared to rat tympanic membrane (Section 4.2). Core-shell collagen fibers were also produced to demonstrate possible bioactive molecule encapsulation for drug delivery applications (Section 4.3).

As spun collagen fibers are not stable in an aqueous environment including cell culture media. Chemical, photochemical and physical crosslinking treatments were applied to enhance fiber aqueous stability (Section 4.4). Subsequently, the change of fiber mechanical properties due to crosslinking were measured using AFM (Section 4.5). In-vitro cell compatibility of the crosslinked collagen fibers was assessed using human lung fibroblasts (Section 4.6).

The following flow-chart illustrates the outline of this chapter.



4.1 Effect of humidity on fiber size and morphology

To produce fibers with uniform morphology and within a particular diameter range, electrospinning processing parameters such as voltage, fiber to collector distance, solution concentration and solution flow rate were studied thoroughly and the results were in consistent with previous studies [67], [84], [89]. It was found that rat tail type I collagen produces bead-free fibers with circular cross-section at a concentration of 20 – 25 wt% in 40 v/v% aqueous acetic acid solution with a 20 cm distance at 20 kV.

On the contrary, the environmental parameters of the electrospinning process are generally less studied. The environmental parameters for fiber formation include temperature and humidity. Between these two parameters, as most experiments are carried out at room temperature, the effect of humidity on fiber production is easier to control. As both collagen and acetic acid are hydrophilic, we hypothesize that environment humidity would have impact towards fiber formation. Thus, we investigated the effects of humidity on collagen fiber size and morphology by changing the humidity at a constant temperature.

Figure 4.1 shows the change of fiber morphology and size with different humidity levels at 22 ± 2 °C. At low humidity levels (20 % and 25 %), large fibers presented ribbon-like morphologies. With increasing humidity, more fibers with a cylindrical cross-section were obtained.

Figure 4.2 indicates that for fibers produced with 25 wt% solution, the average fiber diameter decreases with increasing humidity. The increasing humidity also resulted in a significant reduction in the mean diameter distribution.

To demonstrate that other parameters (i.e. solution concentration) can also affect fiber size and distribution, a lower solution concentration of 22 wt% was used at a constant humidity of 35 % to produce fibers with reduced average fiber diameter and fiber size distribution (the red point in Figure 4.2). Similar effects of solution concentration on fiber diameter have been observed by others [9], [26], [23], [46], [50], [29], [35], [49] .

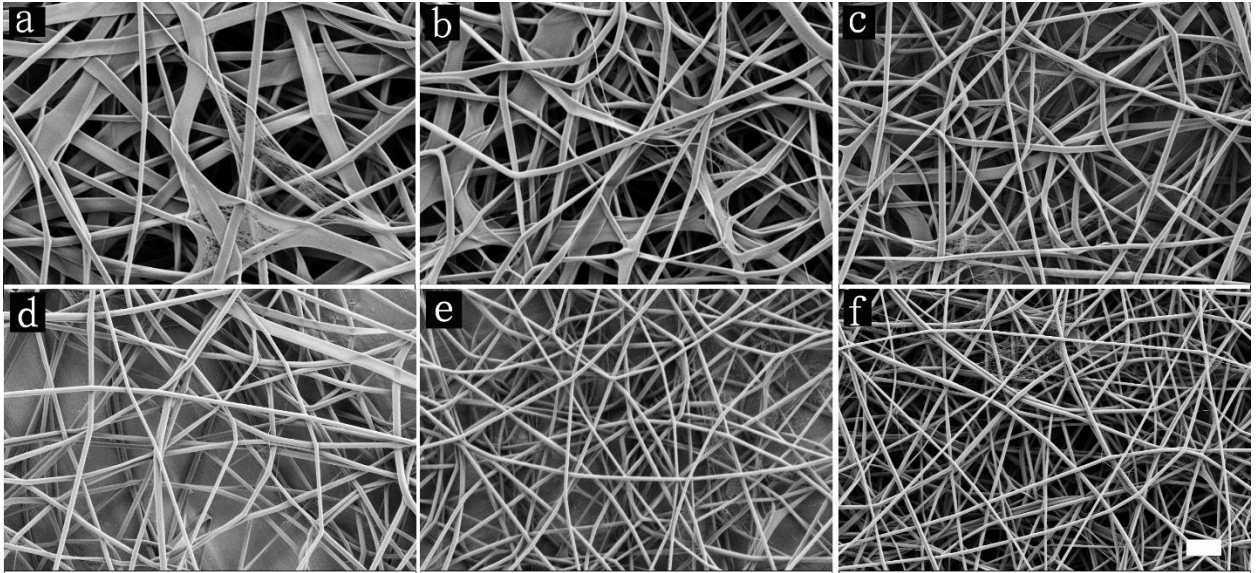


Figure 4.1 SEM images of electrospun collagen fibers spun with 25wt% collagen solution in relative humidity (RH) levels of (a) 20%, (b) 25%, (c) 30%, (d) 35%, (e) 40%, (f) 45%. Scale bar: 1 μ m.

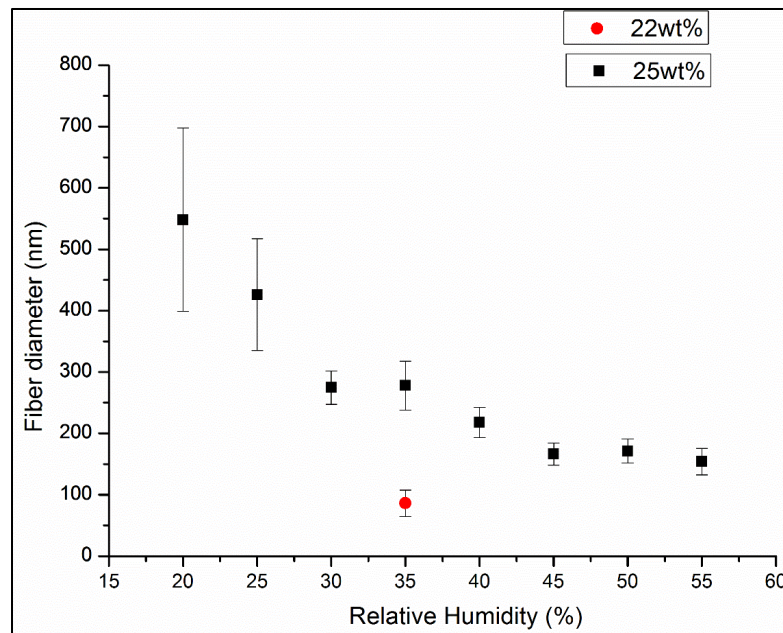


Figure 4.2. Plot of average fiber diameter as a function of relative humidity for a 25 wt% collagen solution (black squares with standar deviations indicated by error bars). Average fiber diameter and fiber size distribution can be further reduced by reducing the solution concentration (red circle).

A similar study of the effect of humidity on electrospun collagen fibers was performed with 5 wt% collagen in HFIP. As seen in Figure 4.4, the dependence of fiber morphology and size on humidity was similar to that seen with 40 v/v% acetic acid as the solvent system. Figure 4.3 shows the change of fiber size and morphology with different humidity levels at room temperature. All SEM micrographs were taken at 5000 X magnification with 3.6 mm working distance (WD) at 1 kV. The low accelerating voltage was used to avoid the use of conductive coatings in SEM to ensure true fiber visualization and fiber size determination. At low humidity (20 % and 25 %), collagen fibers are flat ribbon like and some with dog-bone shaped cross-section due to fast evaporation of the solvent and fiber collapsing (arrows in Figure 4.3a). As humidity level increases, more fibers with cylindrical cross-section were obtained. Increasing humidity level also resulted in a reduction of the fiber diameter distribution (Figure 4.4).

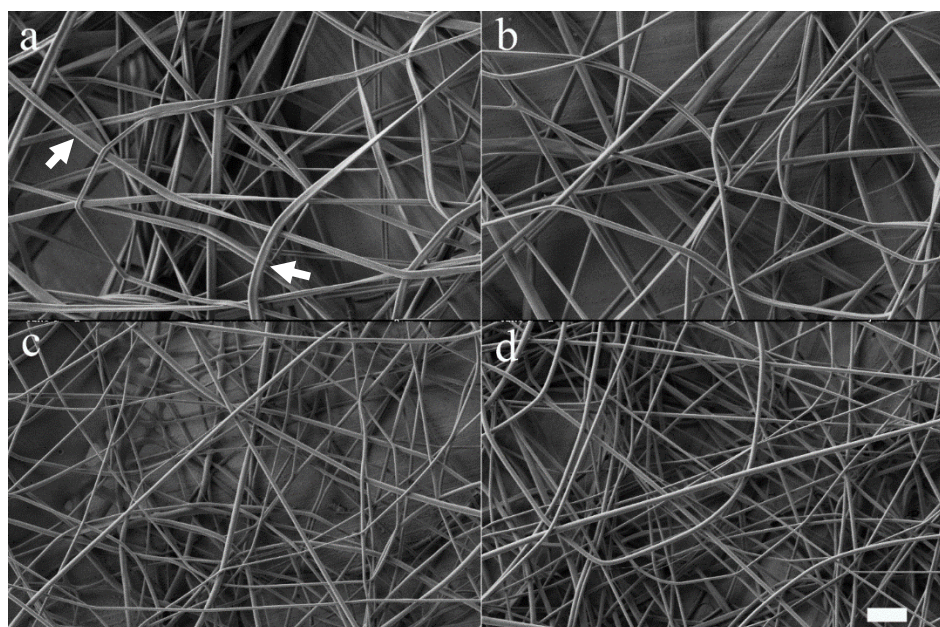


Figure 4.3. SEM images of electrospun collagen fibers spun with 5 wt% collagen solution in HFIP at relative humidity (RH) levels of (a) 25%, (b) 30%, (c) 35%, (d) 40%. Scale bar: 2 μ m.

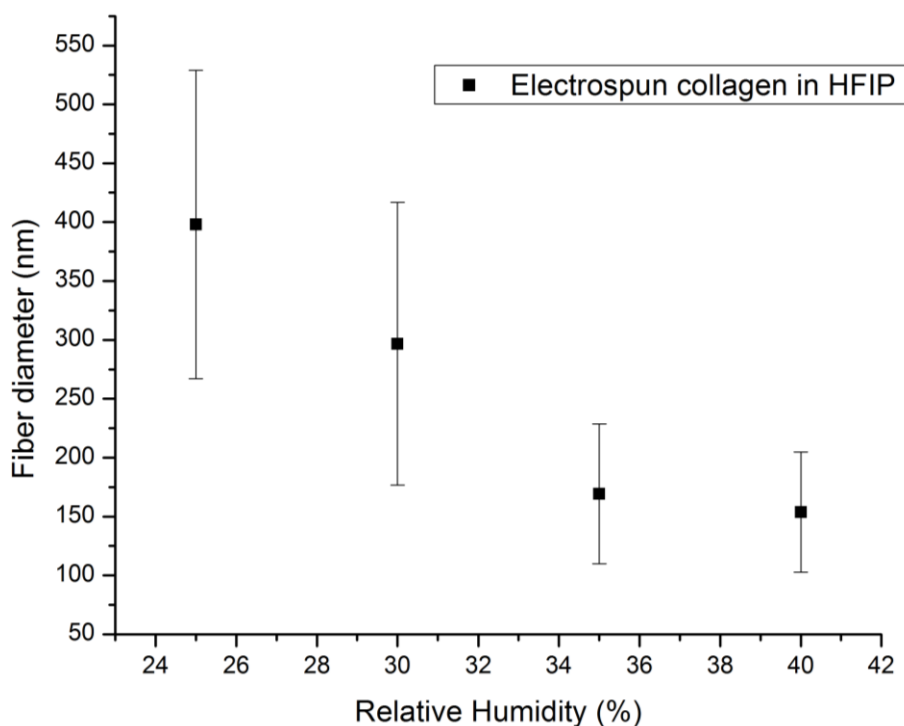


Figure 4.4. Plot of average fiber diameter as a function of relative humidity for a 5 wt% collagen solution in HFIP.

The variation of fiber size and morphology with humidity may be attributed to the hydrophobicity of the solution and change of solution viscosity during the spinning process. In the current study, the solvent system 40 v/v% acetic acid and HFIP are water miscible. While collagen is water soluble, the presence of humidity will decrease collagen solution jet concentration. At higher humidity, solvent evaporation is slower due to the higher water vapor content in the air, so the solution jet remains viscous longer. During which time the electrostatic force allows fiber stretching and thinning. As a result, the solid fiber formation will take longer with smaller fiber diameter. At low humidity, solvent evaporation rate increases, leaves jet stream a shorter whipping and thinning time, results a much faster formation of the dry fibers with larger fiber diameter.

4.2 Other factors affecting fiber morphology and size

Electrospinning is a complicate process involving several parameters. Viscosity of the polymer solution must be high enough to allow polymer entanglement to form fibers

rather than broken beads, but low enough to allow the solution to be extruded as a jet from the spinneret. Thus, only a narrow range of concentration allows the formation of electrospun fibers. Reducing solution concentration to 20wt% collagen in 40 v/v% acetic acid, electrospun fibers can still be formed (Figure 4.5). At low humidity levels (20 – 25 %), flat ribbon fibers formed due to high solvent evaporation rate, fast outer layer formation, and collapse of the fiber center (arrows in Figure 4.5 a). Increasing the humidity allows formation of cylindrical free-standing fibers, however, at higher humidity levels, signs of fiber fusion due to retarded solvent evaporation was observed (arrows in Figure 4.5 c and f).

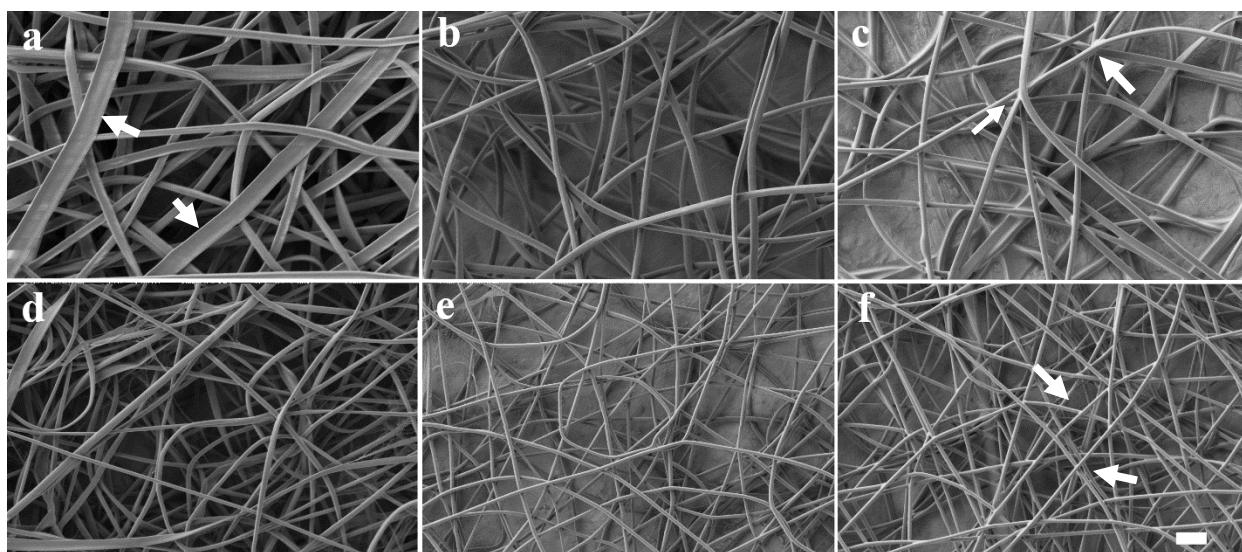


Figure 4.5. SEM images of electrospun collagen fibers spun with 20 wt% collagen solution at a flow rate of 0.1 mL/hr in relative humidity (RH) levels of (a) 20%, (b) 25%, (c) 30%, (d) 35%, (e) 40%, (f) 45%. Scale bar: 2 μ m.

This solvent retardation on fiber fusion is even more noticeable with increased solution flow rate. By increasing solution flow rate from 0.1 mL/hr to 0.15 mL/hr, fewer flat ribbon fibers were seen at low humidity levels (Figure 4.6 a), but fiber fusion was observed at 30 % (Figure 4.6 c arrows). Still higher flow rates resulted in more

cylindrical fibers, larger average fiber size and more fiber fusion.

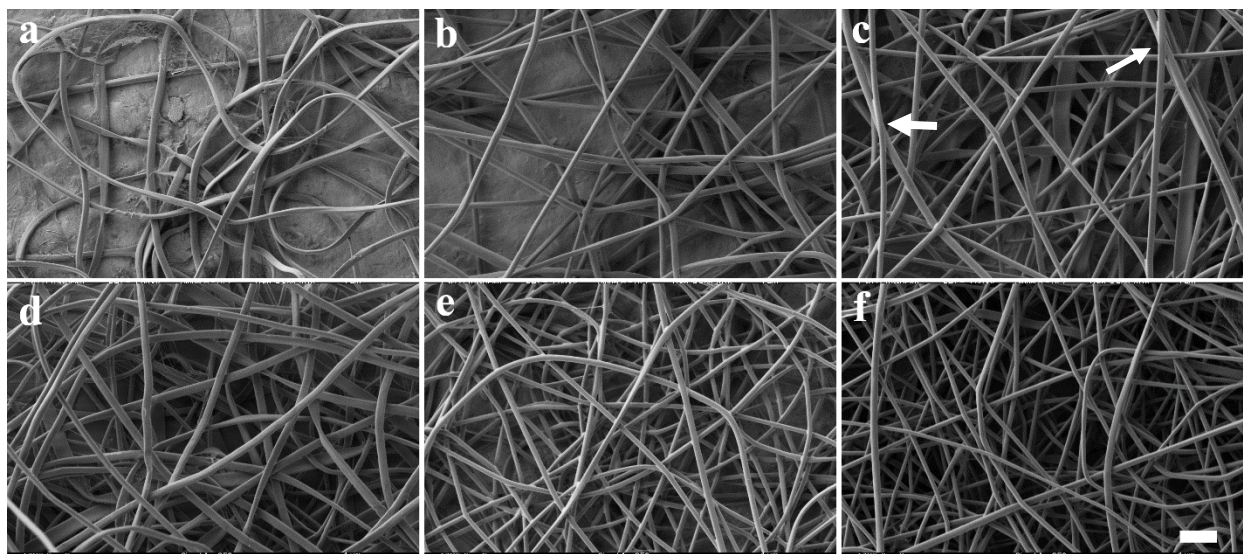


Figure 4.6. SEM images of electrospun collagen fibers spun with 20 wt% collagen solution at a flow rate of 0.15 mL/hr in relative humidity (RH) levels of (a) 20%, (b) 25%, (c) 30%, (d) 35%, (e) 40%, (f) 45%. Scale bar: 2 μ m.

By lowering the solution viscosity through reducing collagen concentration, beaded fibers with a mixture of fibers and beads were obtained (Figure 4.7a). Further lowering the solution concentration to 15 wt% resulted in insufficient inter-chain entanglements to form electrospun fibers. Rather, as spun fibers broke up into droplets due to the effects of surface tension. Therefore, with a 10 wt% collagen in 40 v/v% acetic acid solution collagen beads were electrospayed on the collector. Figure 4.7b shows some of the beads formed through the process. These beads were mostly fused together due to incomplete drying process.

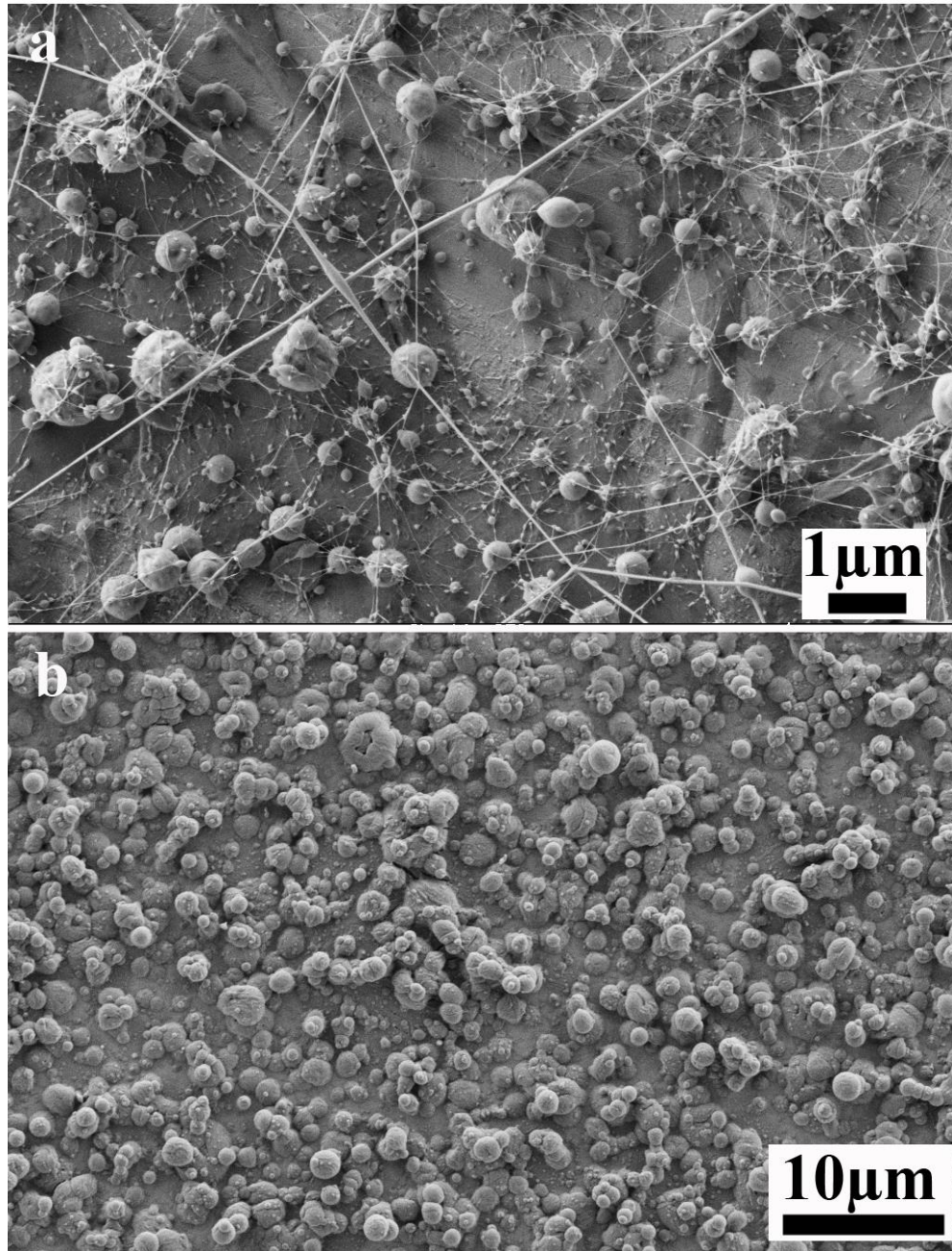


Figure 4.7. SEM micrograph of (a) beaded fibers with 15 wt% collagen solution and (b) electrospayed beads with 10 wt% collagen solution.

4.3 Fiber alignment to mimic tissue structure

Aligned collagen fibers were electrospun with a rotating mandrel at 7400 rpm, a flow rate of 0.15 mL/hr, and an applied voltage of 20 kV. The needle-collector separation distance was 18 cm. The spinning mandrel collector electrode had a diameter of 4.5 cm and all fibers were collected at 30 %. SEM images of one random and one aligned samples are shown in Figure 4.8. Frequency plot of the 2D FFT spectrum were generated to measure the relative scaffold anisotropy and identify the principle axis of fiber orientation (Figure 4.8c and d).

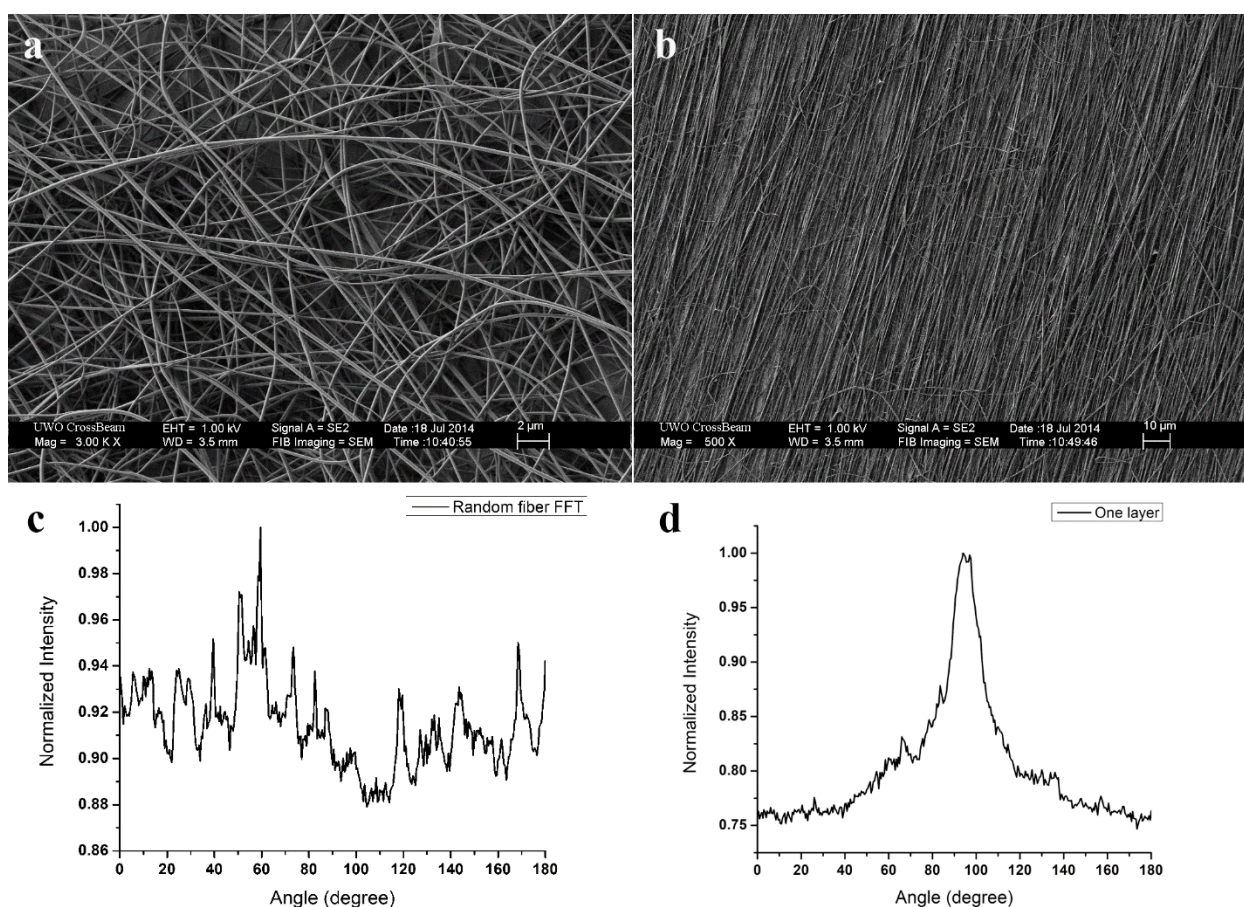


Figure 4.8. (a) random electrospun collagen fibers; (b) aligned electrospun collagen fibers; frequency plot of 2D FFT of (c) random fibers, (d) aligned fibers.

The 2D FFT plot generated from random electrospun collagen fibers shows several peaks (Figure 4.8 a and c). These peaks are caused by a greater disorder or a high degree of

randomness, representing there is presence of fiber aligned in all direction axis. In comparison, the fibers spun with rotating mandrel generated highly aligned fibers as indicated by the 2D FFT frequency plot shows one single narrow peak. This one peak represents the major axis of fiber alignment. The alignment peak is narrow and sharply delineated with minimum peak shoulders, indicating nearly uniform fiber alignment.

To demonstrate that the organized structure of electrospun collagen fibers can mimic the natural tissue, two layers of orthogonally aligned fibers were compared to natural tympanic membrane [218]. SEM micrographs of both structures were taken and analyzed via 2D FFT. The resulting plots give a good comparison of the degree of alignment as well as the relative position of the two layers in the double layer structure (Figure 4.9). Both the tympanic membrane (Figure 4.9 a) and the electrospun scaffold (Figure 4.9 b) possess two distinct peaks offset by 90° , which indicates the orthogonal relationship between the two layers. The overlap of the two spectra indicated the fiber alignment and assemblies mimic the microanatomy of the natural tympanic membrane (Figure 4.9 c).

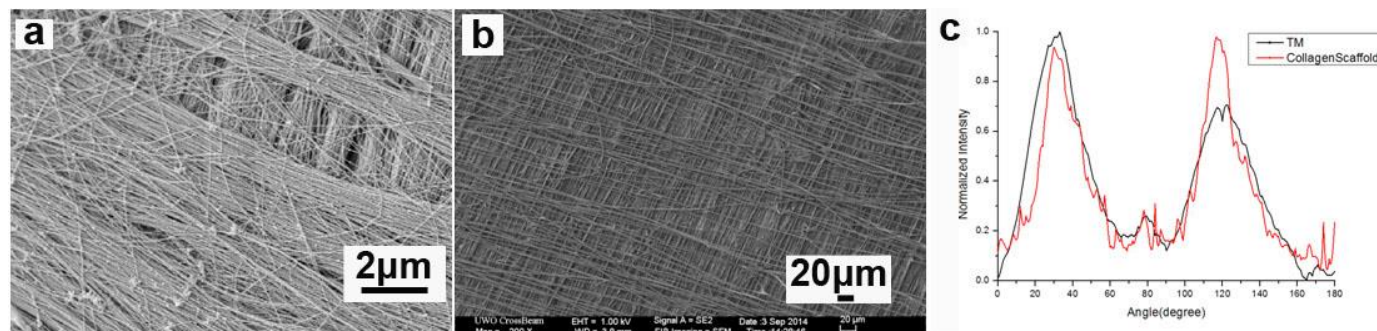


Figure 4.9. (a) SEM image of rat tympanic membrane; (b) SEM image of a two-layer electrospun structure of aligned fibers; (c) frequency FFT plot of fiber alignment for (a) and (b)

4.4 Core-shell fiber fabrication

To create core-shell structures for possible encapsulation of therapeutic agents (e.g., drugs, protein, DNA) coaxial electrospinning was carried out to deliver two polymer solutions independently through a coaxial needle. The process setup and optimization for core-shell preparation has been studied previously [62]. The optimal condition found for electrospinning collagen fibers in HFIP was applied for collagen solution using acetic

acid as solvent system. The core solution was polyethylene glycol (PEG) in 85% ethanol as described previously.

The resulting fibers were imaged using bright field transmission electron microscope (TEM) (Figure 4.10 a and b), core-shell structure of the collagen fibers can be seen in Figure 4.10 a and b with a darker core and lighter shell. From previous studies, structures with a darker core and lighter shell indicates a well-defined core-shell structure [62]. Figure 4.10 a shows a consistent core and shell diameter along the fiber, indicating a uniform distribution of the core-shell material throughout the spinning process. The sharp boundary between the core and shell structure suggests minimum back mixing occurred between the miscible core and shell solutions.

The fibers were stabilized by crosslinking with genipin as the crosslinking agent following an established procedure we developed [62]. Following that, fibers were immersed in water for one day to leach out the core material. The structure of the resulting hollow fibers was imaged using bright field TEM as shown in Figure 4.10 c and d. Due to the removal of core material, the electron beams disintegrate the polymers at 60 kV during TEM imaging and the fiber cross-section can be seen in the TEM images.

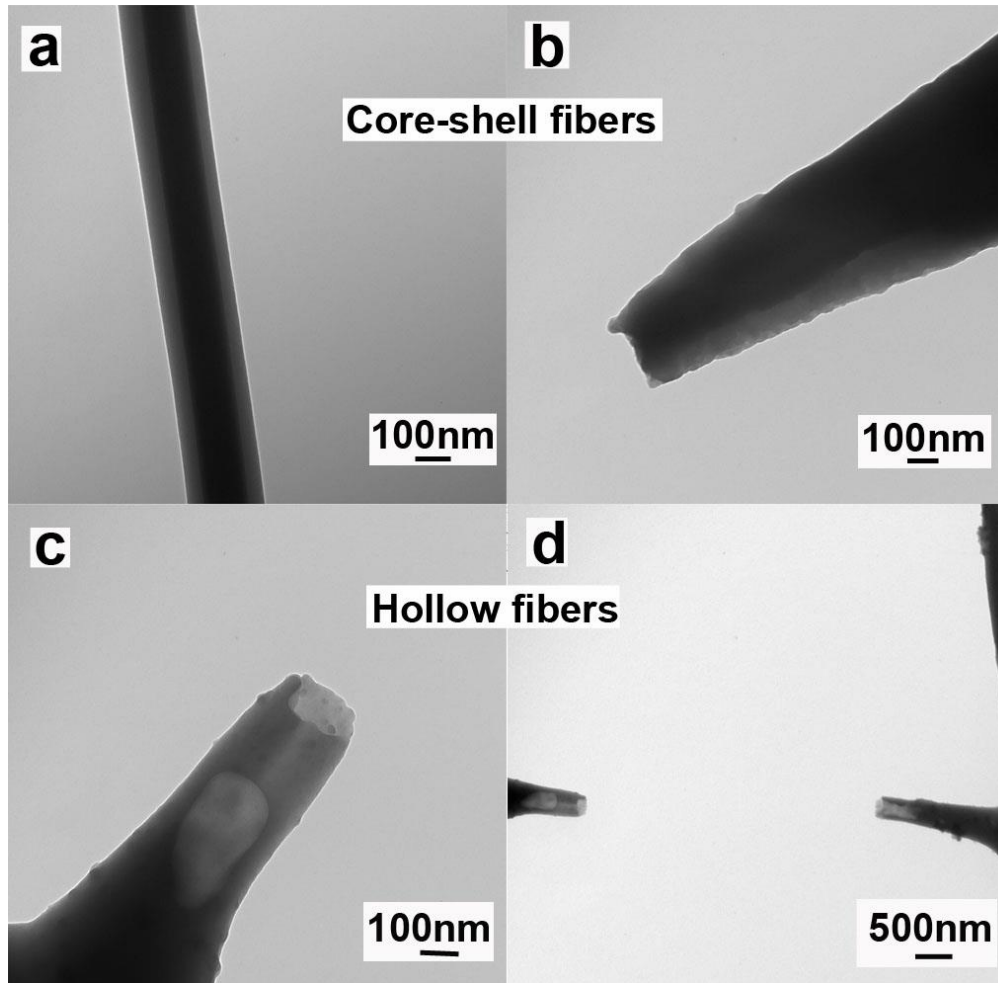


Figure 4.10. TEM images of coaxial electrospun PEG-collagen fibers. (a) and (b) core-shell structure with lighter shell indicating collagen and darker core indicating PEG with collagen; (c) and (d) hollow structure with collagen shell only.

Using electrospinning, collagen fibers with size, morphology and organization mimicking that of the native ECM can be obtained. However, recent studies have shown that collagen does not retain its native structure after the vigorous electrospinning process and becomes water soluble [6], [14], [25], [82]. Subsequent crosslinking methods have been introduced to stabilize the collagen to control its degradation rate and enhance its stability.

4.5 Effect of crosslinking on fiber size, morphology and stability

As the electrospun collagen fibers are not stable in aqueous environment, fibers need to be stabilized for further applications. Figure 4.11 shows as spun fiber morphology before and after fibers were immersed in water for 5 minutes. Before water immersion, as spun fibers are cylindrical and free-standing; after these fibers are exposed to water, they lost their fibrous morphology and gelled into a film.

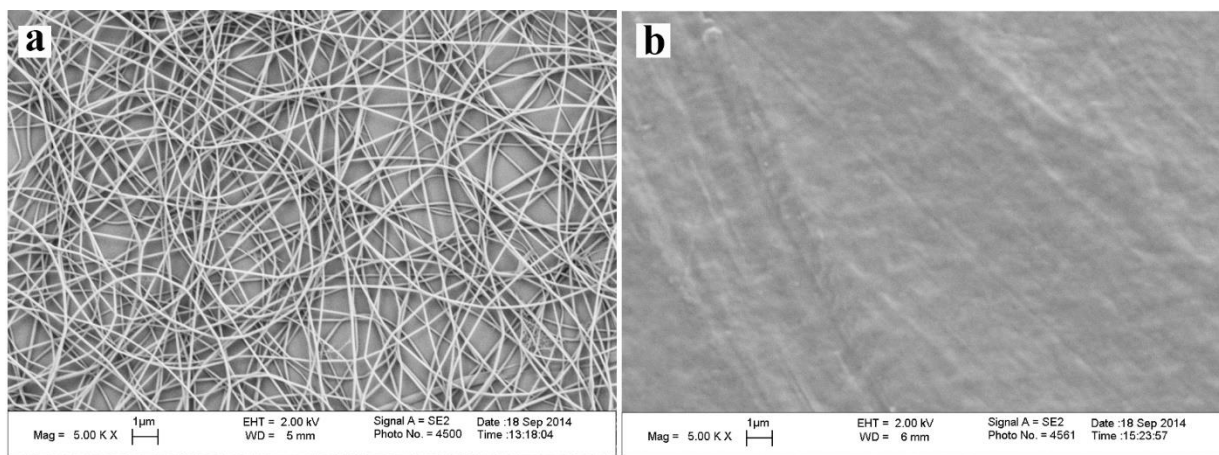


Figure 4.11. (a) as spun collagen fibers; (b) fibers exposed to water and gelled into film.

4.5.1 UV-riboflavin

In this study, UV crosslinking of electrospun collagen fibers was carried out with riboflavin incorporated as a photoinitiator to promote free radical generation and improve crosslinking. Riboflavin incorporated collagen solution was electrospun into free standing cylindrical fibers as shown in Figure 4.12 a. However, a closer look at the fibers reveals features with irregular crystal shapes attributed to undissolved riboflavin particles dispersed in the collagen solution and spun with fiber as a suspension (arrows in Figure 4.12 b and c). As riboflavin is only active in soluble form, to maintain a sufficient amount of soluble riboflavin to produce free radicals for crosslinking, ethanol was used as a solvent system to dissolve the riboflavin while maintaining the fibrous morphology of electrospun collagen fibers.

Several crosslinking durations from 30 min to 600 min at 30 mins intervals were used to determine the optimum exposure time for UV crosslinking. The desirable crosslinking time should be long enough to allow the formation of free radicals which initiate chemical reactions, while short enough to avoid prolonged exposures that might result in an increasing probability of collagen being denatured.

As pure ethanol would absorb moisture from the air water content over time, without carrying out the experiment in a drybox, prolonged exposure resulted in fibers sticking to each other after crosslinking (Figure 4.12 c). Although molecular sieves were later added to the ethanol to absorb the water molecules, the fibers after crosslinking still show similar structure with fibers sticking to each other. Since the overall fibrous morphology was maintained after the crosslinking, these fibers were used to determine crosslinking efficiency.

Based on water stability tests, it was found that the optimum UV crosslinking time is around 180 mins. Compared to other samples for which most of the fibrous features vanished after exposure to water, fibers crosslinked by 180 min of UV illumination remained relatively stable. SEM imaging of the fibers after exposure to water for one hour (Figure 4.12 d-f) show that the overall fibrous features were partially retained. However, the fibers are no longer cylindrical nor free standing, but were flattened with a porous structure.

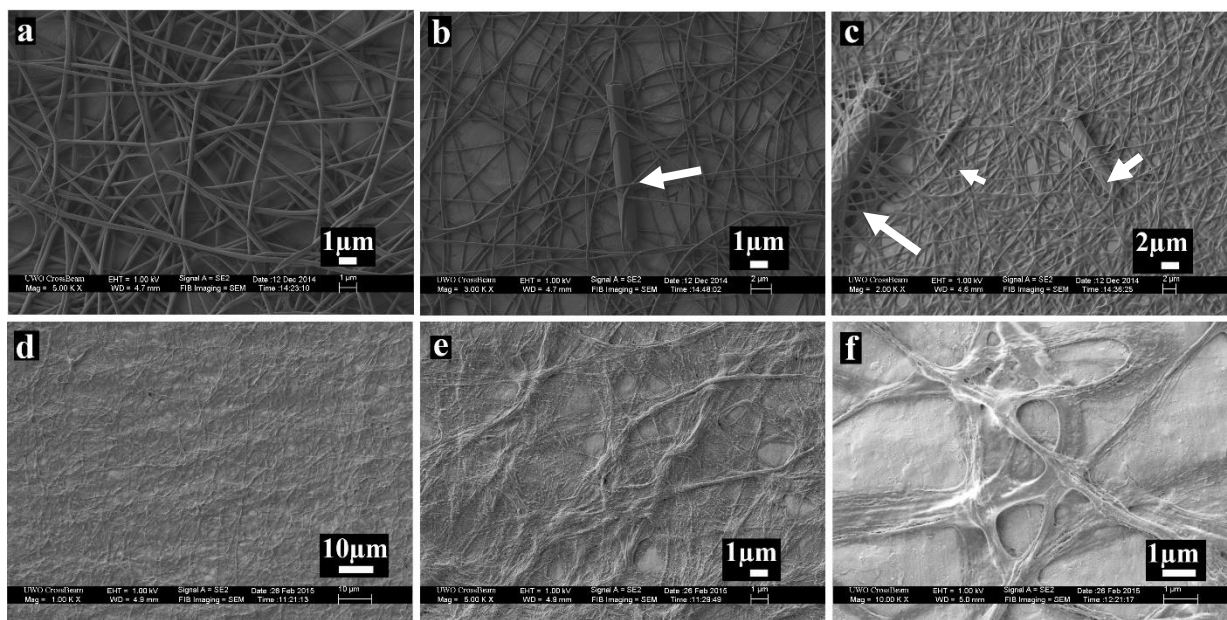


Figure 4.12. (a) riboflavin encapsulated electrospun collagen fibers; (b) pieces of riboflavin encapsulated inside the fiber showing a larger fiber size; (c) fibers crosslinked in pure ethanol for 60 mins; (d)-(f) UV crosslinked fibers after immersed in water for one hour.

4.5.2 Green light and Rose Bengal

Green light was used in combination with Rose Bengal to investigate the crosslinking efficiency and fiber stability. As dissolved Rose Bengal has a characteristic color that acts as a shielding layer for light penetration [162], to improve the crosslinking efficiency, Rose Bengal was incorporated into the solution above the solubility limit (0.1 w/v%). The excess amount Rose Bengal ensures the crosslinking proceed with saturated soluble Rose Bengal in the solvent system.

Figure 4.13 a and b show SEM micrographs of electrospun collagen fibers before and after incorporating Rose Bengal particles into the fibers. Arrow in Figure 4.13 b shows a Rose Bengal particle encapsulated in a fiber. To dissolve the Rose Bengal particles in the fibers at a slow rate while maintaining the fibrous structure and morphology of the electrospun fibers, pure ethanol and pure isopropanol were used as solvent systems for LED crosslinking. Rose Bengal incorporated fibers were immersed in either pure ethanol

or isopropanol and exposed to green light illumination for various durations ranging from 10 mins to 3 days, with 22 hours crosslinking shown to result most stable fibers. Figure 4.13 c to e show SEM images of Rose Bengal incorporated electrospun collagen fibers crosslinked in ethanol solution for 22 hours followed by soaking in water for 24 hours. As can be seen, the fiber diameter increased, while became porous with a rough surface morphology. The porosity and roughness can be attributed to the dissolution and degradation of the fibers during the 24 hours exposure to water. In contrast, when isopropanol was used as the solvent system, the same crosslinking time produced fibers that were more stable with a non-porous structure (Figure 4.13 f-i). Although a certain degree of roughness was still seen.

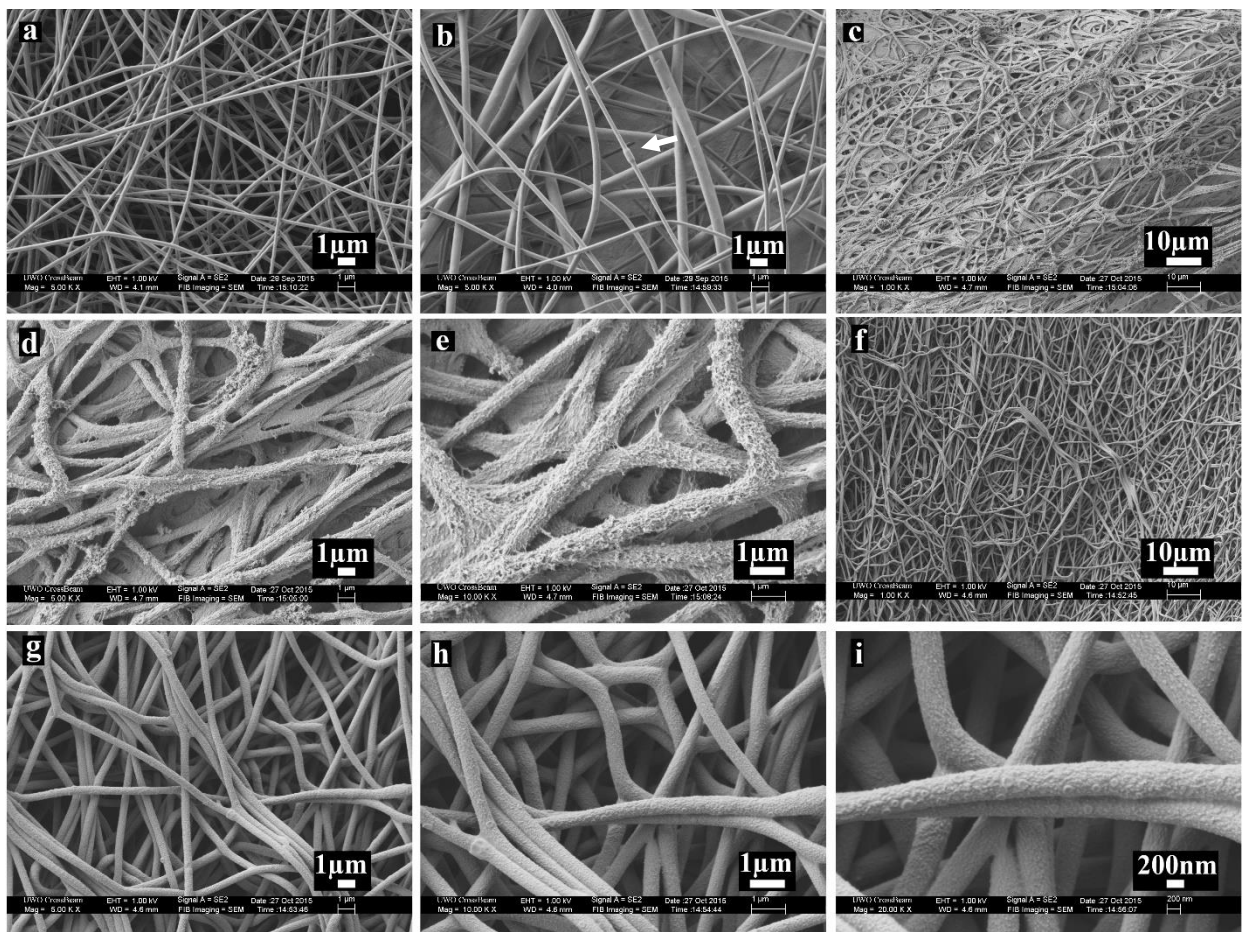


Figure 4.13. SEM micrographs of electrospun collagen fibers containing the photoinitiator Rose Bengal. (a) – (b) as-spun fibers, some of which show irregular shapes indicating encapsulation of Rose Bengal particles. (c) - (e) 24 hours water test

for fibers crosslinked in pure ethanol for 22 hours. (f) – (i) 24 hours water test for fibers crosslinked in isopropanol for 22 hours.

The collagen fibers crosslinked using Rose Bengal in isopropanol were further tested for stability by immersing the fibers in water for 7 days. Figure 4.14 shows the fibers after 7 days water exposure. As can be seen, the overall scaffold structure was maintained, but the fibrous morphology and porosity was lost with all layers of fibers collapsed into a flat mat.

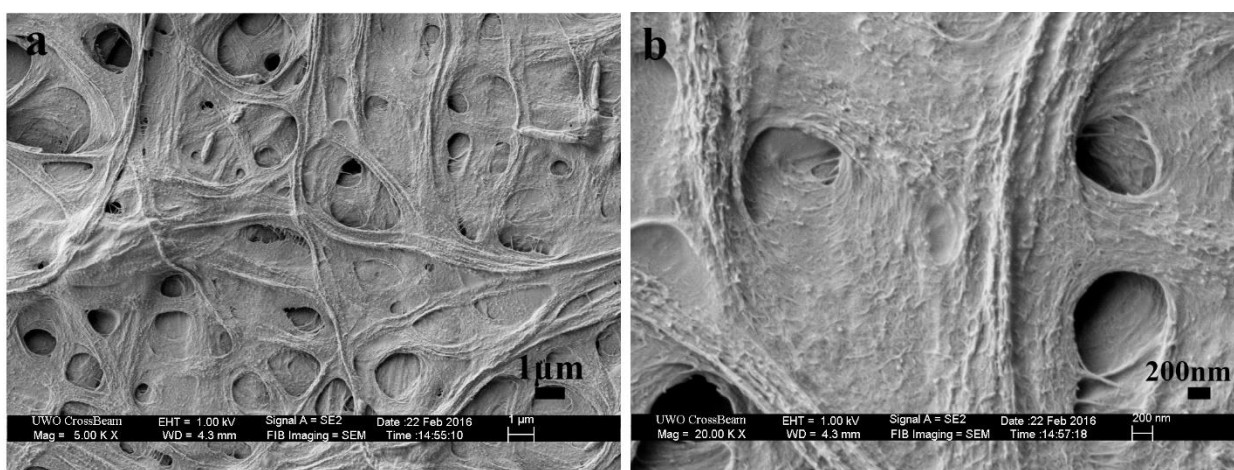


Figure 4.14. SEM micrographs of Rose Bengal incorporated electrospun collagen fibers crosslinked in pure isopropanol for 22 hours and immersed in water for 7 days.

4.5.3 Ion beam implantation

It has been demonstrated by previous studies that ion beam treatment has the potential to selectively induce intrinsic modifications to the mechanical and chemical properties of electrospun fibrous scaffolds [79], [195]. Following procedures described previously, we converted a high energy mono-energetic ion beam generated from a conventional high energy ion beam into a low, poly-energetic beam using a tantalum foil as an energy diffuser.

The energy of the beam is reduced and its distribution is broadened through the collision/straggling process of the ions with the TA atoms in the foil, providing for a widened implantation zone. At the same time, because of the wider distribution of the ions, the energy related damage was minimized to the near surface.

As the electrospun collagen fibers are protein based and more fragile than other polymers, two lower ion dosage levels were used to implant the fibers. Since previous studies showed nitrogen implantation introduced nitrogen based functional groups, which are presented at the sites for cell adhesion, thus nitrogen ion was used to impart fiber stability. The conditions used in preparing the samples are as indicated in Table 4.1.

Table 4.1. Implantation conditions for three samples

	Condition 1	Condition 2	Condition 3
Dosage	8×10^{15} ions / cm^2	4×10^{15} ions / cm^2	4×10^{15} ions / cm^2
Current	800nA – 900 nA	800nA – 900 nA	200 – 300 nA
Cooling method	Air cool	Liquid nitrogen	Liquid nitrogen
Implantation time	~ 6 hours	~2.5 hours	~ 8 hours
Aperture	$3 \times 3 cm^2$	$3 \times 3 cm^2$	$1 \times 1 cm^2$

Table 4.2. Average fiber diameter and standard deviation before and after ion treatment.

Sample	Average fiber diameter (nm)	Standard deviation (nm)
As spun	228.8	38.0
Condition 1	104.9	26.4
Condition 2	145.9	37.3
Condition 3	118.9	32.6

As indicated in Table 4.2, the average fiber diameter before treatment was around 230 nm. Treatment with a high ion dosage (8×10^{15} ions/cm²), average fiber diameter reduced by half to 105 nm. A lower dosage (4×10^{15} ions/cm²) resulted in a lower degree of fiber diameter reduction, with a final average fiber diameter of 145 nm. Surprisingly, reduced current did not further decrease fiber reduction, but produced fibers with an average diameter of 120 nm. Based on the fiber size, condition 2 resulted in fibers with the least size reduction and carbonization. The reduction of average fiber diameter after ion implantation is consistent with previous studies using the same treatment performed on other materials [79].

The diameter distribution of the electrospun collagen samples was determined from 120 randomly chosen fibers on four SEM images captured randomly on the sample. The SEM micrographs and histograms along with best-fit normal distributions are shown in Figure 4.15.

From SEM images, condition 3 with a lower dosage delivered at a lower current over a smaller aperture resulted in fiber fusion, while samples with larger aperture (condition 1

and 2) maintained free standing fibers. Comparing conditions 1 and 2, higher dosage resulted in smaller fibers with more fragile fiber fragments. The broken ends of fibers can be seen in Figure 4.15 d arrow.

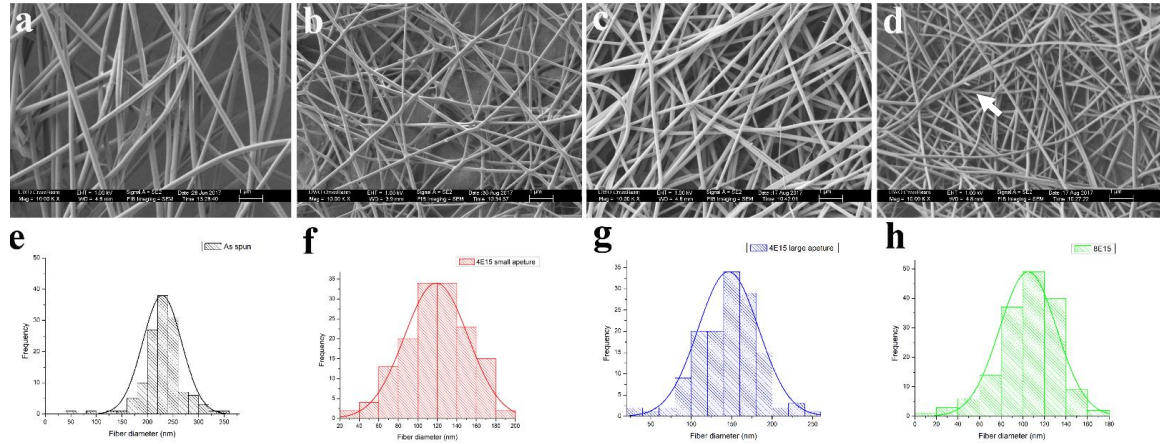


Figure 4.15. SEM micrographs of electrospun collagen scaffolds (a) as-spun, (b) ion implantation with 4×10^{15} ions/cm², 1×1 cm² aperture and 200nA current, (c) ion implantation with 4×10^{15} ions/cm², 3×3 cm² aperture and 900nA current, (d) ion implantation with 8×10^{15} ions/cm², 3×3 cm² aperture and 900nA current; (e)-(h) histograms of fiber diameter distribution for samples in (a)-(d) with best-fit normal distributions.

The fibers crosslinked with condition 1 and 2 were further tested for stability by immersing the fibers in water for 7 days. Figure 4.16 shows the fibers after 7 days water exposure. Not only the overall scaffold structure was maintained, there was no sign of fiber swelling or change of fiber morphology. For the condition 1, average fiber diameter reduced to 96.1 ± 11.2 nm, while for the lower dosage implantation condition 2, the average fiber diameter reduced to 127.8 ± 18.2 nm.

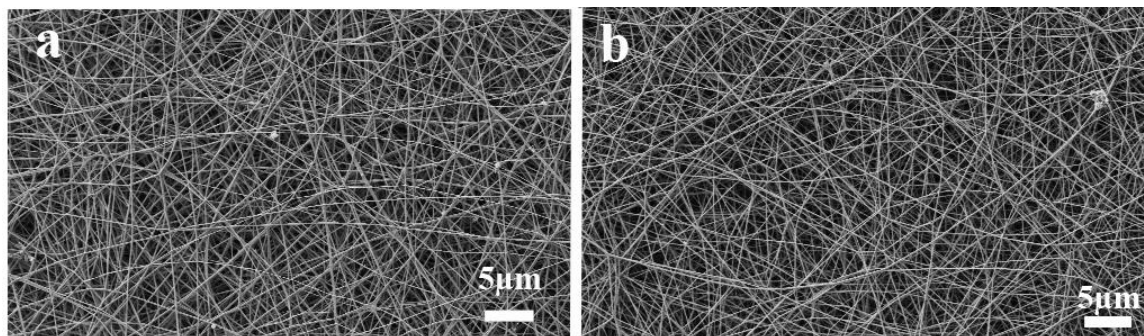


Figure 4.16. SEM micrographs of N⁺ implanted electrospun collagen fibers immersed in water for 7 days. (a) Implantation with 4×10^{15} ions/cm² (b) implantation with 8×10^{15} ions/cm²

4.5.3.1 Effect of ion implantation on chemical structure

Previous work in our group indicated that ion treatment using active N⁺ species can induce chemical modifications that is beneficial for cell attachment. To study the change of chemical structure, XPS was used to analyze the freeze dried collagen, as spun collagen, and nitrogen ion implanted electrospun collagen scaffolds.

XPS survey, C 1s, N 1s and O 1s high resolution spectra were used to examine chemical modification and analyze surface functionalization. The XPS data acquired establish the XPS elemental composition and intensities for the samples. And the percentage fraction of each element is illustrated in Table 4.3.

Table 4.3. Amount of oxygen, nitrogen and carbon present

	O	N	C
Freeze dried collagen	16.1	11.6	72.3
4E15 film	9.6	9.6	79.4
As spun fiber	17.2	17.6	65.4
4E15 fiber	13.0	11.2	73.9
8E15 fiber	11.1	5.4	78.2

From the survey spectra (Figure 4.17 to Figure 4.21), the samples provided very similar elemental composition with the highest contents of carbon, oxygen, nitrogen. Although different protein types may vary in composition to a greater extent and the presence of carbon can be attributed to organic molecules and is ubiquitous and detected on all samples, the change in carbon content can reflect the degree of carbonization during ion implantation. The nitrogen content indicates the presence of nitrogen containing groups that is beneficial for cell adhesion. The freeze-dried type I collagen has a 72.3 % C, 16.1% O and 11.6% N, while by dissolving the collagen in 40 v/v% acetic acid and underwent electrospinning, the as spun collagen fibers has 64.5% C 1s, 17.2 % O and 17.6% N. We theorized the change of C, O and N relative percentage may be attributed to the change of protein folding during protein dissolution and spinning process.

Two levels ion implantation $4 \times 10^{15} \text{ ions/cm}^2$ (4E15) and $8 \times 10^{15} \text{ ions/cm}^2$ (8E15) were carried out on electrospun collagen fibers to stabilize and impart nitrogen containing groups to the scaffold surface. The survey spectra (Figure 4.20 and Figure 4.21) indicated an increase of carbon content and decrease on nitrogen content with increasing ion dosage. The higher levels of carbon and lower levels of nitrogen measured indicating an increase in carbonization and decrease in protein content with increase ion implantation.

By depositing the same dosage ions ($4 \times 10^{15} \text{ ions/cm}^2$) onto both collagen film and electrospun collagen fibers, collagen film exhibited higher C 1s and lower N 1s levels

compared to collagen fibers (Figure 4.18 vs. Figure 4.20). The lower C 1s level of collagen fibers can be attributed to the higher porosity level of collagen fibers allowing faster heat dissipation with higher surface area per unit volume.

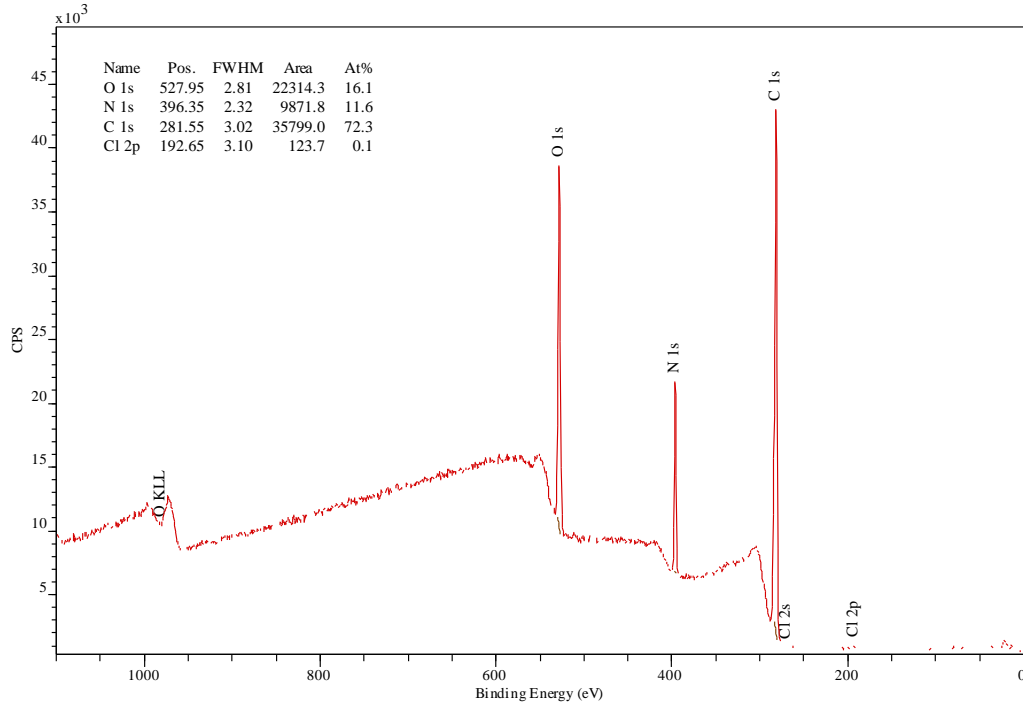


Figure 4.17. Full XPS survey on freeze dried type I collagen.

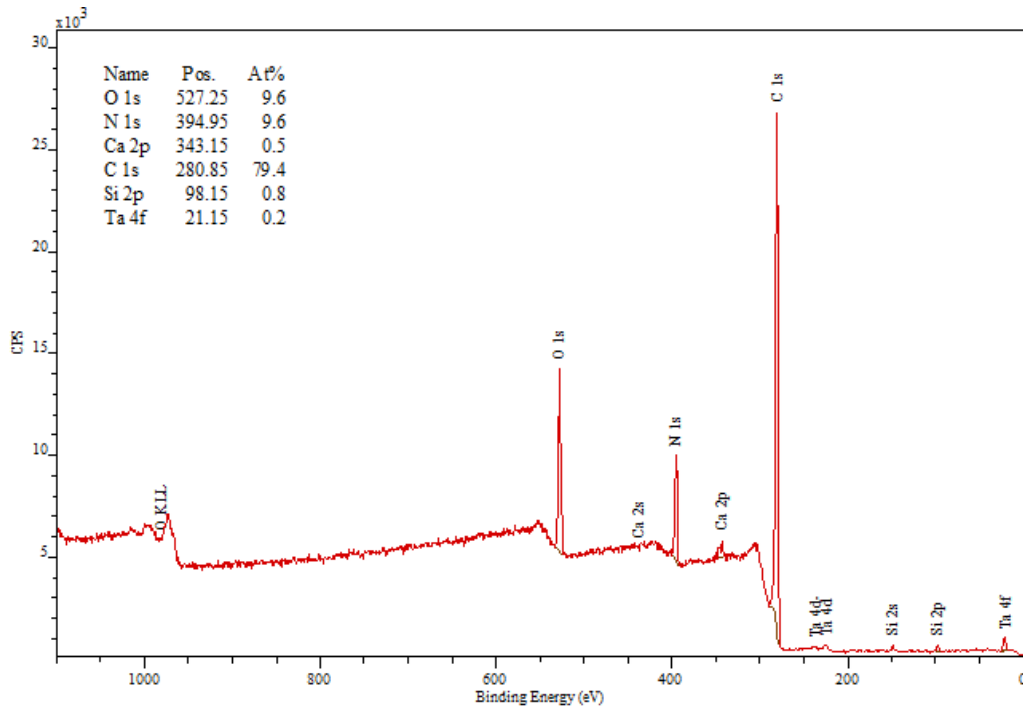


Figure 4.18. Full XPS survey spectrum on 4×10^{15} ions/cm² N⁺ implanted collagen film

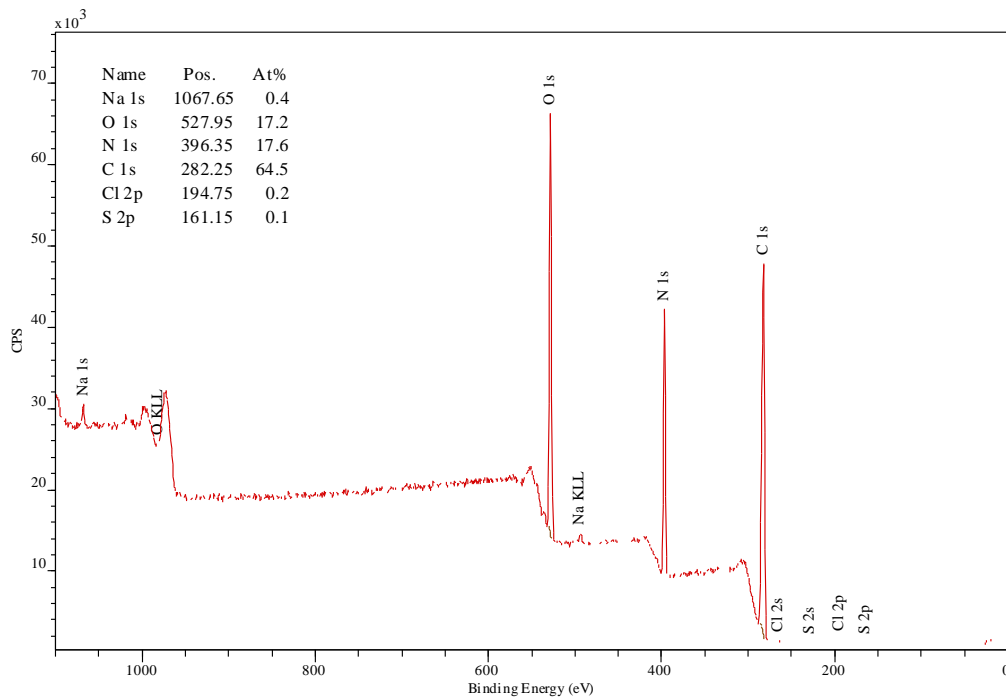


Figure 4.19. Full XPS survey spectrum of as spun collagen fibers

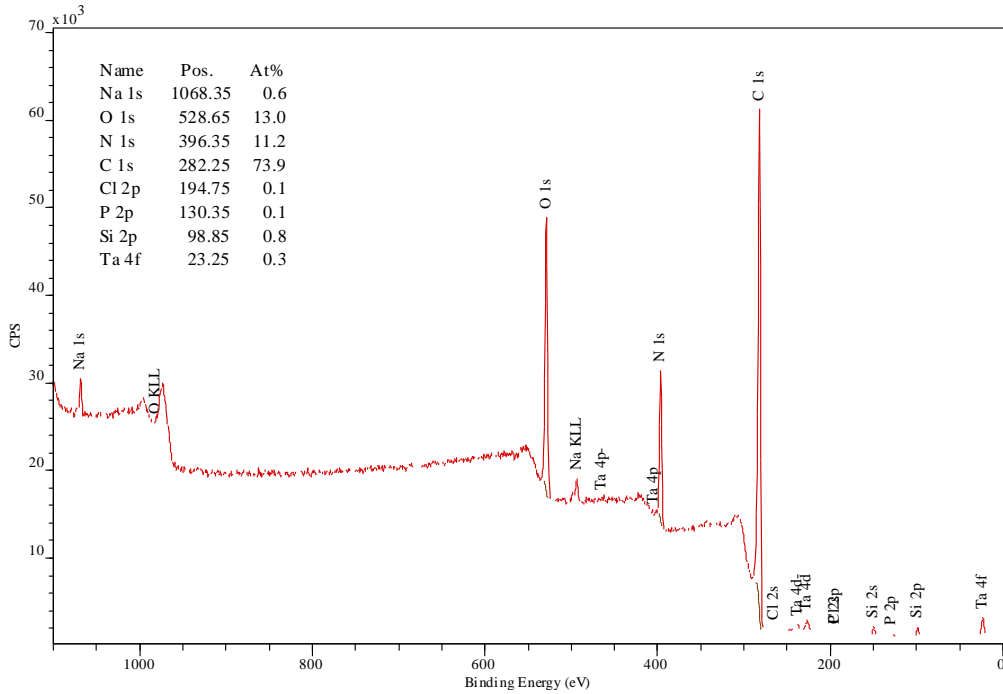


Figure 4.20. Full XPS survey spectrum of 4×10^{15} ions/cm² N⁺ ion implanted electrospun collagen fibers

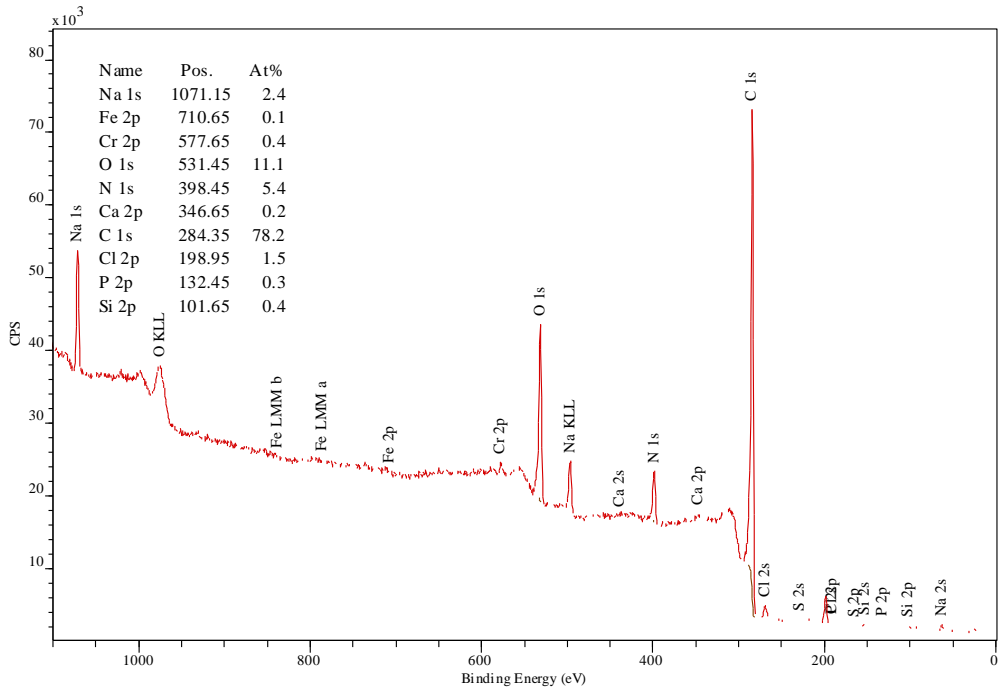


Figure 4.21. Full XPS survey spectrum of 8×10^{15} ions/cm² N⁺ ion implanted electrospun collagen fibers

The N 1s peaks indicated the presence of the amino acid of the protein. The deconvolution of N 1s core level spectra (Figure 4.22 to Figure 4.26) reveals two components, centered around 399 and 400eV, characteristic of nitrogen containing amide groups and amine groups, respectively. As the starting material is collagen protein with presence of amine/amide and carboxy groups, the amine/amide peak are the major components.

Compare to the type I collagen, the as spun fiber resulted a narrower peak with a diminish of the deconvoluted peak at 400eV. With ion implantation treatment, all the implanted samples have much broader peaks compared to the ones without ion implantation (Figure 4.25 and Figure 4.26). The N 1s peak shape and position of 4×10^{15} ions/cm² N⁺ treated fibers were not significantly different from the as spun fiber. Further increase the ion dosage to 8×10^{15} ions/cm² resulted a broader N 1s spectra (Figure 4.26), however, the peak intensity at 400eV is as strong as the amine/amide peak. The appearance and high intensity of NH⁺ peak indicated the possible chemical changes introduced by high dosage ion implantation. Similar result was observed with 4×10^{15} ions/cm² implantation on collagen film (Figure 4.23). Compared to 4×10^{15} ions/cm² implanted collagen fiber, same dosage level resulted the comparative peak intensity of the 8×10^{15} ions/cm² implanted collagen fiber (Figure 4.23 vs. Figure 4.26). Further suggested without the fibrous porosity, samples went through a higher degree chemical changes during ion implantation process.

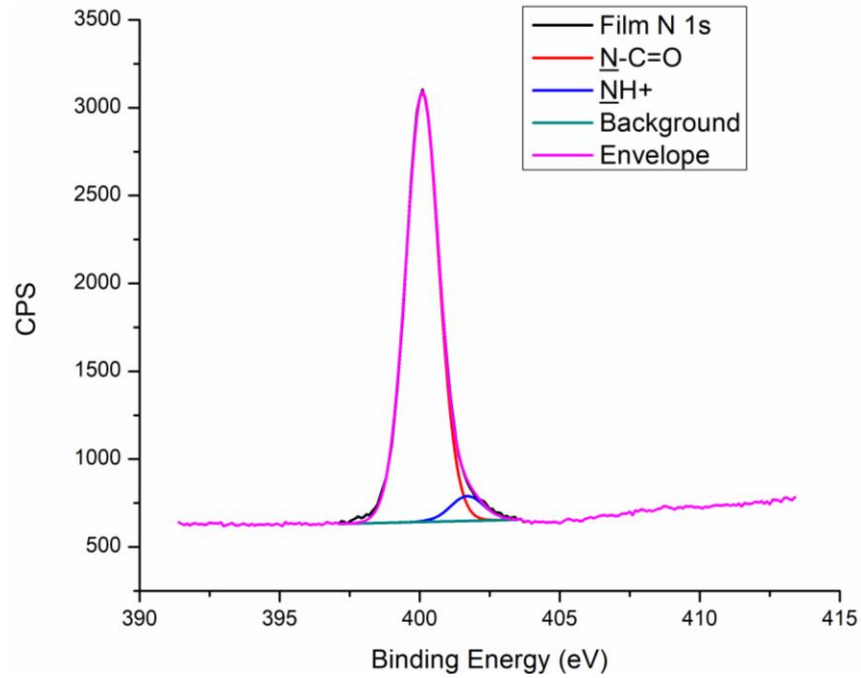


Figure 4.22. High resolution XPS of N 1s for collagen film

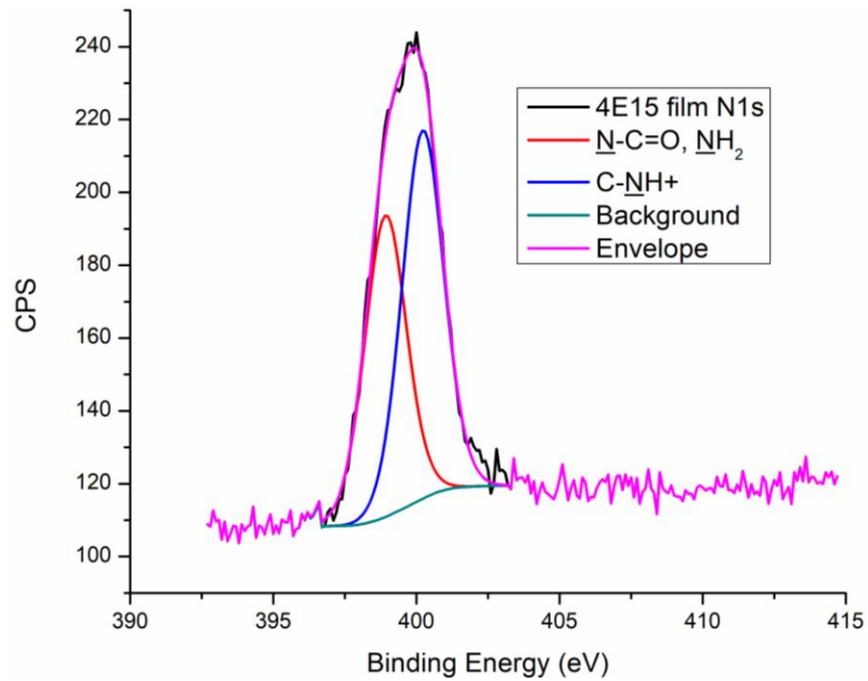


Figure 4.23. High resolution XPS of N 1s for collagen film implanted with 4×10^{15} ions/cm² N⁺

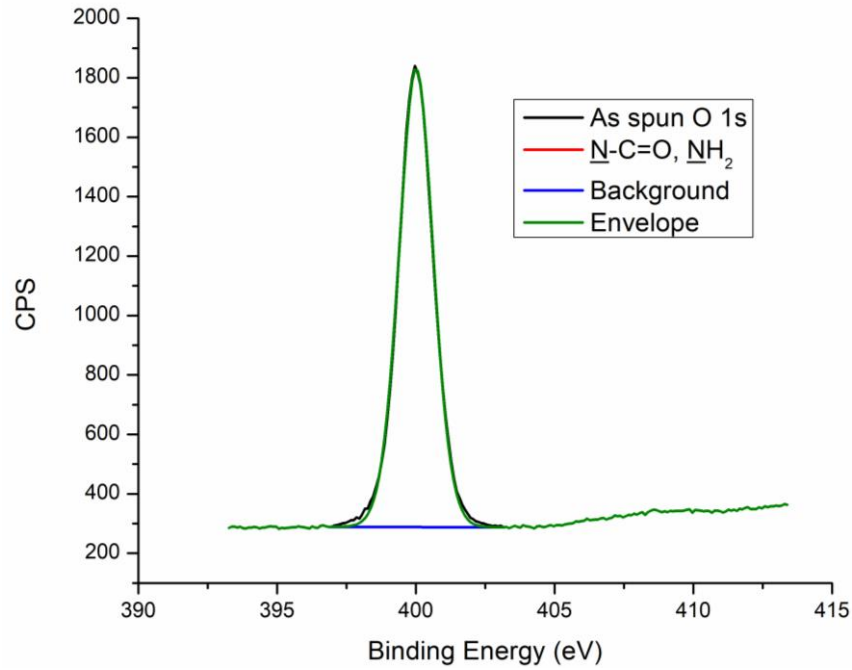


Figure 4.24. High resolution XPS of N 1s for as spun collagen fibers

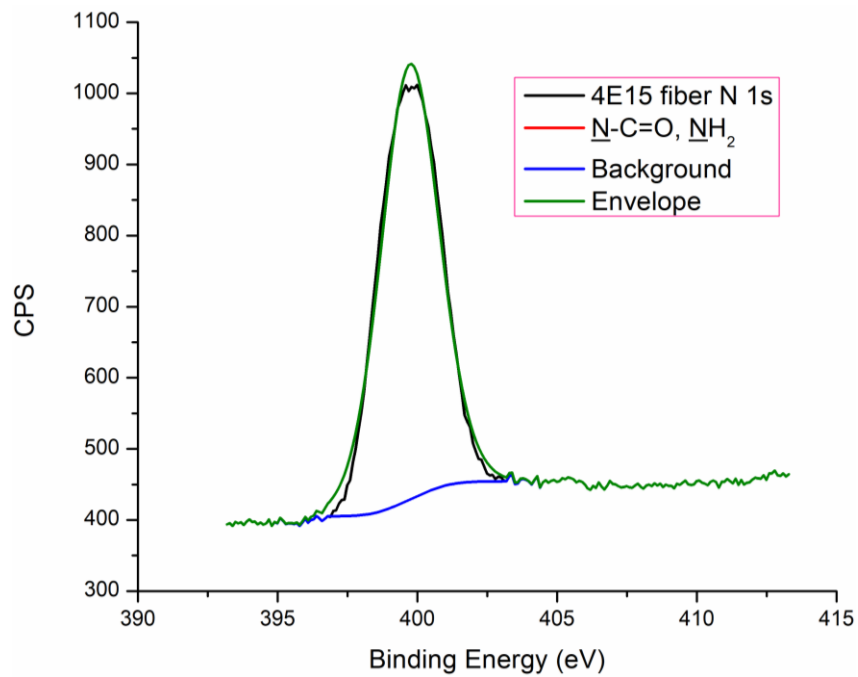


Figure 4.25. High resolution XPS of N 1s for electrospun collagen fibers implanted with 4×10^{15} ions/cm² N⁺

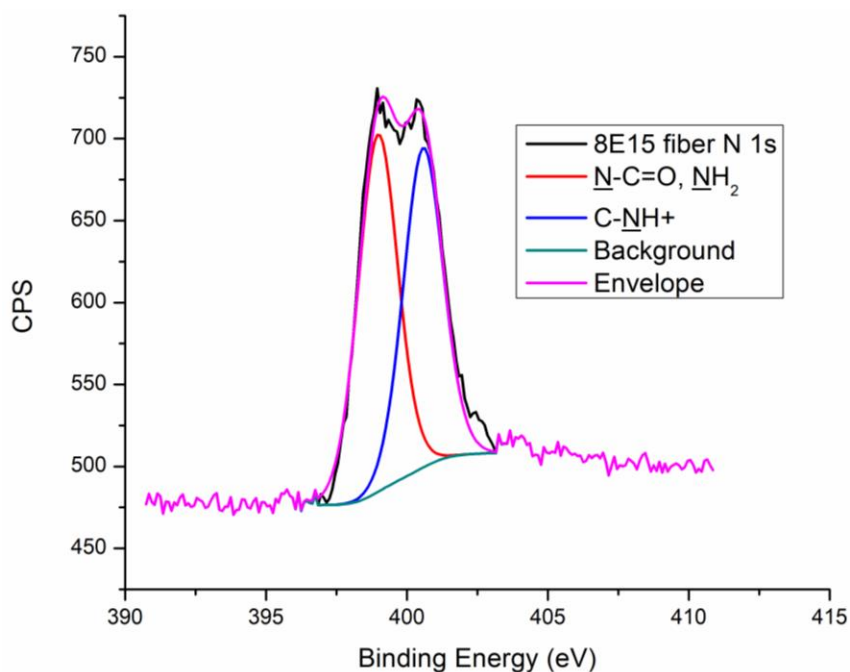


Figure 4.26. High resolution XPS of N 1s for electrospun collagen fibers implanted with 8×10^{15} ions/cm² N⁺

XPS analysis of high resolution C 1s (Figure 4.27 to Figure 4.31) revealed four main chemical components contributing to the spectra, namely C-C and C-H (hydrocarbon), C=O, N-C=O (ketone and aldehyde), C-N, C-NH, C-O (amine/amide and ether), and O-C=O (carboxylic acid and ester). The photoelectron peaks of C 1s were deconvoluted in accordance of the binding energies of C bonds. Compare the high-resolution C 1s spectra, after protein dissolution and electrospinning, the intensity of O-C=O peak diminished while the other peaks remain the same (Figure 4.27 vs. Figure 4.28). The O-C=O peak corresponds to the carboxyl groups in the protein and the nitrogen implanted fibers with both low and high dosages show similar pattern as the film (Figure 4.30 and Figure 4.31 vs. Figure 4.28). The relative peak intensities are slightly different with changing in dosage, but the composition remains the same.

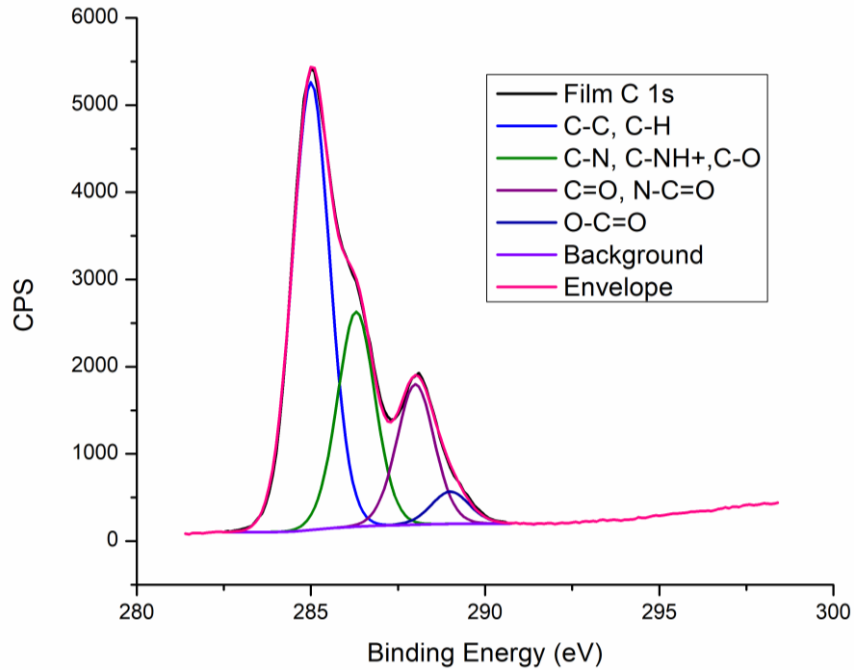


Figure 4.27. High resolution XPS of C 1s for collagen film

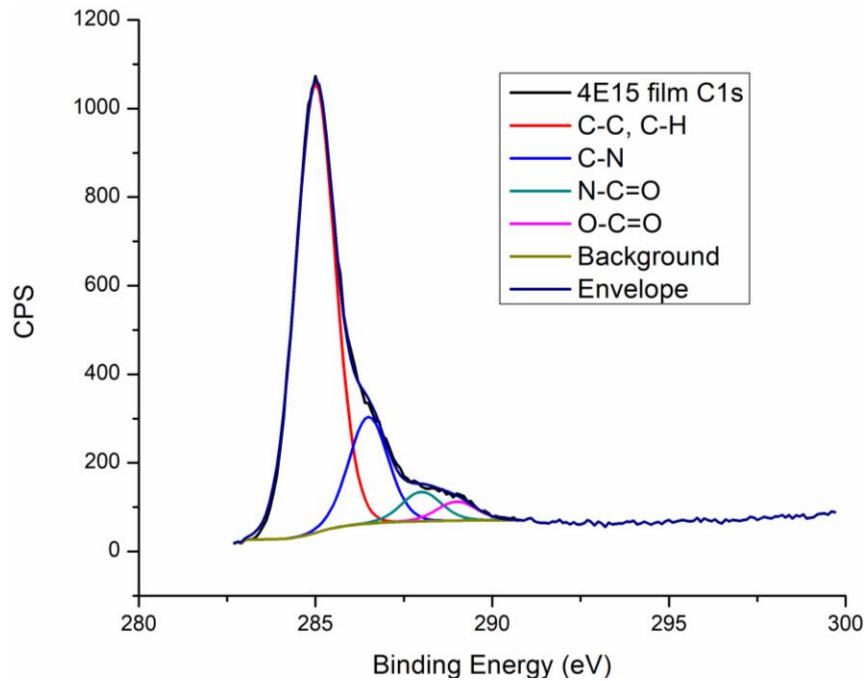


Figure 4.28. High resolution XPS of C 1s for collagen film implanted with 4×10^{15} ions/cm² N⁺

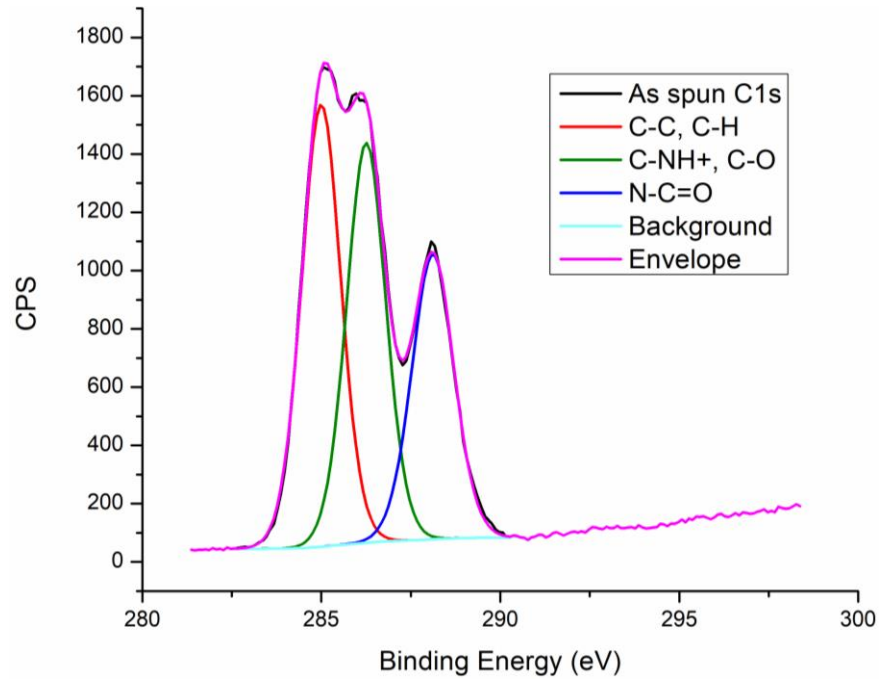


Figure 4.29. High resolution XPS of C 1s for electrospun collagen fibers

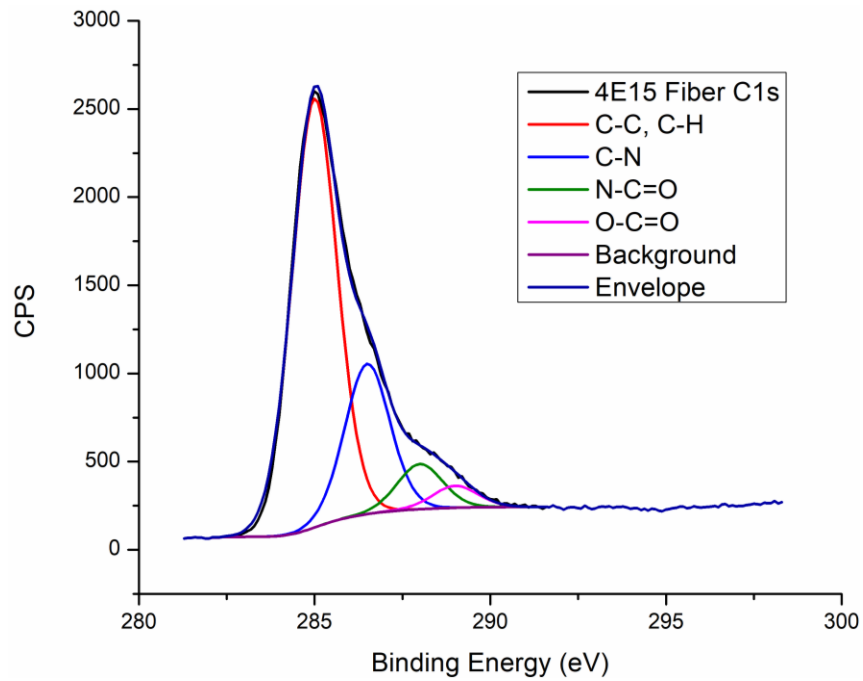


Figure 4.30. High resolution XPS of C 1s for collagen fibers implanted with 4×10^{15} ions/cm² N⁺

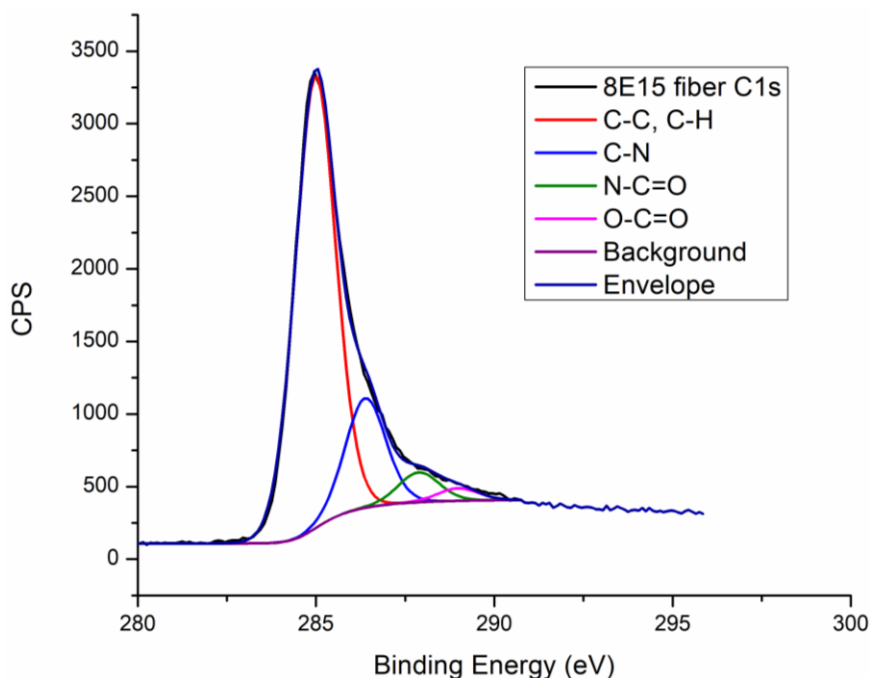


Figure 4.31. High resolution XPS of C 1s for collagen fibers implanted with 8×10^{15} ions/cm² N⁺

The high resolution O 1s shows similar results as C 1s spectrum (Figure 4.32 to Figure 4.36), using 40v/v% acetic acid as solvent, O-C=O peak diminished Figure 4.33 vs. Figure 4.32). Low dosage nitrogen implantation resulted very similar spectra on implanted collagen film, implanted collagen fibers and as spun collagen fiber with small C=O, O-C=O peak and stronger O=C-N peak (Figure 4.33 to Figure 4.35). Higher dosage not only resulted in the change of composition of reappearance of O-C=O peak, along with the emerge of new peak, we hypothesize the emerge of the peak is an indication of high dosage implantation changed chemical composition of collagen fibers (Figure 4.36).

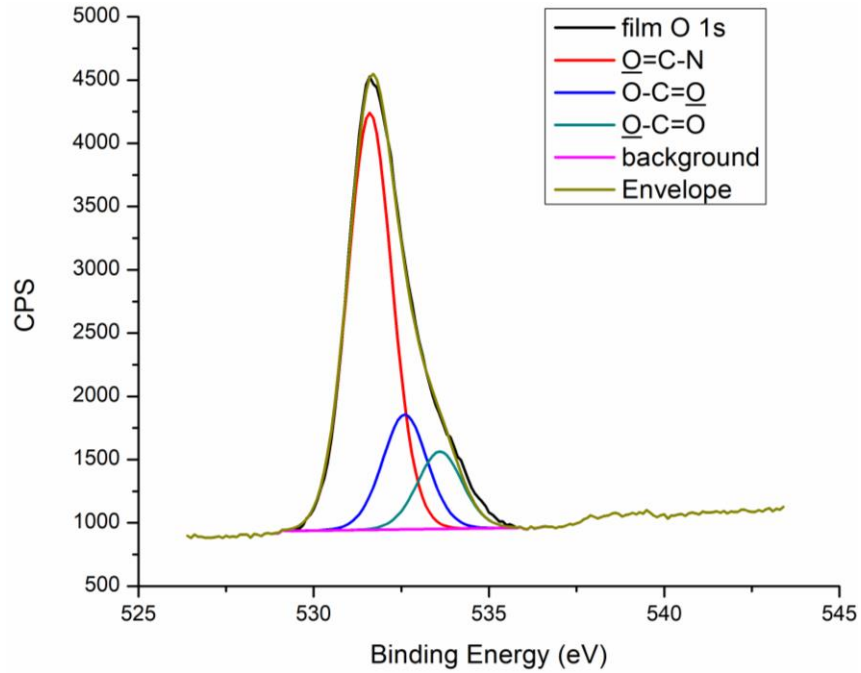


Figure 4.32. High resolution XPS of O 1s for collagen film

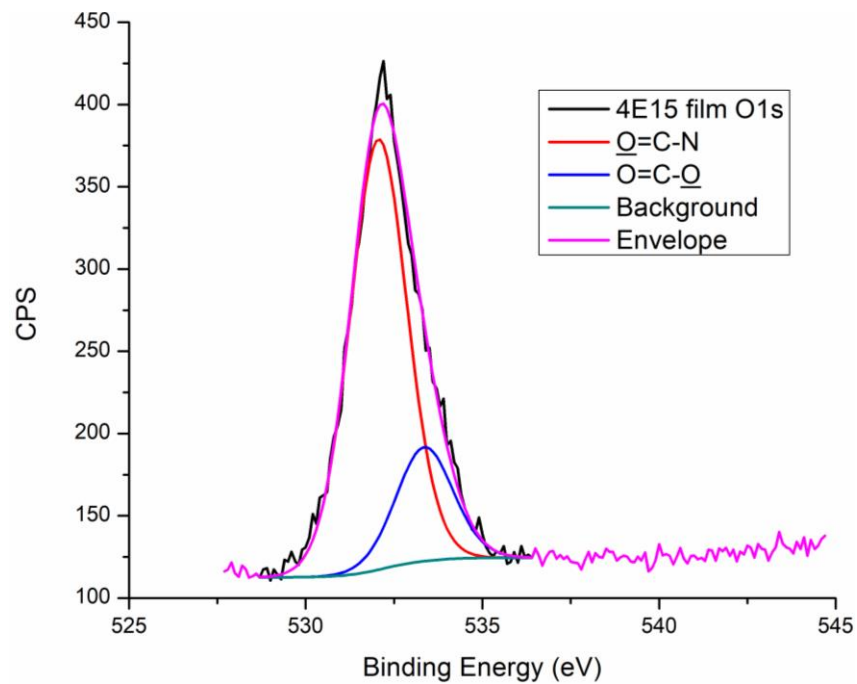


Figure 4.33. High resolution XPS of O 1s for collagen film implanted with 4×10^{15} ions/cm² N⁺

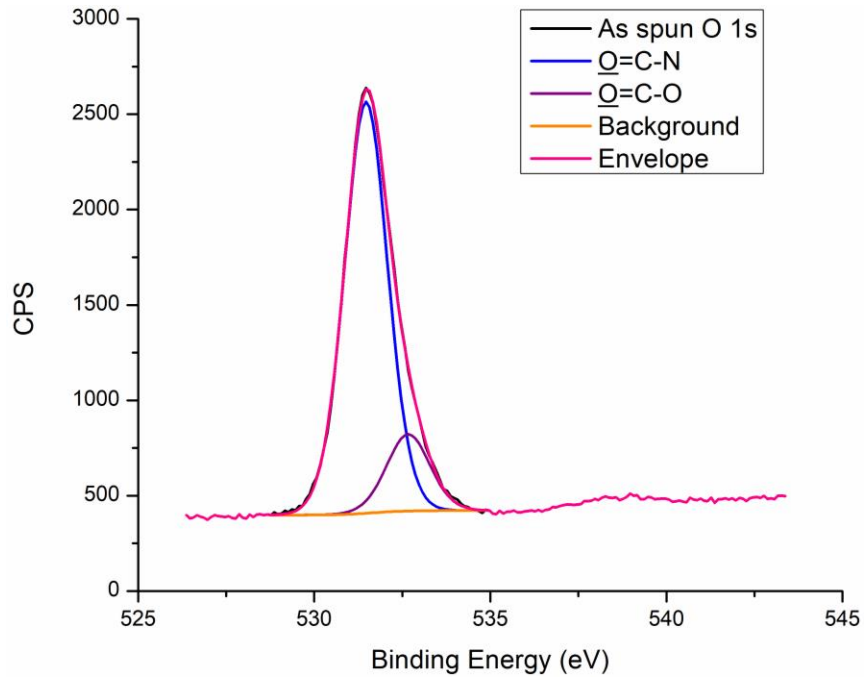


Figure 4.34. High resolution XPS of O 1s for electrospun collagen fibers

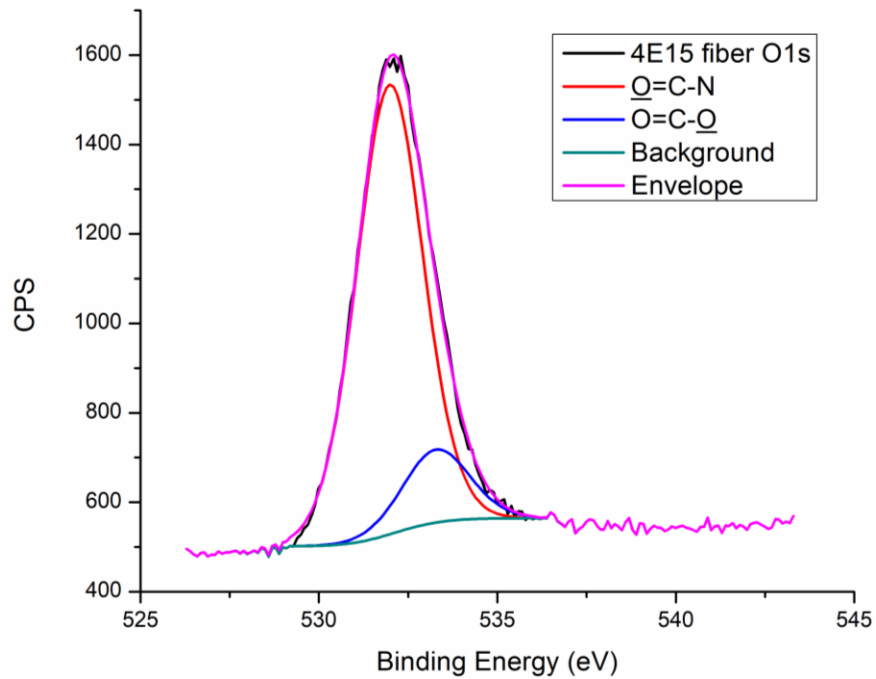


Figure 4.35. High resolution XPS of O 1s for electrospun collagen fibers implanted with 4×10^{15} ions/cm² N⁺

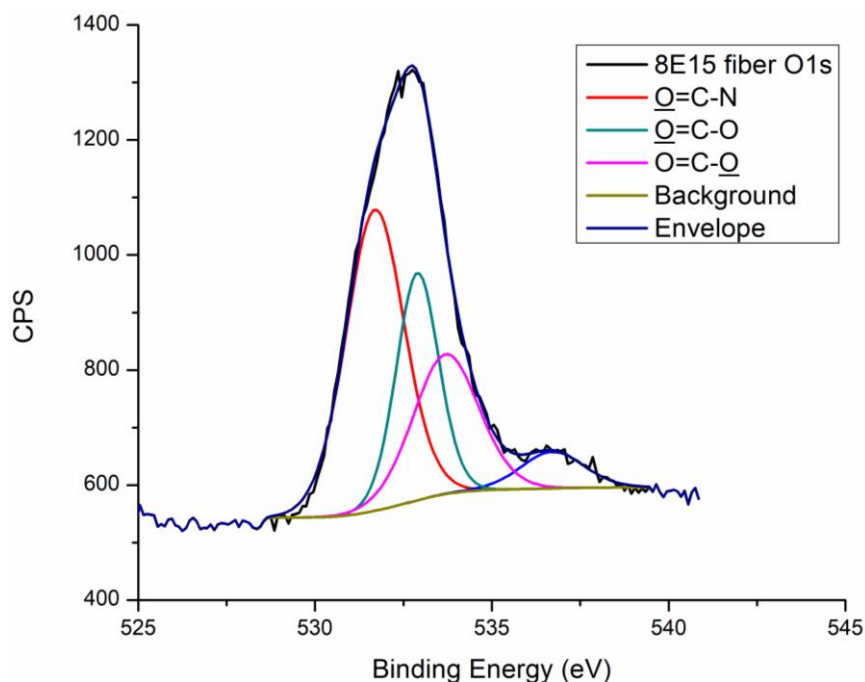


Figure 4.36. High resolution XPS of O 1s for electrospun collagen fibers implanted with 8×10^{15} ions/cm² N⁺

4.6 Mechanical properties of fibers

4.6.1 Vacuum dried electrospun collagen fibers

As spun collagen type I fibers were collected on trenched silicon wafers. These fibers had a uniform appearance and were randomly oriented on the surface (Figure 4.37).

Topographic images of the fibers were obtained using the AFM, and the fiber diameters were determined by the height profiles of each fiber. The average fiber diameter determined by AFM topography profile was 158.2 ± 43.2 nm for as spun collagen fibers fabricated with 25 wt% solution in acetic acid.

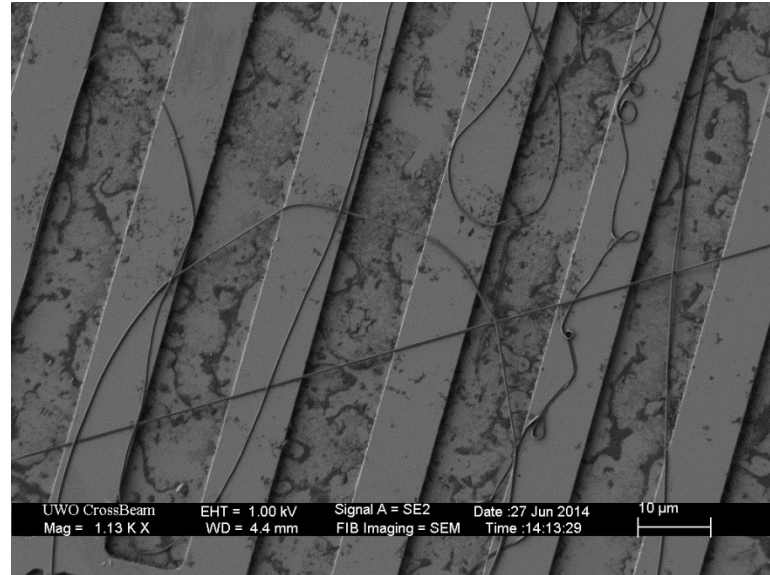


Figure 4.37. SEM image of electrospun collagen type I fibers on trenched silicon wafers. The electrospun fibers are randomly oriented on the surface.

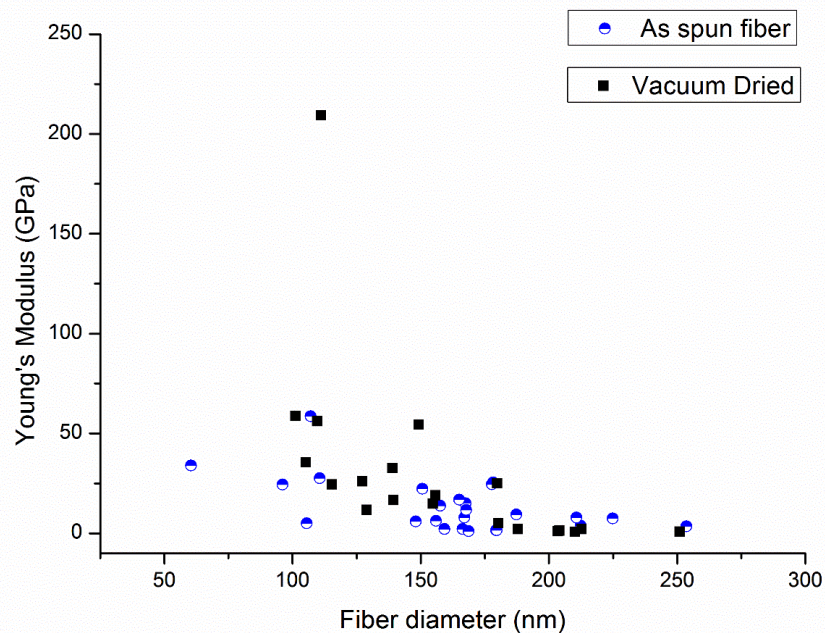


Figure 4.38. Plot of Young's modulus as a function of fiber diameter for as spun electrospun collagen fibers (half blue circles) and vacuum dried as spun fibers (black squares).

Figure 4.38 shows the Young's modulus of as spun electrospun collagen fibers of sizes ranging from 50 nm to 260 nm (half blue circles) as determined by AFM measurements analyzed using the Euler-Bernoulli model. The modulus ranged from 1 GPa to 58 GPa with a slight increase in modulus as fiber size decreases below 200 nm. This trend is more prominent with vacuum dried fibers (black squares). Similar observations of an increase in modulus with decreasing diameter have been reported for studies for other polymer fibers [183], [197], [200], [214], [219], [220].

As both fiber collection and mechanical testing were carried out in 35 %, it is possible that the remaining solvent residue in the fibers may affect their mechanical properties. To test this, the fibers were placed under high vacuum (~8 mtorr) for more than 24 hours. The fibers tested after vacuum drying ranged in diameter from 100 nm to 250 nm. The modulus ranged from 600 MPa to 209 GPa with a drastic increase below 200 nm (Figure 4.38, black squares).

4.6.2 Green light crosslinking

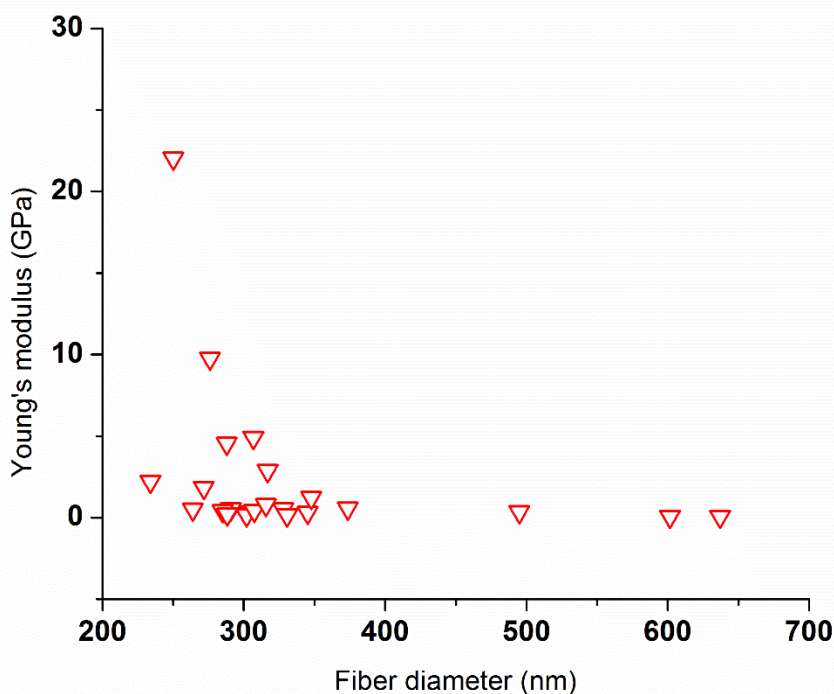


Figure 4.39. Plot of Young's modulus of electrospun Rose Bengal incorporated collagen fibers

Figure 4.39 shows the Young's modulus of fibers containing the photoinitiator Rose Bengal. The Rose Bengal was incorporated at high concentration to ensure abundant photoinitiator within the system during crosslinking. The crosslinking reaction is only active when the photoinitiator is in its soluble state, thus by maintaining abundant photoinitiator within the system, the dissolved photoinitiator would prolong the photochemical crosslinking reaction.

The incorporation of photoinitiator resulted in an increase in fiber size to a range of 240 to 640 nm, while the average Young's modulus was reduced to a range between 75 MPa and 22 GPa. Again an increase in modulus with decreasing diameter was observed, though the onset of size dependence was shifted to ~ 400 nm. A comparison between

fibers incorporating Rose Bengal and freeze dried as spun fibers shows the radical increase of fiber diameter and drastic decrease of fiber elasticity (Figure 4.40).

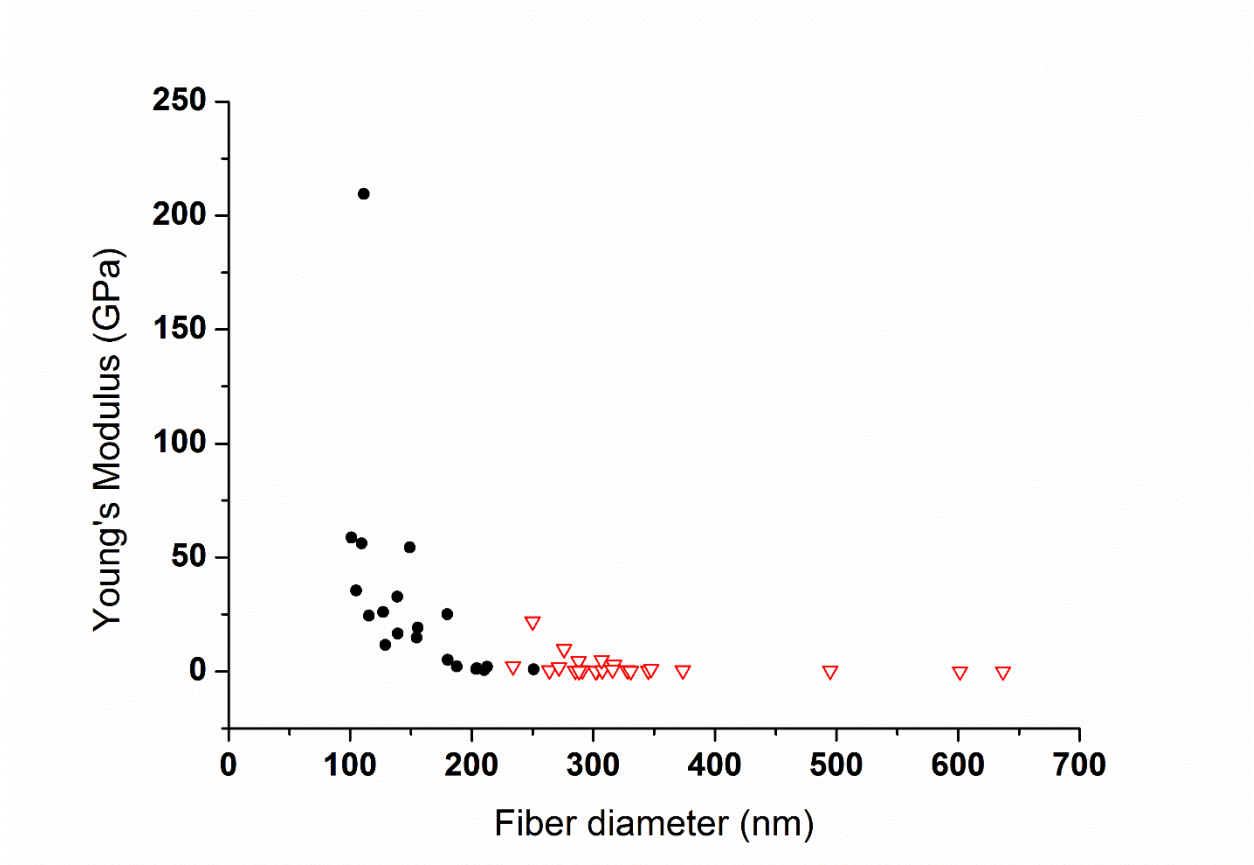


Figure 4.40. Plot of Young's modulus of collagen fibers incorporating photoinitiator (red triangles) and vacuum dried as spun fibers (black disks).

After photochemical crosslinking with green light, the photoinitiator has been consumed for photochemical reaction and the fiber size reduced to 110 nm and 270 nm. The Young's modulus then ranged from 600 MPa to 9 GPa, with an average of around 2.1 GPa. Despite the fact that the fiber size reduced after crosslinking, there is no significant change in fiber elasticity before and after light crosslinking (Figure 4.41). The average Young's modulus of fibers with Rose Bengal before and after photochemical crosslinking are 2.3 ± 4.8 GPa and 2.1 ± 2.3 GPa, respectively.

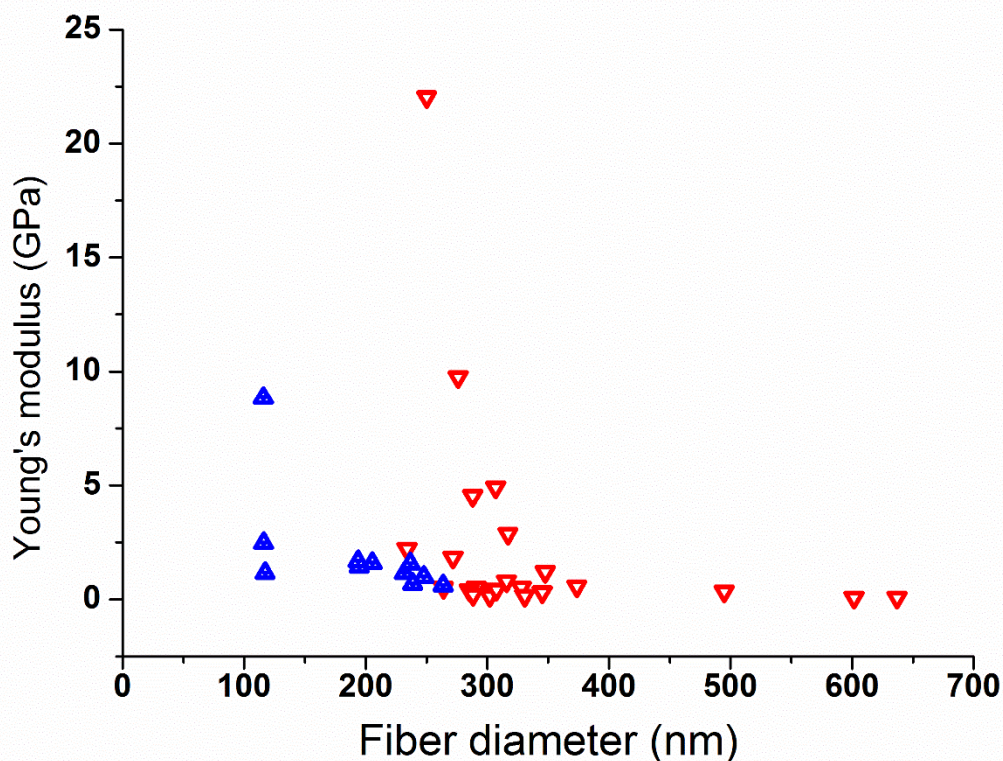


Figure 4.41. Plot of Young's modulus of Rose Bengal incorporated (red triangle) and green light crosslinked (blue triangle) collagen fibers.

4.6.3 Genipin crosslinked electrospun collagen fibers

As genipin crosslinking was carried out in a solvent system containing 3% water, electrospun collagen fibers absorbed water and swelled during crosslinking. As show in Figure 4.42, the fiber size spanned from 70 nm to 1000 nm. This swelling has been reported in previous work on genipin crosslinked electrospun collagen fibers [89], [129]. The Young's modulus of genipin crosslinked fibers show a size dependence for fibers with diameters smaller than 200 nm with fiber elasticity ranging from 5 MPa to 165 GPa.

Genipin crosslinked fibers have a Young's modulus very similar to as spun collagen fibers (Figure 4.42), with a very similar overall trend.

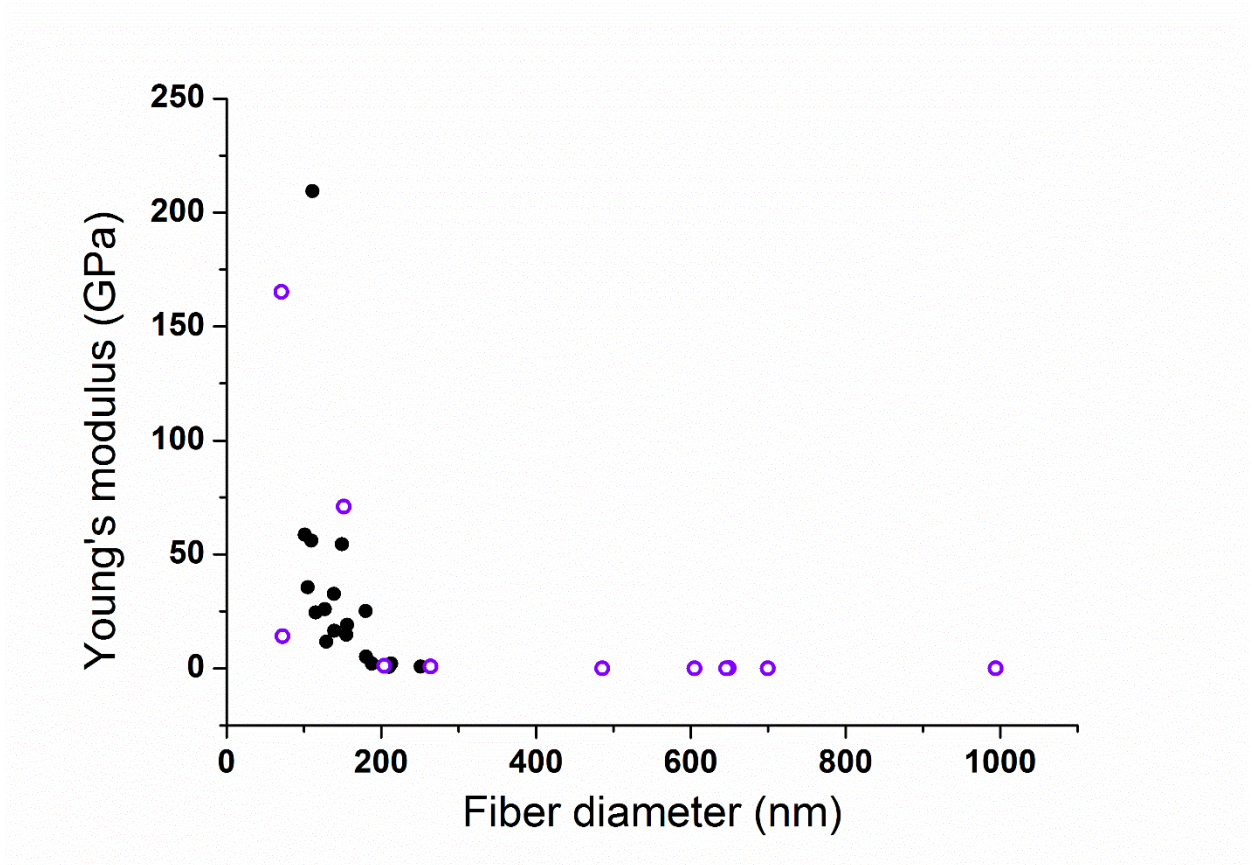


Figure 4.42. Plot of Young's modulus as a function of fiber diameter for genipin-crosslinked collagen fibers (purple circles) and as spun electrospun collagen fibers (black dots).

4.6.4 Ion implantation

Two ion dosage levels were used to treat as spun electrospun collagen fibers, 4×10^{15} ions/cm² (ion4 AA) and 8×10^{15} ions/cm² (ion8 AA). As indicated in the previous section, both treatments resulted in fiber size reduction, size effects in Young's moduli can be observed in both ion treatments (Figure 4.43a and b). The onset for increases in modulus with reduction of fiber diameter is around 170 nm for both cases. By comparing the results from the two ion implantation levels, there is no definitive difference between the two dosages (Figure 4.43c). Unlike other fiber stabilization treatments where fiber mechanical properties changed after the treatments, there is no obvious change in Young's modulus after ion implantation for either dosage levels

(Figure 4.43d). The maintenance of fiber properties after ion treatment can be attributed to the fact that ion implantation is the only physical stabilization treatment that does not introduce or involve other chemicals. The physical treatment allows the preservation of native fiber structures and properties, and produces the fibers most closely resemble the as spun fiber properties.

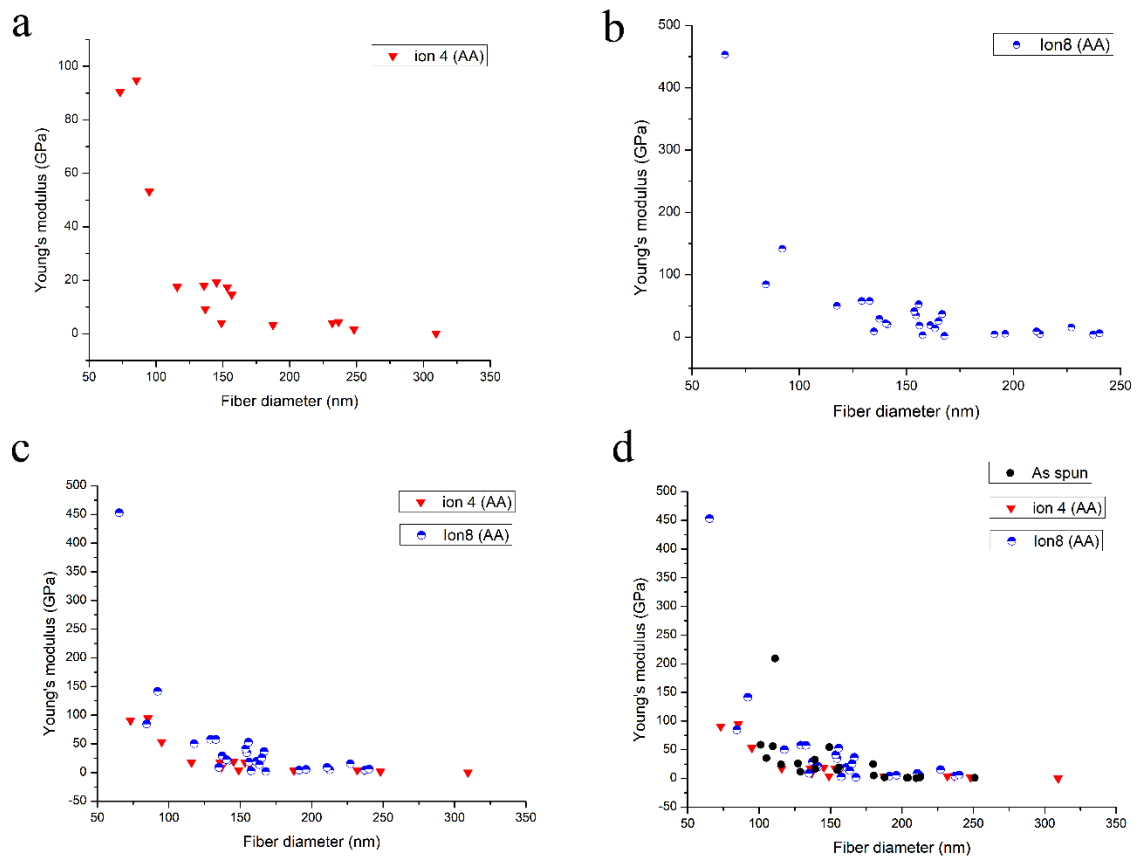


Figure 4.43. Plots of Young's modulus as a function of fiber diameter for (a) nitrogen treatment with dosage of 4×10^{15} ions/cm²; (b) nitrogen treatment with dosage of 8×10^{15} ions/cm²; (c) overlay of the two ion implantation dosages; (d) comparison between ion implanted fibers and as spun collagen fibers.

4.6.5 Change of solvent system

Instead of using 40 v/v% acetic acid as the solvent system for as spun collagen fibers, HFIP was used for comparison. Nitrogen ion treatments with dosage level 4×10^{15} ions/cm² (ion4) and 8×10^{15} ions/cm² (ion8) were applied to the prepared samples. As shown in Figure 4.44a, no difference is evident in the mechanical properties of the resulting fibers. The trends are very similar to those for fibers spun in acetic acid. To further explore the effects of the two different solvent systems, the mechanical properties were compared separately with each ion dosage. It is evident from Figure 4.44 b and c, that the Young's modulus for the two solvent systems extremely similar, although fibers spun with acetic acid system have a more pronounced size effect at low diameters. Presumably the high volatilities of both acetic acid and HFIP allow fast and complete solvent evaporation during the electrospinning process.

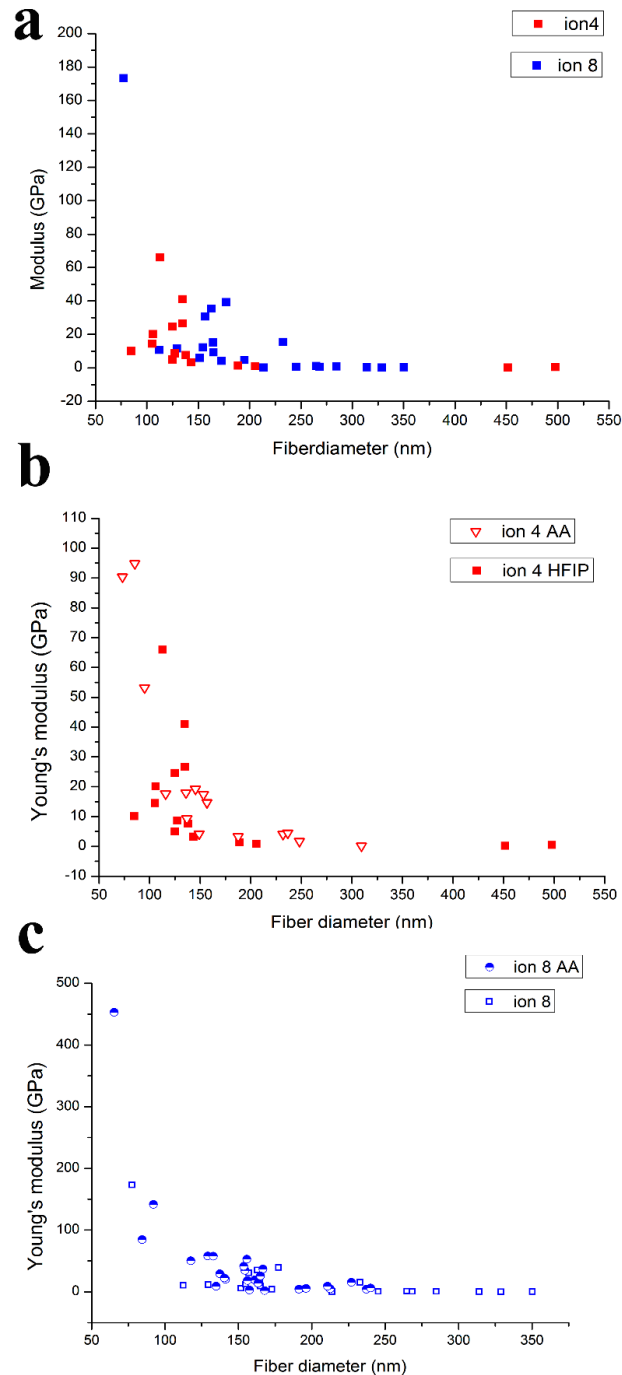


Figure 4.44. Plots of Young's modulus of (a) collagen fibers spun with HFIP solvent system and implanted with different dosage of nitrogen ions; (b) electrospun collagen fibers prepared with HFIP and acetic acid and implanted with 4×10^{15} ions/cm² nitrogen; (c) electrospun collagen fibers prepared with HFIP and acetic acid and implanted with 8×10^{15} ions/cm² nitrogen.

4.7 Cell compatibility of crosslinked collagen fibers

Stabilized electrospun collagen scaffolds can provide the correct structure, geometry, surface chemistry and mechanical properties which mimic that of the native ECM of most tissues. However, cell compatibility of these scaffolds still have to be assessed to determine the performance of the crosslinked fibers.

Human fetal lung (IMR-90) cells were used to determine the aqueous stability of crosslinked electrospun collagen fibers for cell adhesion and proliferation. Nitrogen ion treated collagen film (**film**) and collagen fibers (**4E15**) were used for evaluating the effects of substrate morphology on cell morphology; aligned (**aligned**) and random collagen fibers (**4E15**) were compared to observe the change of cell morphology with substrate organization (i.e. fiber alignment); high and low dosage nitrogen ion treatments (**8E15** vs. **4E15**) were used to identify the effect of ion dosage on cell behavior; photochemical crosslinked and genipin crosslinked electrospun collagen fibers were also used to provide insights in crosslinking methods on cell growth.

Optical images on IMR 90 after 24 hours of cell seeding on culture plates indicate healthy fibroblasts exhibited extended and elongated form to maximize contact area with substrate (Figure 4.45).

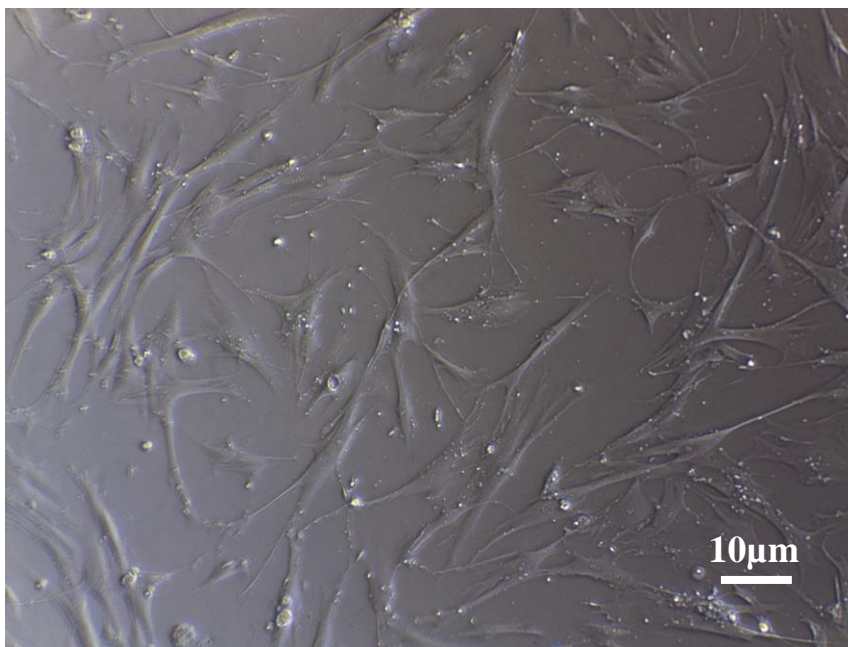


Figure 4.45 Optical image (brightfield) of IMR-90 on culture plate after 24 hours seeding, initial seeding density: 20,000 cells / well.

After seeding the cells on all crosslinked samples, IMR-90 showed good adhesion and spreading on crosslinked film and fibers after 24 hours (Figure 4.46). For the cells on low dosage nitrogen implanted film and random fibers, the cells filopodia spread and extended in all directions, while the cells were stretched into bipolar morphology on other samples (Figure 4.46).

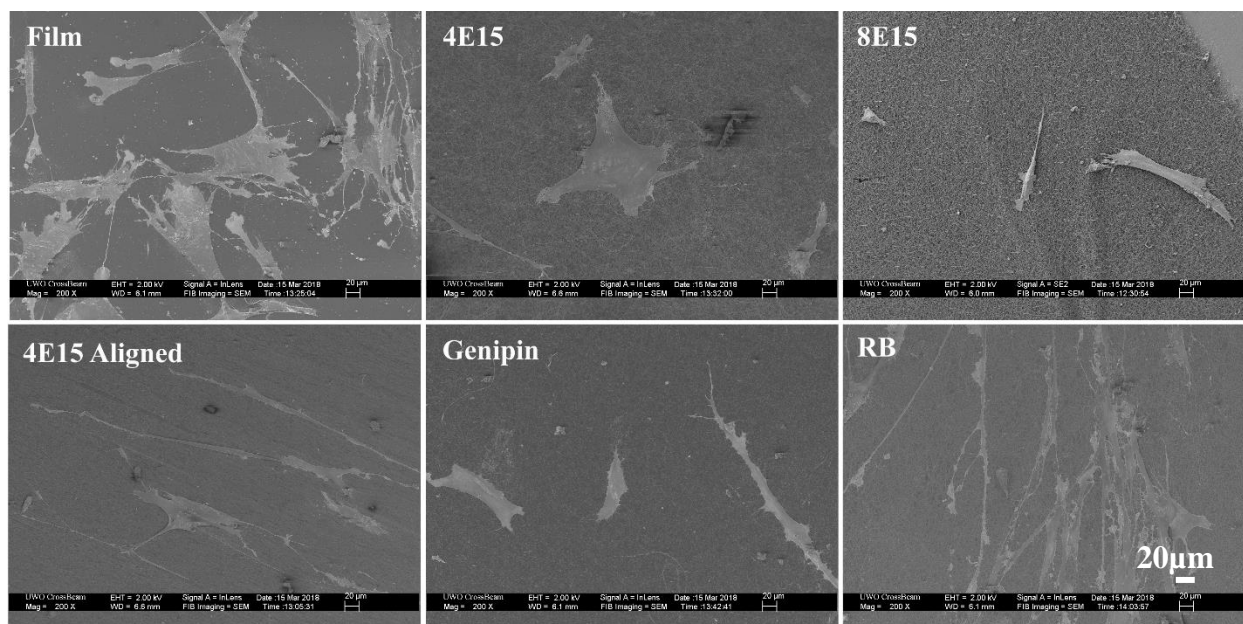


Figure 4.46. SEM images of all crosslinked samples after 24 hours of cell seeding. (All have the scale bar of 20 μm)

Low ion implanted film was used as a positive control to demonstrate the difference in cell morphology when encountering with film versus fibers. The low dosage implanted film showed round cell shape with irregular protrusions in all directions. For all other samples with fibers presented, cells had filopodia protrude from the cells along the direction of the contacted fibers (Figure 4.47 c and d). To form anchorage with substrate, cell filopodia extended towards the fibers until it makes contact with one single fiber, then adhere to the fibers by pulling on them (Figure 4.47a). With higher fiber density, once the filopodia form contact with fiber, they bend and align with the contacted fiber (Figure 4.47c). In some cases, the filopodia would extend to the layer underneath the surface layer and entangled with fiber network (Figure 4.47d). On some samples, the cells infiltrated underneath the surface layer of the sample and grow on the second layer (Figure 4.47b). The layer of fibers lying on top of the cells and the fiber network stay intact around the cells. The length and degree of extension of filopodia differs in each sample. In some samples, filopodia adhere and aligned tightly along the fibers to form long lasting adhesions until it reaches and form contact with adjacent cell filopodia (Figure 4.48a,b). The more than 100 μm long filopodia indicates the active interaction

between filopodia and the fibers, suggests a highly active role of filopodia in mediating initial adhesion events and in exploring their environment.

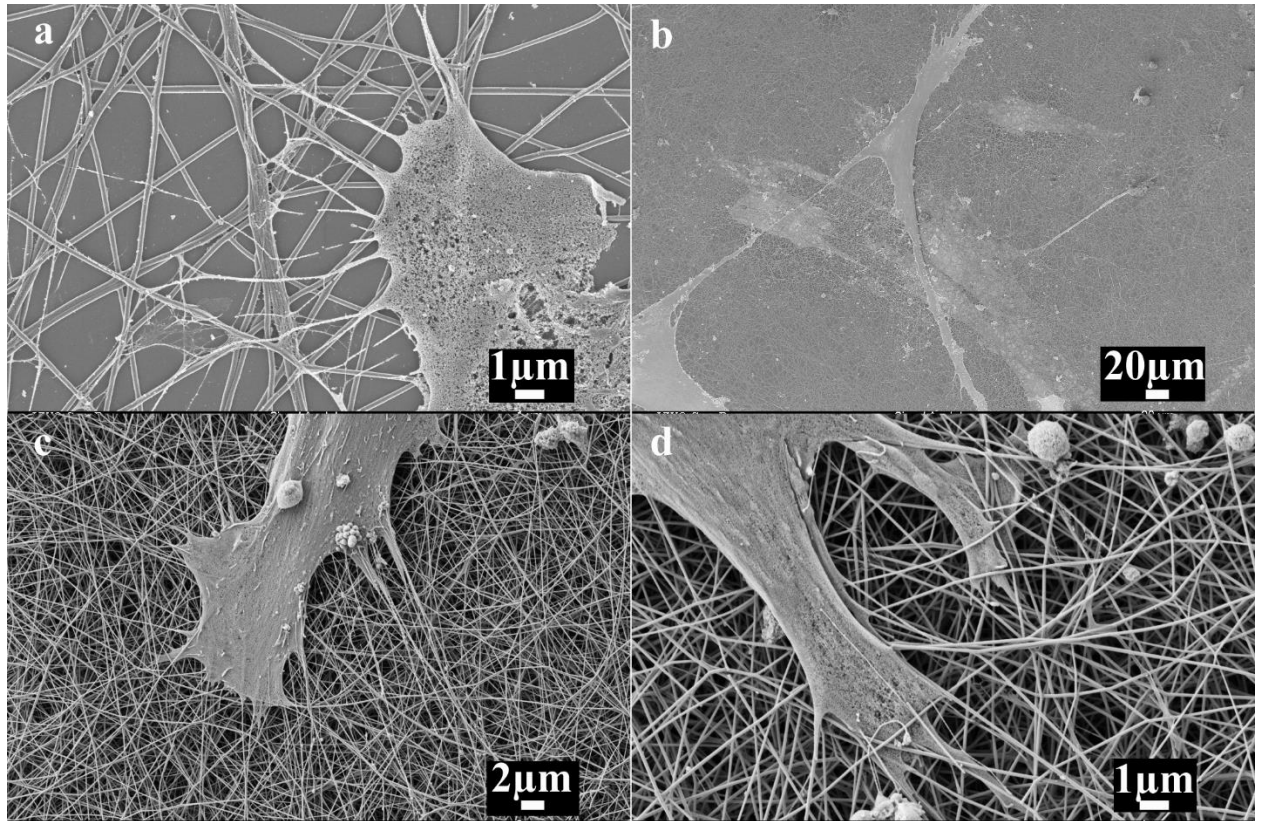


Figure 4.47. SEM images of filopodia extension on crosslinked electrospun collagen. (a) filopodia extended from the cell to reach to genipin crosslinked electrospun collagen fibers. (b) additional cells grow on the bottom of the fiber layer. (c) filopodia reach out, anchor and align with fiber direction. (d) filopodia extended and reached to entangle the fibers underneath the top layer.

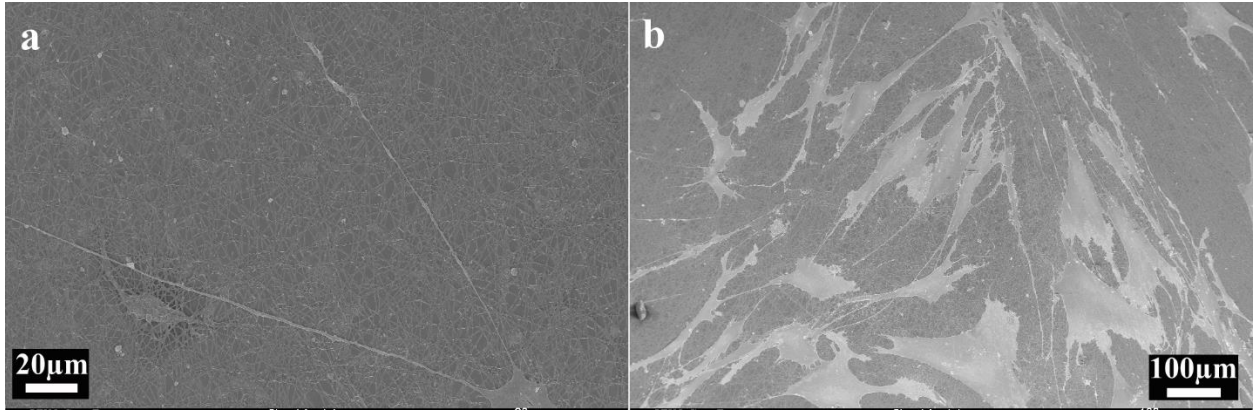


Figure 4.48. SEM images of filopodia extension on LED crosslinked electrospun collagen fibers. (a) long filopodia extension with length of more than 100 μm . (b) filopodia extension and entanglements between cells.

The stellar morphology of all the samples after day 1, day 4 and day 7 can be observed in Figure 4.49, compared to ion implanted films, crosslinked fibers resulted cells elongated into bipolar morphology. All the crosslinked samples have cells with bipolar morphology, while the cells are aligned parallel to the orientation of the aligned fibers.

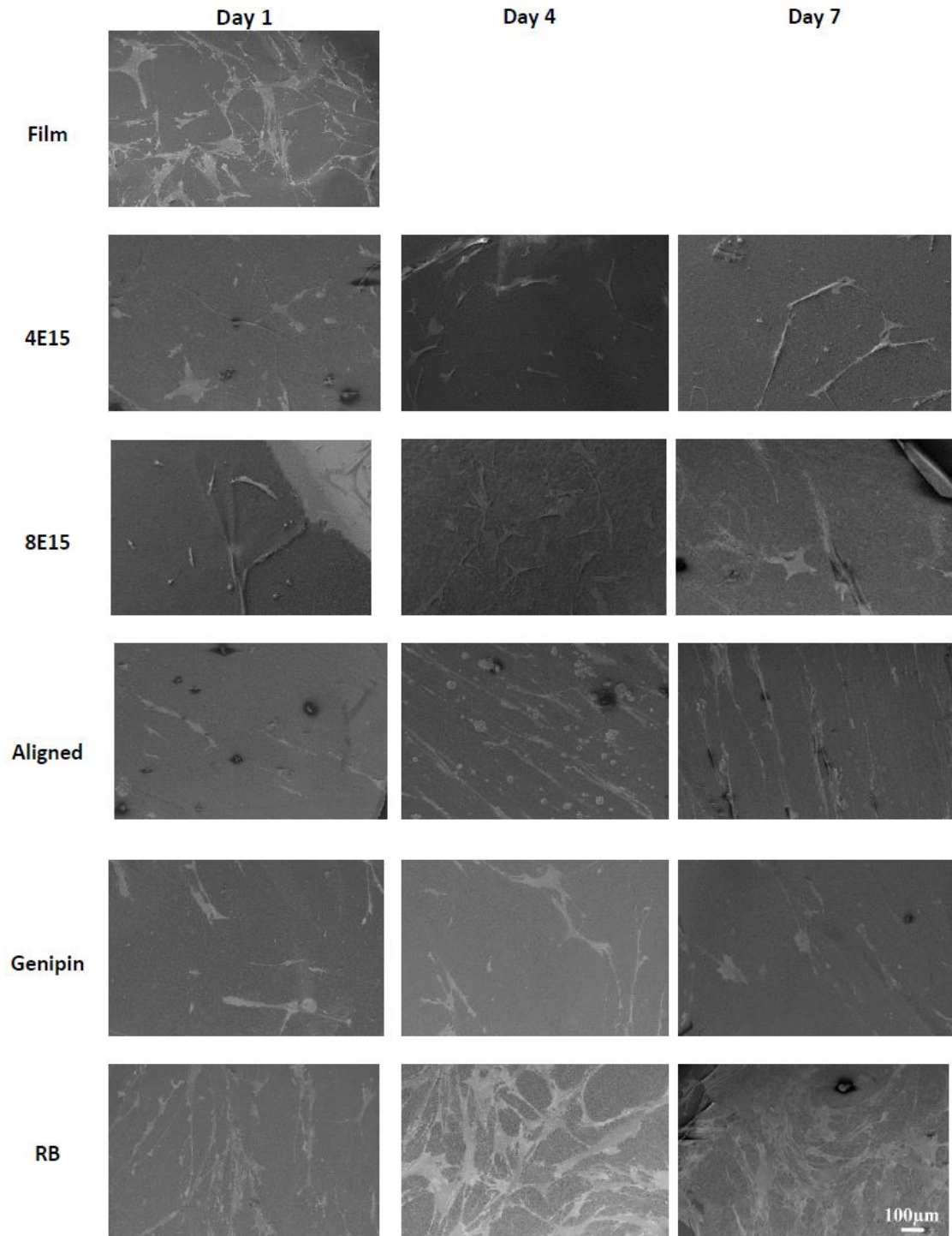


Figure 4.49. SEM images of crosslinked collagen samples after 1, 4 and 7 days of IMR90 culture. (All have the scale bar of 100 μ m)

To further observe the role of the surface topography on the interaction of cells with the fibrous scaffold, cell skeleton and nuclei were stained and imaged using fluorescence microscopy. Figure 4.50 shows by using different excitation and emission wavelength, the cell nuclei and cell skeleton can be clearly distinguished. After 4 days of culture, IMR90 had the bipolar elongation parallel to the orientation of the aligned fibers.

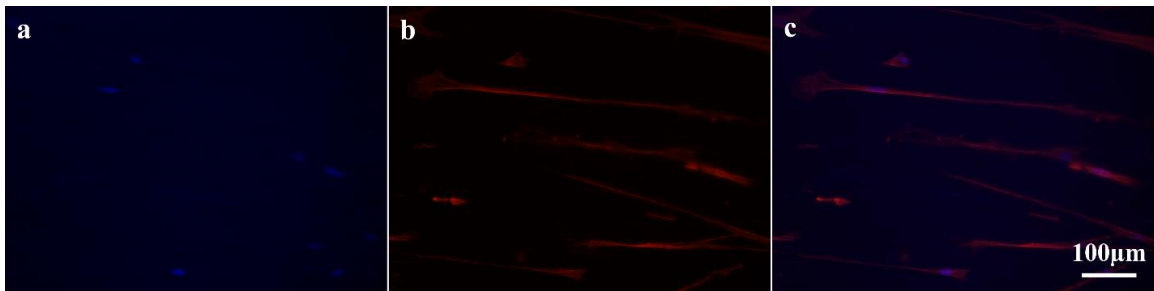


Figure 4.50. Fluorescence images of IMR 90 cultured on aligned crosslinked electrospun collagen nanofiber; a: cell nucleus; b: filamentous actin; c: overlaid image

As a comparison, Figure 4.51 shows the bipolar elongation of cells on aligned fibers while random fibers resulted cells extended in all direction with stellar morphology.

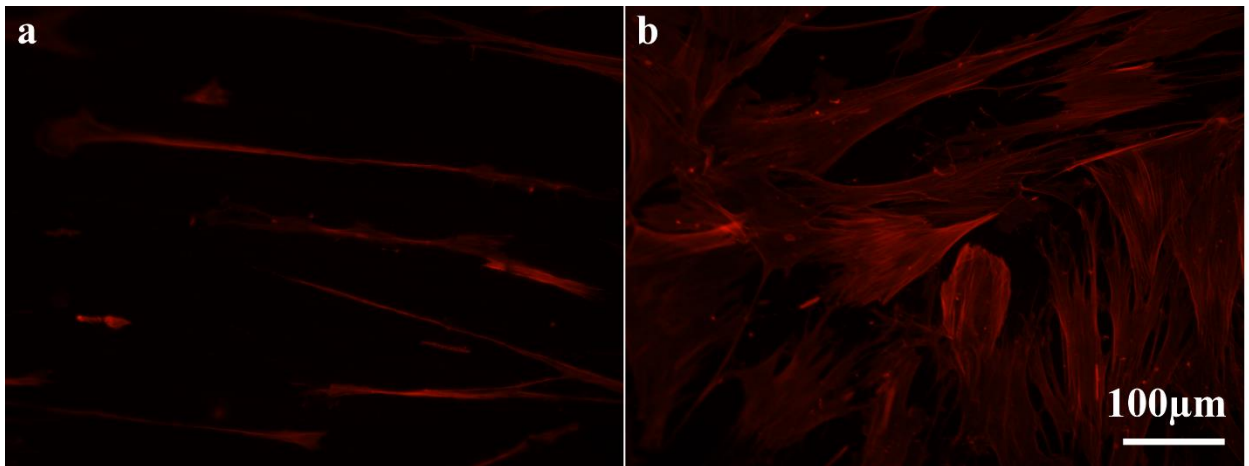


Figure 4.51. Fluorescence image of IMR 90 cultured on aligned vs. random collagen fibers.

5 Discussion

5.1 Tissue engineering

Currently, the most intensively researched approach for the development of medical devices is the tissue engineering / regeneration approach [1], [44], [51], [221]–[225]. This approach attempts to create implants to replace / repair the diseased tissue / organ by making the use of biodegradable materials as template or substrate [19], [20], [146], [222]. The implant is either populated with appropriate types of cells before implantation or would attract local cells after implantation with the help with bioactive molecules such as growth factors [225], [226]. As these cells gradually lay down their own extracellular matrix (ECM) after implantation, the substrate material should be degraded and replaced by living tissue /organ [2], [3].

It is known that extracellular matrix (ECM) provides the structural supports for cell adhesion and cells respond to the structural, chemical, physical and mechanical cues presented in the environment (i.e. ECM) [18], [30], [35], [168], [183], [227]. The importance of ECM in cell behavior regulation inspired researchers to develop biomaterial structures that closely match the target diseased tissue / organ ECM in terms of structure, geometry and properties. The ECM is composed of complex chemically and physically crosslinked network of protein fibers and serves to mechanically support cells in 3-dimensions and provide biochemical signals for cellular activity regulation [34], [39], [39], [51], [62], [75], [228]. To create scaffolds which serve as “synthetic ECM” that replicate the structural, chemical, physical and mechanical aspects of the natural ECM, collagen, the most abundant structural proteins in mammals have been widely used for tissue regeneration applications [11], [13], [228]–[230], [14], [62], [91], [135], [144], [145], [150], [172]. Among the different collagen types, collagen type I, predominantly localized in the skin, tendon, cornea, and bone, is the most abundant in the body and the most widely studied [6], [13], [16], [149], [150], [213], [227], [231]. Amongst the various scaffolding techniques, electrospinning is an outstanding method that is capable of producing non-woven fibrous structure with dimensional constituents similar to those of ECM fibrils. Electrospinning allows fabrication of fibrous scaffolds with controlled geometry and pore dimensions that resembles the fibrillar feature of the ECM. These

fibers provide structural support and mechanical integrity to tissues as well as locations for cell adhesion and can potentially significantly affect cellular behavior [66]. The possible control of fiber arrangement and architecture is also important in affecting cell attachment, proliferation and differentiation [39], [136], [173], [196].

In this work, we used the electrospinning technique to fabricate 3D collagen scaffold with either random or aligned fibers. The as spun collagen fibrous scaffold was not stable in aqueous environment, chemical, photochemical and physical crosslinking were applied to improve fibers aqueous stability. The as spun and treated fibers were subjected to mechanical testing using atomic force microscope to determine the elasticity of individual single fiber. Human fetal lung (IMR-90) cells were used to determine cell compatibility of the scaffolds.

5.2 Preparation of electrospun collagen fibers

The fibrous proteins which provides both structural and adhesive functions in the ECM are approximately 50 – 500 in diameter [18], [227]. Thus, producing nanometer sized fibers is particularly suitable for tissue regeneration applications due to their high surface area to volume ratio and interconnected porous network for cell attachment and infiltration [34], [228]. Fibrous scaffolds can be fabricated with controlled alignment to closely mimic the organized structure of the ECM [34], [39], [113]–[115], [122], [232], [233]. The common approaches used to fabricate fibrous scaffolds include wet spinning, melt spinning, gel spinning, electroblowing, microfluidic device extrusion, template synthesis, drawing, phase-separation, and force spinning [3], [44], [61], [66], [170]. The most common method for the production of nanofibers is electrospinning, which is based on the effect of electrostatic force on liquids and is adopted for the work described in this thesis.

5.2.1 Effect of humidity

Our goal is to fabricate custom designed fibrous scaffolds for tissue engineering applications. We investigated the production of collagen fibers by electrospinning as it is biocompatible and possesses good cell adhesion properties.

In electrospinning, most of the polymer solution properties and process parameters have been well studied, however the environmental parameters including humidity and temperature are probably the ones that have been lesser studied. Based on earlier work by ourselves and others, we fabricated collagen type I fibers by electrospinning and studied the effect of environmental humidity on the resulting fiber diameter and fiber morphology.

We used an aqueous acetic acid solvent system for the preparation of the collagen solution for electrospinning as this system has been reported to allow collagen regeneration that is the least denatured compared to the more popular choice of HFIP. A collagen type I solution of 25 wt % in an aqueous acetic solution of 40 v/v% acetic acid/water was used to produce electrospun collagen fibers over a humidity range of 20 ± 5 to 55 ± 5 %. Similarly, 5 wt% collagen type I solution in HFIP was used to produce electrospun collagen fibers over a humidity range of 25 ± 5 to 40 ± 5 %.

As show in Figure 4.1 and Figure 4.3, under the electrospinning conditions used, diameter of the fibers produced falls within the range of 150 to 700 nm. The effect of humidity on fiber diameter follows a trend such that the diameter decreases monotonically with increasing humidity for both solvent systems (Figure 4.2 and Figure 4.4). These results illustrate the importance of taking the environmental parameters such as humidity into consideration to ensure experimental reproducibility. It also demonstrated that humidity is an experimental parameter that can be used to tune the diameter of the fibers that is desired for a given tissue engineering application.

There is no comparable results of humidity effect on electrospun collagen fiber in the literature. However, the trend of decreasing fiber diameter with increasing humidity is an interesting one and is comparable to that reported for the PEO – water system. This correlation could be explained in terms of collagen – acetic acid – water and collagen – HFIP - water interaction. Since both acetic acid and HFIP are miscible with water and collagen is highly hydrophilic and lyophilized collagen is soluble in acetic acid, an increase in environmental humidity of the electrospinning process serves to increase the dilution of the collagen solution with water, delaying phase separation (fiber

solidification) to allow further stretching of the liquid polymer jet in the electric field before reaching the collector electrode thus leading to a decrease in fiber diameter.

Collagen fiber morphology under various humidities are collected in Figure 4.1, Figure 4.3, Figure 4.5 and Figure 4.6. Depending on the specific humidity, fiber morphology can range from ribbons to cylindrical fibers. The difference in fiber morphology can be attributed to the solvent evaporation process at different humidity levels. At low humidity level, solvent evaporation rate would be fast, a solid fiber outlayer is formed, while the inner core is still a fluid. As the inner layer solvent evaporated diffusively through the outlayer, the overall structure collapsed to form the ribbon dog bone shape fibers (Figure 4.1 a, b, and Figure 4.3 a). While as seen in Figure 4.1 e, f and Figure 4.3 d, at higher humidity level, with sufficient time given to allow the solvent to evaporate completely before the dry fibers arrive at the collector electrode, cylindrical free standing fibers without fusion of overlapping fibers can be obtained. Further increase the humidity level, solvent evaporation may be retarded, fibers may stick to each other on the collector (Figure 5.1). Thus, the difference in solvent evaporation process determine the morphology and size of the obtained fibers.

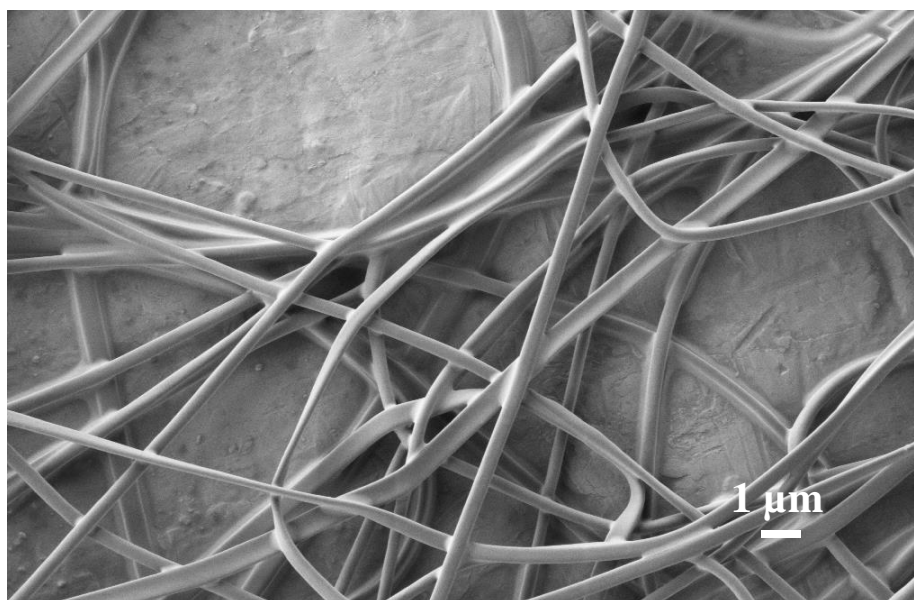


Figure 5.1. Fibers sticking to collector and with each other

The control of fiber size and morphology via humidity control allows tuning the collagen fiber diameter for an intended applications. For example, the average diameter of collagen fibril in ECM is between 10 nm to 500nm depending on the target tissue. For example, a recent report of the structure of the tympanic membrane indicated this tissue is composed of two layers of collagen fibers with diameter in a narrow range centered around 30nm. For tympanic membrane repair, it is desirable to have fibers with diameter range similar to that of the natural tissue to construct the scaffold for tympanoplasty. Our results suggest that the humidity parameter can be used advantageously to tune fiber diameters to the appropriate range for target applications such as tympanic membrane repair.

5.2.2 Other parameters

The increasing interest in using electrospinning in the field of biomedical and tissue engineering can be attributed to several factors. Electrospinning is known for its capacity to make fibrous and porous structure that are similar to natural ECM, its ability to control fiber size from micro- to nano-scale allows creating relatively large surface to volume ratio for cell adhesion [44], [49], [50], [66], [70], [84], [108]. Moreover, electrospinning is highly versatile in terms of choice of materials, spinning process parameters and resulting product qualities [63], [84].

Following previous study on the effect of humidity on fiber size and morphology, we extended our study to other parameters to demonstrate the versatility and controllability of electrospinning process.

In the interest of fiber diameter control, we have also investigated the effect of changing collagen solution concentration. The effect of solution concentration on electrospun collagen fibers were studied previously with collagen in HFIP. Collagen solution at concentrations below 5wt% and above 10wt% are either not electrospinnable to produce fibers or too viscous to allow fiber drawing from the tip of the solution droplet [129]. For collagen in 40v/v% acetic acid, by decreasing the collagen solution concentration from 25 wt% to 22 wt % and under similar electrospinning conditions and environmental humidity, average fiber diameter is decreased from around 280 nm to 85 nm (Figure 4.2

red circle). This result is consistent with other studies on effect of polymer concentration on fiber diameters [3], [64], [68], [102], [112].

The change in solution concentration directly affect solution viscosities. If the viscosity is too low with not enough polymer chain entanglement, the electrospinning process failed to be carried out, rather droplets are formed during the process (electrospraying). As shown in Figure 4.7, both beads and a mixture of beads and fibers can be formed with lower solution concentration. A reduced collagen concentration to 15 wt% resulted in a mixture fiber and beads (Figure 4.7 a), while a 10 wt% collagen solution resulted only in beads formation (Figure 4.7 b). Although electrospraying process is not the focus of this study, these collagen beads can be used as drug delivery vehicles and can either be coated or encapsulated for other tissue engineering applications.

Another parameter we explored was solution flow rate. Two flow rates (0.15 mL and 0.1 mL) were used to produce fibers at various humidity level (Figure 4.5 vs. Figure 4.6). At higher humidity level, both flow rate levels resulted in smooth fibers, while at low humidity levels, less flat ribbon fibers were seen for the higher flow rate sample (Figure 4.5 a vs. Figure 4.6 a).

The use of HFIP and acetic acid for producing collagen fibers also indicates the solvent properties can affect fiber spinning process, attributing to solvent vapor pressure and dissolution ability on the choice of material. The standard deviation of average fiber diameter in Figure 4.4 is much larger than the values shown in Figure 4.2. This difference can be attributed to the choice of solvent used in the spinning process alter the bending instability, splaying and splitting of the solution jet [147]. Compare to HFIP, acetic acid resulted in a more stable jet, the resultant fibers are more uniform with smaller fiber size variation.

These results demonstrate the versatility and controllability of electrospinning process, depends on the target applications, fibers, beads, beaded fibers, ribbon like fibers, cylindrical fibers, fibers with ranges of diameters can be achieved by adjusting the influential process parameters and choice of solvent systems. These parameters directly

affect surface to volume ratio, porosity, and fiber density, which are all important for specific target tissue regeneration.

5.3 Fiber alignment and 2D FFT

Tissue mechanical properties derive from the heterogeneous composition and anisotropic organization of the tissue's microstructure. For many tissues, including skin, ligaments, and arteries, the organization of the collagen fibrils control the tissues mechanical functionality. Consequently, in order to produce scaffolds as functional replacement tissue, it is necessary to recapitulate the tissue's organization in the engineered construct. In this work, we tried to produce aligned collagen fibers to demonstrate the feasibility of fiber alignment to mimic tissue organization.

Highly aligned collagen fibers were fabricated in this work (Figure 4.8 b). To quantify the degree of alignment, 2D FFT function converts the pixels that depict the spatial organization of the constituent fibers to mathematically defined frequency domain that maps and contains quantitative information concerning the orientation of the objects in the image [113]. The frequency plot of the 2D FFT function was used to measure relative scaffold anisotropy and identify the principal axis of the fiber orientation. By comparing the aligned fiber to random fibers, Figure 4.8 c and d demonstrate the difference between the random and aligned fibers. The degree of alignment reflected in the plot with higher the intensity and fewer occurrences of the peaks on the plot indicate that the alignment of fibers. Figure 4.8c consists of multiple peaks with various intensities while Figure 4.8 d display one peak with high intensity indicating one primary align axis exist for the Figure 4.8b and most fibers aligned along the primary axis.

To demonstrate the resemblance between aligned collagen fibers and organized tissue, the collagen fiber construct was compared to the simplest organized tissue in body, tympanic membrane. Tympanic membrane, also called ear drum, is mainly composed of two layers orthogonally aligned collagen fibers. As shown in Figure 4.9, by comparing the SEM image of a two layer orthogonal collagen fibers (Figure 4.9 b) to tympanic membrane (Figure 4.9 a) at microscopic level using 2D FFT, the two images are very similar in degree of alignment, relative position of the two layers in the double layer

structure and the amplitudes which correspond to the intensity of the fibers. Both the tympanic membrane and the electrospun scaffold possessed two distinct peaks offset by 90°, indicate the orthogonal relationship between the two layers. The similarity in peak amplitude and width suggested fiber density in electrospun collagen sample resembles that of the tympanic membrane.

Recent studies on contact surface guidance revealed that cellular orientation can be induced by substrate alignment [26], [28]–[30], [33], [42], [115], [234], [235]. Since cell alignment would induce aligned ECM deposition [119], [236], [237], by reproducing and controlling the alignment of both cells and scaffold organization, a more physiological representation of human tissues could be achieved.

5.4 Core-shell fiber

For tissue engineering applications, besides cells and scaffolds, it is desirable to encapsulate bioactive molecules such as growth factors to stimulate critical phenomena in tissue development [103]. Cell attachment, motility, proliferation, aggregation and gene expression, are all influenced by those soluble signaling proteins of varied growth factors. These bioactive molecules should be delivered in a controlled and sustained manner without loss of its bioactivity.

As previous studies have provided the basis for design and optimization of coaxial electrospinning process to control the nanostructure of core-shell composite nanofibers, coupled with morphological mimicking of the nanofiber scaffolds to the target tissue structure, we can provide both morphological and biochemical clues for the regenerating tissue [62], [103], [238].

The core-shell fibers obtained in this study have well defined core-shell structure with darker core and lighter shell in bright field TEM (Figure 4.10 a and b). The thickness of the core and shell are uniform along the fiber, the successful removal of the core material further proved the distinct boundary between the core and shell indicated no back mixing between the two materials (Figure 4.10 c and d). The versatility of coaxial electrospinning provides an alternative and simple means to encapsulate drugs. Two

components can be coaxially and simultaneously electrospun through coaxial needle. Further crosslinking of the core-shell fiber can be used to modify and determine the mechanism and rate of drugs or bioactive molecule release. Depends on the degree of crosslinking and permeability of the chemicals through shell material, drug molecules can diffuse through the shell or can be held over a period of time until release when the shell material starts to degrade or in a combination of the two mechanisms. The use of core-shell structured nanofibers for encapsulating bioactive molecules and conducting controlled release has yet to be explored.

5.5 Collagen fiber stabilization and aqueous stability

The use of collagen as a biomaterial for tissue engineering has many advantages, including being abundant and biocompatible [136]. Electrospinning has been widely used to fabricate collagen fibers to closely mimic the fibrous structure of the natural extracellular matrix [13], [239]. However, recent studies have shown that collagen does not retain its native structure and undergoes some conformation changes during electrospinning [136]. As shown in Figure 4.11 b, the solubility of collagen is drastically changed after electrospinning, the water-insoluble freeze dried collagen becomes water soluble. This change in solubility post electrospinning has been attributed to the conformation change of collagen [7], [136].

As one of the most important criteria for tissue engineering scaffold is its controlled aqueous stability in cell culture media, it is necessary to introduce crosslinks into the molecular structure of collagen to control its degradation rate and enhance its mechanical stability [25]. Hence, crosslinking has been used to stabilize the electrospun collagen mats for widening the possibility of using it in tissue regeneration and biomedical applications. The most commonly used crosslinking methods include chemical crosslinking using reagents such as aldehydes, carbodiimides, and plant extracts, physical crosslinking using dehydrothermal and UV irradiation and biological methods such as transglutaminase [25].

The use of glutaraldehyde for crosslinking of collagen has been studied extensively [3], [6], [16], [144], [174]. The reactions involved during glutaraldehyde crosslinking is very

complex and many reaction can occur during crosslinking. These crosslinking reactions introduce cytotoxic aldehyde groups into the scaffold and remain non-specifically bound to the collagen even after exhaustive rinsing [10], [14], [144], [151]. As a result, glutaraldehyde is considered to be cytotoxic as a crosslinking reagent [3], [7], [10], [25], [89], [129], [151], [153], [160].

Our group has been working with genipin, a plant extract, for electrospun collagen crosslinking extensively due to its comparatively low cytotoxicity [45], [89], [129], [131], [136], [158]. Our previous work on genipin crosslinked electrospun collagen fibers indicate genipin crosslinking would enhance fiber stability in aqueous media but with increase in average fiber diameter due to swelling [89], [129].

Another approach to crosslink collagen is via UV irradiation. Riboflavin is widely used in ophthalmic applications to enhance stroma strength through UV irradiation, while the combination of Rose Bengal and visible light for collagen crosslinking has been established for keratoconus and other ectatic disorders treatments [159], [160], [162], [240]. Since both treatments are accomplished by strengthening the collagen presented in cornea, these methods were later adapted to stabilize collagen based materials [7], [159], [160], [163], [240]. In the current study, riboflavin with UV irradiation and Rose Bengal with green light exposure were used to photochemically crosslink electrospun collagen fibers. Figure 4.12 illustrate the fiber morphology and size before and after riboflavin loading (Figure 4.12 a and b), after UV illumination (Figure 4.12 c) and post water test (Figure 4.12 d – f). Although fibers are more stable than as spun fibers, one hour aqueous stability test shows flat porous structure indicating collagen is partially dissolved and degraded within the test duration. On the other hand, Figure 4.13 a and b show SEM images of free standing fibers obtained for as spun Rose Bengal incorporated fibers, Figure 4.13 c – i show SEM images of fibers crosslinked in two different solvent systems (pure ethanol and pure isopropanol) for 22 hours followed by 24 hours of water test. By using these two solvent systems, collagen fibers maintain their fibrous structure while the rate and degree of dissolution and degradation are different. Fibers crosslinked in ethanol have porous structure (Figure 4.13 d and e) while fibers crosslinked in isopropanol have rough surface after water test. The size difference in average fiber diameter after water

uptake and the duration of fiber swelling suggested that the extent of crosslinking varies in each sample. If the degree of crosslinking is not sufficient to resist swelling, fibers will disintegrate and dissolve after prolonged water exposure.

Both chemical and photochemical crosslinking approaches result in stabilization with fairly significant fiber swelling and alteration of fiber morphology (Figure 4.12, Figure 4.13 and Figure 4.14). Moreover, these chemical approaches also has the potential of introducing cytotoxicity into the crosslinked fiber. Alternative methods that can control post stabilization swelling of the fibers and at the same time eliminate the introduction of potential cytotoxicity with the use of crosslinking chemical reagents would be highly desirable. An approach that may allow us to achieve this is via ion implantation.

Our group is one of the first to use ion implantation to modify and impart aqueous stability to polymer materials [58], [79], [195]. Although previous work use ion implantation as a secondary modification method for surface modification and material stability [58], [79], [195], our most recent work on ion implanted electrospun collagen fibers shows that ion implantation not only successfully crosslinked fibers, it also resulted least fiber swelling over 7 days [75]. In our current work, ion implantation was carried out according to a previously established procedure [75] and as shown in Figure 4.16, fibers fabricated with the same source collagen and ion implantation procedure, fiber stability is comparable to previous work. After immersed in water for 7 days, fibers show no sign of swelling. The reduction in fiber diameter can be attributed to fiber degradation over the test period. Among all the crosslinking methods used in this work, ion implantation resulted in very effective stabilization with no sign of swelling and no alternation of fiber morphology.

Our results indicate that each crosslinking method has demonstrated a different degree of structural stability, largely attributed to the different crosslinking mechanisms and degree of crosslinking. By only looking at fiber size changes, it seems ion implantation is the most effective in collagen crosslinking. However, as the fiber degradation / disintegration rate should match that of the ECM deposition rate by the cells populated on the scaffold, the degree of crosslinking or degree of stability of the fibers should be tailored

accordingly to match that of the ECM deposition rate. Thus, the choice of ideal crosslinking method should not only depend on degree of crosslinking, degree of fiber swelling and degradation, but also depend on other aspects such as the rate of degradation relative to tissue regeneration rate, functional groups on the surface of the fibers, cell compatibility and mechanical properties of the scaffolds.

The availability and variability in fiber crosslinking methods, resultant fiber morphology, size and stability provide flexibility in choosing crosslinking methods for target applications. For example, the difference in resultant fiber morphology (smooth, rough and porous) with each crosslinking method allows further tuning on fiber structure and scaffold surface area to volume ratio. The rough surface and porous fibers obtained with green light crosslinking can provide high surface area for cell adhesion and drug loading for tissue engineering and biomedical applications.

It should be also noted that fiber swelling were only tested in water in the current study. The degree of fiber swelling and fiber degradation could be much different when samples are placed in cell media such as DMEM and RPMI. The presence of salts in the cell media will change fiber solution interaction, result in different dissolution and degradation rate of the collagen protein. As shown in previous work [75], during aqueous stability test, ion implanted fibers showed higher fiber swelling in DMEM than in water. The difference in fiber swelling can be attributed to the differences in solution composition, where the ionic species present in the cell culture media can interact with the collagen molecules to promote water ingress into the fiber that lead to faster dissolution and degradation. In this work, water exposure is used to establish the feasibility of different crosslinking methods in imparting collagen crosslinking and fiber stability.

5.5.1 Change of chemical structure of ion implantation (XPS)

The successfulness of a tissue engineering scaffold largely depends on the favorable material-tissue interaction [2], [3]. Thus, the surface chemistry of biomaterials plays a significant role in determining the outcome of the tissue-scaffold interactions. With the

appropriate modification, a material's surface can be tailored to improve biocompatibility, adhesion and cell interactions [54]–[56], [58], [59].

As mentioned in the previous section, the benefit of ion implantation over other crosslinking methods includes minimum cytotoxicity with no additional chemical crosslinking agents added so that the chemical structure of the ion implanted samples should closely resemble that of the native material. During ion implantation process, the ions have energies high enough to break the chemical bonds while allowing new bonds forming. This bond breaking and reforming process leads to the crosslinking / stabilization of the structure. With the removal of chemical bonds and the formation of new bonds, chemical changes could have taken place. As nitrogen ion is an active ion species, it serves two different roles in the ion implantation process, it transfers kinetic energy to the bonds to break them allowing new bonds formation for crosslinks, and it can introduce itself into the structure during the process.

Our previous work showed N^+ implantation introduce nitrogen contain functional groups into polyvinyl alcohol (PVA) fibers, and the following cell compatibility study showed the small amount of nitrogen introduction drastically improved cell adhesion / compatibility [79]. This suggests the amount of nitrogen present in the material determines the cell adhesion/compatibility. However, our previous work on N^+ implanted electrospun collagen fibers indicated that implantation resulted in decrease in nitrogen content [75]. This is because PVA has no nitrogen present in its chemical structure, the use of N^+ resulted in the introduction of nitrogen contain groups. While collagen already have nitrogen contain groups such as amine and amide, the ion interaction can result in both nitrogen bond formation and removal. Due to the high energy of the nitrogen ions, most ions would penetrate through the samples and the bond removal is more favorable compare to the formation. Hence, nitrogen content would decrease with ion implantation. As the difference in nitrogen contents and the amount of amide in the ion implanted fibers can have important implications when being considered for tissue engineering applications, our goal is to look at the nitrogen content change, minimize the nitrogen loss and maintain the amine / amide groups for cell adhesion.

In order to understand the chemical and structural changes taking place in the ion implantation process, XPS was employed to assess the element fraction of nitrogen calculated using an assumption of depth homogeneity [241].

From the survey spectra in Figure 4.17– Figure 4.21, all samples have very similar elemental compositions (N, O, C), indicating all samples are mainly composed of protein. The bulk protein samples provide a reference for protein composition, although different treatment (e.g. electrospinning and ion implantation) may change the relative composition. The nitrogen content in native collagen is determined to be 11.6% (Figure 4.17), after ion implantation, the collagen film nitrogen content dropped to 9.6% (Figure 4.18). By dissolving the collagen in acetic acid and electrospun into fibers, the nitrogen content increased to 17.6% (Figure 4.19). The increase in nitrogen content can be attributed to dissolution process and high energy input from electrospinning, resulting in the unfolding of collagen structure, exposing more nitrogen containing groups.

With 4×10^{15} ions/cm² N⁺ implantation, the nitrogen content on the electrospun collagen reduced to 11.2% (Figure 4.20), which is very similar to native collagen (Figure 4.17). A higher dosage implantation resulted in further reduction in nitrogen content (Figure 4.21). As summarized in Table 4.3, within all the samples, as spun fibers have the highest nitrogen content and high dosage (8×10^{15} ions/cm²) implanted electrospun collagen fibers have the lowest nitrogen content.

The reduction of nitrogen content for all implanted sample can be attributed to the change of chemical structure by ion implantation, the high energy ions favor nitrogen groups removal than bonds formation. The higher ion dosage resulted more nitrogen bonds removal and higher nitrogen content loss.

We also looked at the change of chemical structure by focusing on the nitrogen peaks using high resolution XPS scans. Since peptide bonds (amide) are known to be essential for cell adhesion on substrates, one of our goals would be to maximize the amide contents on the crosslinked fibers. The high resolution XPS N1s scans are shown in Figure 4.22- Figure 4.26. Both the freeze-dried type I collagen and as-spun collagen fibers have one main peak at 400 eV representing amine/amide group (Figure 4.22 and Figure 4.24).

Comparing to the nitrogen implanted samples, low dosage ion implanted fibers maintained the main amine/amide peak with no additional peaks indicating minimum structural change (Figure 4.25). Ion implanted film and high dosage implanted fibers showed additional imide peak (Figure 4.23 and Figure 4.26), indicating the possible chemical changes introduced by implantation. Both C 1s (Figure 4.27 to Figure 4.31) and O 1s (Figure 4.32 to Figure 4.36) are used to confirm the samples have chemical structures representing functional groups in protein. The elemental analysis and high resolution XPS spectra suggest low dosage ion implantation resulted close resemblance of chemical structure between implanted fibers and freeze-dried collagen. However, when choosing a scaffold for specific tissue engineering application, other aspects such as degradability, morphology and mechanical properties should also be taking into consideration.

5.6 Mechanical properties

For many applications in the biomedical areas including tissue regeneration, three dimensional (3D) nanofibrous scaffold with controlled fiber orientation simulates the extracellular matrix (ECM) environment [42], [79], [242]. Cells which are in direct contact with the scaffold can sense and respond to the stimulation from the surrounding including mechanical stimuli [18], [18], [30], [35]. Hence, the scaffold should not only have optimal fiber diameters that mimic the structure but also have mechanical properties of the native ECM [50], [78], [154], [204], [226], [243], [244]. Since the overall property of the scaffold is determined by the organization and property of the individual fiber, and the cells are sensing individual fiber properties at the microscopic level, it is important to determine the mechanical property of single fibers that constitute the 3D scaffold [245][246][152], [159], [169], [172]. As the fibers produced in this work is in the submicron range, conventional method cannot be used to measure fiber properties and nanofiber properties can be significantly different from their macroscopic counterparts as the fiber size is reduced to the nanoscale[79], [149], [172], [180], [191], [193], [196], [199].

During AFM measurements, each fiber was treated as an individually isolated sample and measured independently, thus there is no standard deviation on the modulus

measurements [74], [190], [200], [219], [247]–[249] Although the as spun collagen fibers have comparatively high Young's modulus (Figure 4.38), by adding photoinitiators into the fiber, the fiber modulus reduced by a factor of 10 (Figure 4.40). Similar effects due to inclusion of other components resulted in reduced overall composite stiffness was observed in other studies and were attributed to the difference in loading and aspect ratios of reinforced components [185], [196], [209], [250]. After visible light crosslinking, fiber size drastically reduced due to the depletion of the photoinitiators, while the overall mechanical properties remained similar to those prior to crosslinking (Figure 4.41). On the other hand, genipin crosslinking resulted in fiber swelling while the overall Young's modulus of the fibers remained similar to the as spun fiber (Figure 4.42).

It was suggested that the mechanical properties of electrospun collagen nanofibers can be adjusted by controlling the crosslinking parameters. For genipin crosslinking and visible light crosslinking, concentration of the crosslinker and reaction / irradiation time and energy of the LED would affect the overall degree of crosslinking. Similarly, for ion implantation, it was expected the change of ion dosage and ion current would affect the degree of crosslinking, thus the mechanical properties of the fibers. However, as seen for ion implanted electrospun nanofibers, no significant difference was observed on mechanical properties between two ion dosages (Figure 4.43). This result contradicts with previous work ion implanted electrospun PVA fibers where increase in nitrogen ion dosage increased PVA fiber average elasticity [79]. However, taking the average of the fiber elasticity can be misleading as we observed size dependence on fiber properties. Depends on the number of fibers taken in the ranges of fiber size, the average fiber elasticity can be skewed towards smaller fibers with higher elasticities. The overlapping of the sets of data provides a more direct comparison between the samples and showed the consistency and matching of fiber elasticities with various treatments.

Although acetic acid was suggested as an alternative to HFIP with less collagen denaturation, no mechanical property variation was observed in the Young's modulus of fibers spun with acetic acid of HFIP (Figure 4.44). This could be attributed to the vigorous electrospinning process where most of the solvent should be evaporated by the

time fibers reach to the collector, small or no solvent residue was left in the fibers. The fiber structure and properties remain similar regardless of the type of solvent being used.

Table 5.1. Summary comparison of collagen Young's moduli

Papers	Collagen fibers	Conditions	Range of diameters (nm)	Moduli
Yang et al. [87]	Electrospun type I collagen Non crosslinked	dry	179-356	1.4-7.5 Gpa
Yang et al. [87]	Electrospun type I collagen Glutaldehyde crosslinked	dry	191-450	1.3-7.8 GPa
Yang et al. [87]	Electrospun type I collagen Glutaldehyde crosslinked	PBS buffer	210-425	0.07-0.26 GPa
Carlisle et al. [149]	Electrospun type I collagen	dry	180-800	0.1-10 Gpa
Yang et al. [192]	Native type I bovine Achilles tendon	dry	200-300	1.0-3.9 GPa
Yang et al. [192]	Native type I bovine Achilles tendon	PBS buffer	200-300	0.07-0.17 GPa
Graham et al. [229]	<i>In vitro</i> assembled type I collagen fibril from human fibroblasts	dry	10-30	32 mPa
Eppell et al. [246]	Single type I collagen fibrils from sea cucumber	hydrated	10-500	550 mPa
This work	Electrospun type I collagen as spun	dry	60 - 280	2.33-51.68 GPa
This work	Electrospun type I collagen genipin crosslinked	dry	71-667	0.01-61.98 GPa
This work	Electrospun type I collagen + Rose Bengal	dry	227-642	0.07-15.62 GPa
This work	Electrospun type I collagen 520nm crosslinked	dry	110-270	0.93 – 36 GPa
	Electrospun type I collagen ion implantation	dry	72- 680	0.1 – 174 GPa

The young's moduli of collagen from literature are summarized in Table 5.1. Yang et al. performed AFM bending tests on electrospun collagen fibers to obtain bending and shear moduli c . The Young's modulus was found to be between 1.4 and 7.5 GPa. These values are significantly lower than the moduli obtained from the as spun fibers in the current study. This could be attributed to a different collagen source (type I collagen from calf skin) of the fibers. Another study performed on collagen fibrils from bovine Achilles tendon measured a Young's moduli of 1.0 to 3.9 GPa with fiber diameters of 187-305 nm [192]. In both works, it was observed that the bending modulus increased as the fiber diameter decreased. A similar trend was observed by other groups on single electrospun collagen type I fiber, where a modulus between 0.1 and 10 GPa was measured [149]. Graham et al. stretched in vitro assembled type I collagen fiber obtained from human fibroblasts using the AFM and obtained a Young's modulus of 32 MPa [229]. Feijen's group carried out several studies on the mechanical properties of native collagen fibers and found a modulus of about 1-7 GPa [87], [251]. Compared to previously published studies [87], [149], [192], the electrospun type I collagen fibers obtained in this study have mechanical properties similar to native collagen fibers. For each set of data, there also seem to be a size dependence on mechanical properties.

Yang et al. performed mechanical testing on electrospun collagen fibers and native collagen fibrils in both dry and wet conditions [87], [192]. The Young's modulus obtained in PBS is ten times smaller than the ones in dry condition. The difference of Young's modulus in dry and wet condition indicates the crosslinked fibers may resemble different mechanical characteristics in physiological relevant conditions such as PBS. As previous section indicated fiber morphology and sizes change in aqueous condition, the mechanical properties can be quite different among the crosslinking treatments.

The variation of fiber mechanical properties among different crosslinking treatments suggest that we can chose and adjust our crosslinking system to obtain fiber properties in a wide range to accommodate different mechanical needs and provide cells with various degree of mechanical stimuli.

5.7 Cell compatibility

The purpose of a tissue engineering scaffold is to replace and repair damaged tissues, the scaffold-cell interaction determines the effectiveness of the scaffold. To evaluate the performance of the scaffold, it is important to determine the cell-scaffold interaction in vitro. Cell compatibility tests were performed on crosslinked electrospun fibers.

Human fetal lung (IMR-90) cell line were seeded on crosslinked electrospun collagen fibers for up to 7 days. As shown in Figure 4.46, cells show good adhesion and spread out in all directions on chemical and photochemical crosslinked and ion implanted samples. The highly involvement and entanglement of filopodia with fibers (Figure 4.47) indicating the role of filopodia in topography sensing thus directing cell migration and enable cell orientation [252]. As indicated in Figure 4.46 and Figure 4.48 b, the majority of cells showed typical spindle-shaped with abundant filopodia formation [253]. The observed filopodia were extended towards all directions on the surface of the samples (Figure 4.47 and Figure 4.48 a), implying that these cells were actively exploring the surrounding surfaces before migrating [252]. Partridge and Marcantonio verified that filopodia containing both integrin and actin formed the initial cell-matrix contacts and further generated mature focal adhesions [254].

By observing the surface area coverage with cells in Figure 4.49, photochemical crosslinked resulted in highest surface area coverage. By day 7, the surface coverage reaches 70 – 80% confluence, which is similar to cell propagated on cell culture plates. Genipin crosslinking resulted in the lowest surface area coverage. The low cell coverage combined with our previous work on hydrogel/ fiber composite on neural stem cell fate suggests that although genipin is considered to have much reduced cytotoxicity compare to glutaraldehyde, it may still impair biocompatibility of the crosslinked scaffold [158].

Although ion implantation resulted moderate surface area coverage compared to Rose Bengal incorporated photochemical crosslinking, physical crosslinking best preserved fiber morphology with least change in fiber size over seven days cell growth. The ion implanted fibers are the most stable with least swelling among all samples. Along with the XPS results indicating the lower carbonization level with lower dosage implantation,

low dosage N^+ implantation should be the most desirable based on its stability and biocompatibility.

To mimic the three-dimensional (3D) environment of natural tissues, aligned electrospun collagen fibers were prepared and crosslinked with ion implantation. These fibers were approximately 120 nm in diameter and comprised the aligned topographical features on the scaffold surface. After IMR-90 seeded on the fibers for 1 day, the cells are deformed to align along the fiber direction (Figure 5.2).



Figure 5.2 IMR 90 seeded on N^+ implanted aligned fibers for 24 hours.

Similar results have been demonstrated by several other studies. Works have been done to investigate the influences of feature alignment on cell alignment, Lowe et al. found that dermal fibroblasts aligned and extended in the direction of the larger, aligned scaffold features [122], Yang et al. seeded stem cells onto oriented nano- and microfibers of PLLA and found that the direction of cellular elongation and neurite outgrowth was parallel to the direction of PLLA fibers [255]. Schnell et al. found that collagen containing PCL fibers provided an excellent scaffold for Schwann cell migration and growth while the cells approximately obeyed the directionality of the underlying

nanofibers [235]. Combined with our current result where IMR90 elongated along the fiber alignment direction, it is reasonable to believe the topographical cues presented by aligned fibers were sufficient to orientated contacted cells. The aligned cells would induce aligned extracellular matrix deposition, which is critical for generating functional tissues.

6 Conclusion

Since many tissues possess highly organized structure, it is necessary to have the structure of the tissue engineering scaffold to closely resemble that of the tissue it is replacing. An example is the tympanic membrane or ear drum, the fibrous structure of the ECM consists of collagen fibers arranged in organized orientations. In this work, we aimed at developing scaffold consisting electrospun collagen fibers that mimic the chemical, structural, organization and mechanical aspects of the native ECM. The electrospun fibers were successfully produced in both random and organized orientation by electrospinning and various parameters were adjusted to tune the fiber morphology and diameters. As electrospun collagen fibers are unstable in aqueous environment, chemical, photochemical crosslinking and ion implantation were performed to impart aqueous stability into the collagen fibers. Our aqueous stability tests demonstrated improved fiber stability in water and it is possible to obtain fibers with different structure and morphologies to increase scaffold surface area for cell adhesion and drug loading. Not only the nanofibers have unique mechanical properties from its bulk counterparts at the submicron scale, but also the mechanical properties of individual fibers can be adjusted by different crosslinking methods. In vitro cell compatibility assessment indicated good adhesion and spreading of the IMR 90 fibroblasts. Rose Bengal and green light crosslinked samples resulted highest surface coverage of the cells while aligned fibers treated with N^+ beam induced the cell morphology deformation and cell alignment along the fiber.

The results in this study demonstrate that it is possible to control fiber size, morphology, structure, stability, degradation and mechanical properties through the versatile electrospinning and crosslinking process. By adjusting electrospinning parameters and crosslinking conditions, scaffolds with tunable structures and properties can serve as a great candidate for next generation of implantable medical device and tissue engineering scaffolds.

7 Future work

A successful tissue engineering scaffold should be able to fill the tissue void, provide structural support and to deliver appropriate bioactive signals to direct and promote cells to form tissues within the body upon implantation.

Our work has demonstrated the ability to create scaffold that can mimic native tissue environment in terms of structural, morphological, chemical and mechanical aspects, carry and encapsulate molecules for delivery applications and good cell adhesion properties.

Collagen scaffold is biodegradable and it serves as a temporary templates for cell seeding, proliferation and growth prior to the regeneration of nature ECM, thus, the scaffold degradation rate should match the ECM deposition rate of the target tissue. In the future, the fiber stability tests should be conducted in physiological conditions such as PBS, cell culture media in addition to water. And it is also necessary to perform degradation test to determine and tune the degradation rate of the scaffold to match that of the target tissue regeneration rate.

To demonstrate bioactive molecule encapsulation and control delivery, growth factors should be encapsulated and a controlled release study should be carried out to determine the release rate of the bioactive molecules. By determining the release mechanism and kinetics, crosslinking condition can be adjusted accordingly to delivery appropriate cellular signals efficiently.

Although our work indicated good cell adhesion, this study is very preliminary in terms of determine cell compatibility. More detailed cell compatibility studies are necessary to ascertain our current results.

In our current work, fiber mechanical properties were determined under ambient conditions in air. For tissue engineering applications, scaffolds will be used in a physiological relevant environment consists of an aqueous fluid, cell behavior will be depending on the fibers' "wet" mechanical properties. For both in vivo and in vitro

studies, it is necessary to determine mechanical properties of these scaffolds in fluid such as PBS or cell culture media.

Reference

- [1] D. Howard, L. D. Buttery, K. M. Shakesheff, and S. J. Roberts, "Tissue engineering: Strategies, stem cells and scaffolds," *J. Anat.*, vol. 213, no. 1, pp. 66–72, 2008.
- [2] B. P. Chan and K. W. Leong, "Scaffolding in tissue engineering: General approaches and tissue-specific considerations," *Eur. Spine J.*, vol. 17, no. SUPPL. 4, 2008.
- [3] S. Khorshidi *et al.*, "A review of key challenges of electrospun scaffolds for tissue-engineering applications," *Journal of Tissue Engineering and Regenerative Medicine*, vol. 10, no. 9. 2016.
- [4] D. R. Eyre and J. J. Wu, "Collagen cross-links," *Top. Curr. Chem.*, vol. 247, pp. 207–229, 2005.
- [5] a Gaspar, L. Moldovan, D. Constantin, a M. Stanciuc, P. M. Sarbu Boeti, and I. C. Efrimescu, "Collagen-based scaffolds for skin tissue engineering.," *J. Med. Life*, vol. 4, no. 2, pp. 172–7, May 2011.
- [6] R. Parenteau-Bareil, R. Gauvin, and F. Berthod, "Collagen-based biomaterials for tissue engineering applications," *Materials (Basel)*, vol. 3, no. 3, pp. 1863–1887, 2010.
- [7] T. Liu, W. K. Teng, B. P. Chan, and S. Y. Chew, "Photochemical crosslinked electrospun collagen nanofibers: Synthesis, characterization and neural stem cell interactions," *J. Biomed. Mater. Res. Part A*, vol. 95A, no. 1, pp. 276–282, 2010.
- [8] S. Baker *et al.*, "The mechanical properties of dry, electrospun fibrinogen fibers," *Mater. Sci. Eng. C*, vol. 32, no. 2, pp. 215–221, 2012.
- [9] A. Elamparithi, A. M. Punnoose, and S. Kuruvilla, "Electrospun type 1 collagen matrices preserving native ultrastructure using benign binary solvent for cardiac tissue engineering.," *Artif. cells, nanomedicine, Biotechnol.*, vol. 1401, no. January

2016, pp. 1–8, 2015.

- [10] A. Fiorani *et al.*, “Comparative performance of collagen nanofibers electrospun from different solvents and stabilized by different crosslinkers,” *J. Mater. Sci. Mater. Med.*, vol. 25, no. 10, pp. 2313–2321, 2014.
- [11] J. Bürck *et al.*, “Resemblance of electrospun collagen nanofibers to their native structure,” *Langmuir*, vol. 29, no. 5, pp. 1562–1572, 2013.
- [12] D. G. Simpson *et al.*, “Electrospun collagen: A tissue engineering scaffold with unique functional properties in a wide variety of applications,” *J. Nanomater.*, vol. 2011, 2011.
- [13] L. Buttafoco *et al.*, “Electrospinning of collagen and elastin for tissue engineering applications,” *Biomaterials*, vol. 27, no. 5, pp. 724–734, 2006.
- [14] B. Dong, O. Arnoult, M. E. Smith, and G. E. Wnek, “Electrospinning of Collagen Nanofiber Scaffolds from Benign Solvents,” *Macromol. Rapid Commun.*, vol. 30, no. 7, pp. 539–542, 2009.
- [15] N. H. Fujiwara, D. F. Kallmes, S.-T. Li, H.-B. Lin, and K. D. Hagspiel, “Type 1 collagen as an endovascular stent-graft material for small-diameter vessels: a biocompatibility study,” *J. Vasc. Interv. Radiol.*, vol. 16, no. 9, pp. 1229–36, 2005.
- [16] J. A. Matthews, G. E. Wnek, D. G. Simpson, and G. L. Bowlin, “Electrospinning of collagen nanofibers,” *Biomacromolecules*, vol. 3, no. 2, pp. 232–238, 2002.
- [17] G. Charras and E. Sahai, “Physical influences of the extracellular environment on cell migration,” *Nat. Rev. Mol. Cell Biol.*, vol. 15, no. 12, pp. 813–824, Oct. 2014.
- [18] B. M. Baker *et al.*, “Cell-mediated fibre recruitment drives extracellular matrix mechanosensing in engineered fibrillar microenvironments,” *Nat. Mater.*, vol. 14, no. 12, pp. 1262–1268, 2015.

- [19] B. N. Mason, J. P. Califano, and C. A. Reinhart-king, “Engineering Biomaterials for Regenerative Medicine,” pp. 19–38, 2012.
- [20] P. Lu, K. Takai, V. M. Weaver, and Z. Werb, “Extracellular matrix degradation and remodeling in development and disease,” *Cold Spring Harb Perspect Biol*, vol. 3, no. 12, pp. 1–24, 2011.
- [21] T. Koide, “Triple helical collagen-like peptides: Engineering and applications in matrix biology,” *Connect. Tissue Res.*, vol. 46, no. 3, pp. 131–141, 2005.
- [22] S. A. Sell, P. S. Wolfe, K. Garg, J. M. McCool, I. A. Rodriguez, and G. L. Bowlin, “The use of natural polymers in tissue engineering: A focus on electrospun extracellular matrix analogues,” *Polymers (Basel)*, vol. 2, no. 4, pp. 522–553, 2010.
- [23] T. J. Wess, “Collagen fibrillar structure and hierarchies,” *Collagen Struct. Mech.*, pp. 49–80, 2008.
- [24] H. Fernandes, L. Moroni, C. Van Blitterswijk, and J. De Boer, “Extracellular matrix and tissue engineering applications,” *J. Mater. Chem.*, vol. 19, no. 31, pp. 5474–5484, 2009.
- [25] L. M. Delgado, Y. Bayon, A. Pandit, and D. I. Zeugolis, “To cross-link or not to cross-link? Cross-linking associated foreign body response of collagen-based devices,” *Tissue Eng. Part B. Rev.*, vol. 21, no. 3, pp. 298–313, 2015.
- [26] A. I. Teixeira, “Epithelial contact guidance on well-defined micro- and nanostructured substrates,” *J. Cell Sci.*, vol. 116, no. 10, pp. 1881–1892, 2003.
- [27] R. B. Dickinson, S. Guido, and R. T. Tranquillo, “Biased cell migration of fibroblasts exhibiting contact guidance in oriented collagen gels,” *Ann. Biomed. Eng.*, vol. 22, no. 4, pp. 342–356, 1994.
- [28] P. P. Provenzano, D. R. Inman, K. W. Eliceiri, S. M. Trier, and P. J. Keely, “Contact Guidance Mediated Three-Dimensional Cell Migration is Regulated by

- Rho/ROCK-Dependent Matrix Reorganization,” *Biophys. J.*, vol. 95, no. 11, pp. 5374–5384, 2008.
- [29] J. Meyle, K. Gültig, M. Brich, H. Hämmerle, and W. Nisch, “Contact guidance of fibroblasts on biomaterial surfaces,” *J. Mater. Sci. Mater. Med.*, vol. 5, no. 6–7, pp. 463–466, 1994.
- [30] M. K. Driscoll, X. Sun, C. Guven, J. T. Fourkas, and W. Losert, “Cellular contact guidance through dynamic sensing of nanotopography,” *ACS Nano*, vol. 8, no. 4, pp. 3546–3555, 2014.
- [31] F. Grinnell, “Fibroblast biology in three-dimensional collagen matrices,” *Trends Cell Biol.*, vol. 13, no. 5, pp. 264–269, May 2003.
- [32] F. Grinnell, Chin-Han Ho, E. Tamariz, D. J. Lee, and G. Skuta, “Dendritic Fibroblasts in Three-dimensional Collagen Matrices,” *Mol. Biol. Cell*, vol. 14, no. February, pp. 384–395, 2003.
- [33] C. Londono *et al.*, “Nonautonomous contact guidance signaling during collective cell migration,” *Proc. Natl. Acad. Sci.*, vol. 111, no. 5, pp. 1807–1812, 2014.
- [34] C. Y. Xu, R. Inai, M. Kotaki, and S. Ramakrishna, “Aligned biodegradable nanofibrous structure: A potential scaffold for blood vessel engineering,” *Biomaterials*, vol. 25, no. 5, pp. 877–886, 2004.
- [35] D. E. Discher, P. Janmey, and Y.-L. Wang, “Tissue cells feel and respond to the stiffness of their substrate.,” *Science*, vol. 310, pp. 1139–1143, 2005.
- [36] T. Yeung *et al.*, “Effects of substrate stiffness on cell morphology, cytoskeletal structure, and adhesion,” *Cell Motil. Cytoskeleton*, vol. 60, no. 1, pp. 24–34, 2005.
- [37] E. S. Place, J. H. George, C. K. Williams, and M. M. Stevens, “Synthetic polymer scaffolds for tissue engineering,” *Chem. Soc. Rev.*, vol. 38, no. 4, pp. 1139–51, Apr. 2009.

- [38] P. B. Warren, P. Huebner, J. T. Spang, R. A. Shirwaiker, and M. B. Fisher, “Engineering 3D-Bioplotted scaffolds to induce aligned extracellular matrix deposition for musculoskeletal soft tissue replacement,” *Connect. Tissue Res.*, vol. 00, no. 00, pp. 1–13, Dec. 2016.
- [39] H. Aubin *et al.*, “Directed 3D cell alignment and elongation in microengineered hydrogels,” *Biomaterials*, vol. 31, no. 27, pp. 6941–6951, 2010.
- [40] C. Mota *et al.*, “Multiscale fabrication of biomimetic scaffolds for tympanic membrane tissue engineering,” *Biofabrication*, vol. 7, no. 2, p. 025005, 2015.
- [41] H. Zhang, C. Zhao, Y. Zhao, G. Tang, and X. Yuan, “Electrospinning of ultrafine core/shell fibers for biomedical applications,” *Sci. China Chem.*, vol. 53, no. 6, pp. 1246–1254, Jun. 2010.
- [42] J. Yan *et al.*, “Effect of fiber alignment in electrospun scaffolds on keratocytes and corneal epithelial cells behavior,” *J. Biomed. Mater. Res. Part A*, vol. 100A, no. 2, pp. 527–535, Feb. 2012.
- [43] E. S. Place, N. D. Evans, and M. M. Stevens, “Complexity in biomaterials for tissue engineering,” *Nat. Mater.*, vol. 8, no. 6, pp. 457–70, Jun. 2009.
- [44] J. Lannutti, D. Reneker, T. Ma, D. Tomasko, and D. Farson, “Electrospinning for tissue engineering scaffolds,” *Mater. Sci. Eng. C*, vol. 27, no. 3, pp. 504–509, 2007.
- [45] N. G. Rim, C. S. Shin, and H. Shin, “Current approaches to electrospun nanofibers for tissue engineering,” *Biomed. Mater.*, vol. 8, no. 1, p. 014102, Jan. 2013.
- [46] F. J. O’Brien, B. a Harley, M. a Waller, I. V Yannas, L. J. Gibson, and P. J. Prendergast, “The effect of pore size on permeability and cell attachment in collagen scaffolds for tissue engineering,” *Technol. Health Care*, vol. 15, no. 1, pp. 3–17, Jan. 2007.
- [47] M. M. Stevens and J. H. George, “Exploring and engineering the cell surface

- interface.,” *Science*, vol. 310, no. 5751, pp. 1135–8, Nov. 2005.
- [48] R. Nayak, R. Padhye, I. L. Kyratzis, Y. B. Truong, and L. Arnold, “Recent advances in nanofibre fabrication techniques,” *Text. Res. J.*, vol. 82, no. 2, pp. 129–147, 2012.
- [49] Q. P. Pham, U. Sharma, and A. G. Mikos, “Electrospinning of Polymeric Nanofibers for Tissue Engineering Applications: A Review,” *Tissue Eng.*, vol. 0, no. 0, p. 060509065116001, 2006.
- [50] N. Bhardwaj and S. C. Kundu, “Electrospinning: A fascinating fiber fabrication technique,” *Biotechnol. Adv.*, vol. 28, no. 3, pp. 325–347, 2010.
- [51] D. W. Hutmacher, “Scaffolds in tissue engineering bone and cartilage.,” *Biomaterials*, vol. 21, no. 24, pp. 2529–43, Dec. 2000.
- [52] P. Martin, “Wound Healing--Aiming for Perfect Skin Regeneration,” *Science (80-.)*, vol. 276, no. 5309, pp. 75–81, Apr. 1997.
- [53] H.-T. Hu, S.-Y. Lee, C.-C. Chen, Y.-C. Yang, and J.-C. Yang, “Processing and properties of hydrophilic electrospun polylactic acid/beta-tricalcium phosphate membrane for dental applications,” *Polym. Eng. Sci.*, vol. 53, no. 4, pp. 833–842, Apr. 2013.
- [54] D. J. Li, F. Z. Cui, and H. Q. Gu, “F⁺ Ion implantation induced cell attachment on intraocular lens,” *Biomaterials*, vol. 20, no. 20, pp. 1889–1896, 1999.
- [55] M. Kusakabe *et al.*, “Control of Endothelial Cell Adhesion to Polymer Surface by Ion Implantation,” vol. 460, no. February 2000, pp. 6–7, 2001.
- [56] K. Kurotobi, Y. Suzuki, H. Nakajima, H. Suzuki, and M. Iwaki, “Platelet adhesion and plasma protein adsorption control of collagen surfaces by He⁺ ion implantation,” *Nucl. Instruments Methods Phys. Res. Sect. B Beam Interact. with Mater. Atoms*, vol. 206, pp. 532–537, 2003.

- [57] A. Tuross, J. Jagielski, L. Slusarski, and N. K. Madi, "Ion beam modification of surface properties of polyethylene," *Vacuum*, vol. 70, pp. 201–206, 2003.
- [58] K. K. Ho Wong, M. Zinke-Allmang, and W. Wan, "N⁺ surface doping on nanoscale polymer fabrics via ion implantation," *Nucl. Instruments Methods Phys. Res. Sect. B Beam Interact. with Mater. Atoms*, vol. 249, no. 1–2 SPEC. ISS., pp. 362–365, 2006.
- [59] K. H. Wong, M. Zinke-Allmang, W. K. Wan, J. Z. Zhang, and P. Hu, "Low energy oxygen ion beam modification of the surface morphology and chemical structure of polyurethane fibers," *Nucl. Instruments Methods Phys. Res. Sect. B Beam Interact. with Mater. Atoms*, vol. 243, pp. 63–74, 2006.
- [60] M. Guenther, K. Sahre, G. Suchanek, G. Gerlach, and K. J. Eichhorn, "Influence of ion-beam induced chemical and structural modification in polymers on moisture uptake," *Surf. Coatings Technol.*, vol. 142–144, pp. 482–488, 2001.
- [61] Y. Li and W. Wan, "Exploring Polymer Nanofiber Mechanics: A review of the methods for determining their properties.," *IEEE Nanotechnol. Mag.*, vol. 11, no. 3, pp. 16–28, Sep. 2017.
- [62] Y. Li *et al.*, "Optimization of the Electrospinning Process for Core–Shell Fiber Preparation," *J. Biomater. Tissue Eng.*, vol. 4, no. 11, pp. 973–980, Nov. 2014.
- [63] D. Rodoplu and M. Mutlu, "Effects of electrospinning setup and process parameters on nanofiber morphology intended for the modification of quartz crystal microbalance surfaces," *J. Eng. Fiber. Fabr.*, vol. 7, no. 2, pp. 118–123, 2012.
- [64] C. J. Thompson, G. G. Chase, a. L. Yarin, and D. H. Reneker, "Effects of parameters on nanofiber diameter determined from electrospinning model," *Polymer (Guildf.)*, vol. 48, no. 23, pp. 6913–6922, Nov. 2007.
- [65] A. Haider, S. Haider, and I. K. Kang, "A comprehensive review summarizing the effect of electrospinning parameters and potential applications of nanofibers in

- biomedical and biotechnology,” *Arabian Journal of Chemistry*. 2015.
- [66] A. Frenot and I. S. Chronakis, “Polymer nanofibers assembled by electrospinning,” *Curr. Opin. Colloid Interface Sci.*, vol. 8, no. 1, pp. 64–75, Mar. 2003.
- [67] V. Beachley and X. Wen, “Effect of electrospinning parameters on the nanofiber diameter and length,” *Mater. Sci. Eng. C. Mater. Biol. Appl.*, vol. 29, no. 3, pp. 663–668, Apr. 2009.
- [68] C. L. Casper, J. S. Stephens, N. G. Tassi, D. B. Chase, and J. F. Rabolt, “Controlling surface morphology of electrospun polystyrene fibers: Effect of humidity and molecular weight in the electrospinning process,” *Macromolecules*, vol. 37, no. 2, pp. 573–578, 2004.
- [69] S. Tripatanasuwan, Z. Zhong, and D. H. Reneker, “Effect of evaporation and solidification of the charged jet in electrospinning of poly(ethylene oxide) aqueous solution,” *Polymer (Guildf.)*, vol. 48, no. 19, pp. 5742–5746, 2007.
- [70] D. H. Reneker and A. L. Yarin, “Electrospinning jets and polymer nanofibers,” *Polymer (Guildf.)*, vol. 49, no. 10, pp. 2387–2425, May 2008.
- [71] D. Li, J. T. McCann, Y. Xia, and M. Marquez, “Electrospinning: A Simple and Versatile Technique for Producing Ceramic Nanofibers and Nanotubes,” *J. Am. Ceram. Soc.*, vol. 89, no. 6, pp. 1861–1869, Jun. 2006.
- [72] A. Stanishevsky, S. Chowdhury, P. Chinoda, and V. Thomas, “Hydroxyapatite nanoparticle loaded collagen fiber composites: Microarchitecture and nanoindentation study,” *J. Biomed. Mater. Res. Part A*, vol. 86A, no. 4, pp. 873–882, Sep. 2008.
- [73] M. G. McKee, G. L. Wilkes, R. H. Colby, and T. E. Long, “Correlations of Solution Rheology with Electrospun Fiber Formation of Linear and Branched Polyesters,” *Macromolecules*, vol. 37, no. 5, pp. 1760–1767, Mar. 2004.

- [74] S. Curgul, K. J. Van Vliet, and G. C. Rutledge, "Molecular Dynamics Simulation of Size-Dependent Structural and Thermal Properties of Polymer Nanofibers," *Macromolecules*, vol. 40, no. 23, pp. 8483–8489, Nov. 2007.
- [75] N. Sharma, "Electrospun nanofibers for tissue engineering," 2017.
- [76] N. Khan, "Applications of electrospun nanofibers in the biomedical field," vol. 5, no. 2, pp. 63–73, 2012.
- [77] R. D. Blank and A. L. Boskey, "Genetic collagen diseases: Influence of collagen mutations on structure and mechanical behavior," *Collagen Struct. Mech.*, pp. 447–474, 2008.
- [78] T. J. Sill and H. A. von Recum, "Electrospinning: applications in drug delivery and tissue engineering.," *Biomaterials*, vol. 29, no. 13, pp. 1989–2006, May 2008.
- [79] K. K. H. Wong, J. L. Hutter, M. Zinke-Allmann, and W. Wan, "Physical properties of ion beam treated electrospun poly(vinyl alcohol) nanofibers," *Eur. Polym. J.*, vol. 45, no. 5, pp. 1349–1358, May 2009.
- [80] S. Chan, H. Yang, F. Ko, C. Ayranci, S. Basu, and A. Note, "Tensile Stress-Strain Response of Small-diameter Electrospun Fibers," *Appl. Note*, pp. 1–4, 2012.
- [81] F. Croisier *et al.*, "Mechanical testing of electrospun PCL fibers," *Acta Biomater.*, vol. 8, no. 1, pp. 218–224, Jan. 2012.
- [82] D. Liang, B. S. Hsiao, and B. Chu, "Functional electrospun nanofibrous scaffolds for biomedical applications.," *Adv. Drug Deliv. Rev.*, vol. 59, no. 14, pp. 1392–412, Dec. 2007.
- [83] S. A. Theron, E. Zussman, and A. L. Yarin, "Experimental investigation of the governing parameters in the electrospinning of polymer solutions," *Polymer (Guildf)*, vol. 45, no. 6, pp. 2017–2030, Mar. 2004.
- [84] S. Saehana, F. Iskandar, and M. Abdullah, "Optimization of Electrospinning

- Parameter by Employing Genetic Algorithm in Order to Produce Desired Nanofiber Diameter,” *Int. J. Chem. Nucl. Metall. Mater. Eng.*, no. 1, pp. 78–83, 2013.
- [85] R. M. Nezarati, M. B. Eifert, and E. Cosgriff-Hernandez, “Effects of humidity and solution viscosity on electrospun fiber morphology,” *Tissue Eng. Part C. Methods*, vol. 19, no. 10, pp. 810–9, Oct. 2013.
- [86] a. Subbotin, R. Stepanyan, a. Chiche, J. J. M. Slot, and G. ten Brinke, “Dynamics of an electrically charged polymer jet,” *Phys. Fluids*, vol. 25, no. 10, p. 103101, 2013.
- [87] L. Yang, C. F. C. Fitié, K. O. van der Werf, M. L. Bennink, P. J. Dijkstra, and J. Feijen, “Mechanical properties of single electrospun collagen type I fibers,” *Biomaterials*, vol. 29, no. 8, pp. 955–962, 2008.
- [88] O. Hardick, B. Stevens, and D. G. Bracewell, “Nanofibre fabrication in a temperature and humidity controlled environment for improved fibre consistency,” *J. Mater. Sci.*, vol. 46, no. 11, pp. 3890–3898, 2011.
- [89] Y. Li, J. Liu, J. R. De Bruyn, W. Wan, J. R. de Bruyn, and W. Wan, “Optimization of the Electrospinning Process for Core – Shell Fiber Preparation,” *J. Biomater. Tissue Engineerng*, vol. 4, no. 11, pp. 973–980, Nov. 2014.
- [90] A. G. Kanani and S. H. Bahrami, “Effect of Changing Solvents on Poly (ϵ - Caprolactone) Nanofibrous Webs Morphology,” vol. 2011, 2011.
- [91] K. S. Rho *et al.*, “Electrospinning of collagen nanofibers: Effects on the behavior of normal human keratinocytes and early-stage wound healing,” *Biomaterials*, vol. 27, no. 8, pp. 1452–1461, 2006.
- [92] X. Geng, O.-H. Kwon, and J. Jang, “Electrospinning of chitosan dissolved in concentrated acetic acid solution,” *Biomaterials*, vol. 26, no. 27, pp. 5427–32, Sep. 2005.

- [93] B. Ghorani, S. J. Russell, and P. Goswami, "Controlled Morphology and Mechanical Characterisation of Electrospun Cellulose Acetate Fibre Webs," *Int. J. Polym. Sci.*, vol. 2013, pp. 1–12, 2013.
- [94] H. Homayoni, S. A. H. Ravandi, and M. Valizadeh, "Electrospinning of chitosan nanofibers: Processing optimization," *Carbohydr. Polym.*, vol. 77, no. 3, pp. 656–661, Jul. 2009.
- [95] H. Liu and C. Tang, "Electrospinning of Cellulose Acetate in Solvent Mixture N,N-Dimethylacetamide (DMAc)/Acetone," *Polym. J.*, vol. 39, no. 1, pp. 65–72, Dec. 2006.
- [96] Q. Iqbal, P. Bernstein, Y. Zhu, J. Rahamim, P. Cebe, and C. Staii, "Quantitative analysis of mechanical and electrostatic properties of poly(lactic) acid fibers and poly(lactic) acid—carbon nanotube composites using atomic force microscopy," *Nanotechnology*, vol. 26, no. 10, p. 105702, Mar. 2015.
- [97] S. Tungprapa *et al.*, "Electrospun cellulose acetate fibers: effect of solvent system on morphology and fiber diameter," *Cellulose*, vol. 14, no. 6, pp. 563–575, Mar. 2007.
- [98] S. C. Chen, X. B. Huang, X. M. Cai, J. Lu, J. Yuan, and J. Shen, "The influence of fiber diameter of electrospun poly(lactic acid) on drug delivery," *Fibers Polym.*, vol. 13, no. 9, pp. 1120–1125, Nov. 2012.
- [99] S. Megelski, J. S. Stephens, D. Bruce Chase, and J. F. Rabolt, "Micro- and nanostructured surface morphology on electrospun polymer fibers," *Macromolecules*, vol. 35, no. 22, pp. 8456–8466, 2002.
- [100] C. T. Lim, E. P. S. Tan, and S. Y. Ng, "Effects of crystalline morphology on the tensile properties of electrospun polymer nanofibers," *Appl. Phys. Lett.*, vol. 92, no. 14, p. 141908, Apr. 2008.
- [101] L. Huang, N. N. Bui, S. S. Manickam, and J. R. McCutcheon, "Controlling electrospun nanofiber morphology and mechanical properties using humidity," *J.*

- Polym. Sci. Part B Polym. Phys.*, vol. 49, no. 24, pp. 1734–1744, 2011.
- [102] J. . Deitzel, J. Kleinmeyer, D. Harris, and N. . Beck Tan, “The effect of processing variables on the morphology of electrospun nanofibers and textiles,” *Polymer (Guildf)*, vol. 42, no. 1, pp. 261–272, Jan. 2001.
- [103] Y. Z. Zhang, X. Wang, Y. Feng, J. Li, C. T. Lim, and S. Ramakrishna, “Coaxial electrospinning of (fluorescein isothiocyanate-conjugated bovine serum albumin)-encapsulated poly(epsilon-caprolactone) nanofibers for sustained release,” *Biomacromolecules*, vol. 7, no. 4, pp. 1049–57, Apr. 2006.
- [104] R. Hashizume *et al.*, “Morphological and mechanical characteristics of the reconstructed rat abdominal wall following use of a wet electrospun biodegradable polyurethane elastomer scaffold,” *Biomaterials*, vol. 31, no. 12, pp. 3253–3265, Apr. 2010.
- [105] K. Ohkawa, D. Cha, H. Kim, A. Nishida, and H. Yamamoto, “Electrospinning of Chitosan,” *Macromol. Rapid Commun.*, vol. 25, no. 18, pp. 1600–1605, Sep. 2004.
- [106] V. E. Kalayci, P. K. Patra, Y. K. Kim, S. C. Ugbolue, and S. B. Warner, “Charge consequences in electrospun polyacrylonitrile (PAN) nanofibers,” *Polymer (Guildf)*, vol. 46, no. 18, pp. 7191–7200, 2005.
- [107] M. M. Hohman, M. Shin, G. Rutledge, and M. P. Brenner, “Electrospinning and electrically forced jets. I. Stability theory,” *Phys. Fluids*, vol. 13, no. 8, p. 2201, 2001.
- [108] D. H. Reneker and L. Chun, “Nanometre diameters of polymer, produced by electrospinning,” *Nanotechnology*, vol. 7, pp. 216–223, 1996.
- [109] C. Zhang, X. Yuan, L. Wu, Y. Han, and J. Sheng, “Study on morphology of electrospun poly(vinyl alcohol) mats,” *Eur. Polym. J.*, vol. 41, no. 3, pp. 423–432, 2005.
- [110] Z. Li and C. Wang, “One-Dimensional nanostructures,” pp. 15–29, 2013.

- [111] R. Konwarh, N. Karak, and M. Misra, “Electrospun cellulose acetate nanofibers: the present status and gamut of biotechnological applications.,” *Biotechnol. Adv.*, vol. 31, no. 4, pp. 421–37, 2013.
- [112] T. A. Kowalewski and S. Barral, “Experiments and modelling of electrospinning process,” vol. 53, no. 4, pp. 385–394, 2005.
- [113] C. E. Ayres *et al.*, “Measuring fiber alignment in electrospun scaffolds: a user’s guide to the 2D fast Fourier transform approach,” *J. Biomater. Sci. Polym. Ed.*, vol. 19, no. 5, pp. 603–621, 2008.
- [114] C. Chaubaroux *et al.*, “Cell Alignment Driven by Mechanically Induced Collagen Fiber Alignment in Collagen/Alginate Coatings.,” *Tissue Eng. Part C. Methods*, vol. 21, no. 9, pp. 881–888, Sep. 2015.
- [115] S. Y. Chew, R. Mi, A. Hoke, and K. W. Leong, “The effect of the alignment of electrospun fibrous scaffolds on Schwann cell maturation,” *Biomaterials*, vol. 29, no. 6, pp. 653–661, 2008.
- [116] D. Li, Y. Wang, and Y. Xia, “Electrospinning of polymeric and ceramic nanofibers as uniaxially aligned arrays,” *Nano Lett.*, vol. 3, no. 8, pp. 1167–1171, 2003.
- [117] J. I. Kim, T. I. Hwang, L. E. Aguilar, C. H. Park, and C. S. Kim, “A Controlled Design of Aligned and Random Nanofibers for 3D Bi-functionalized Nerve Conduits Fabricated via a Novel Electrospinning Set-up,” *Sci. Rep.*, vol. 6, no. 1, p. 23761, 2016.
- [118] D. Mounier, C. Poilane, C. Bucher, and P. Picart, “Evaluation of transverse elastic properties of fibers used in composite materials by laser resonant ultrasound spectroscopy,” no. April, pp. 1247–1250, 2012.
- [119] S. Singh, S. B. Bandini, P. E. Donnelly, J. Schwartz, and J. E. Schwarzbauer, “A cell-assembled, spatially aligned extracellular matrix to promote directed tissue development,” *J. Mater. Chem. B*, vol. 2, no. 11, p. 1449, 2014.

- [120] Y. Ji *et al.*, “Confinement-induced super strong PS/MWNT composite nanofibers,” *EPL (Europhysics Lett.)*, vol. 84, no. 5, p. 56002, Dec. 2008.
- [121] X. Li, W. Lou, and R. Song, “Experimental Investigation of Polyurethane Electrospun Nanofibers Mat---Relationship Between Mechanical Property and,” *Wjoe.Hebeu.Edu.Cn*, pp. 1–2, 1969.
- [122] C. J. Lowe, I. M. Reucroft, M. C. Grotta, and D. I. Shreiber, “Production of Highly Aligned Collagen Scaffolds by Freeze-drying of Self-assembled, Fibrillar Collagen Gels,” *ACS Biomater. Sci. Eng.*, vol. 2, no. 4, pp. 643–651, 2016.
- [123] S. Chakraborty, I. Liao, A. Adler, and K. W. Leong, “Electrohydrodynamics : A facile technique to fabricate drug delivery systems ☆,” *Adv. Drug Deliv. Rev.*, vol. 61, no. 12, pp. 1043–1054, 2009.
- [124] L. A. Smith and P. X. Ma, “Nano-fibrous scaffolds for tissue engineering.,” *Colloids Surf. B. Biointerfaces*, vol. 39, no. 3, pp. 125–31, Dec. 2004.
- [125] C. C. Helms and M. Guthold, “The Mechanical Stress – Strain Properties of Single Electrospun Collagen Type I Nanofibers,” 2010.
- [126] N. Sharma, J. Liu, S. Karamdoust, D. Boughner, and W. Wan, “Effect of ion implantation on electrospun collagen fiber properties,” in *10th World Biomaterials Congress*, 2016.
- [127] S. C. Baker *et al.*, “Characterisation of electrospun polystyrene scaffolds for three-dimensional in vitro biological studies,” *Biomaterials*, vol. 27, no. 16, pp. 3136–3146, 2006.
- [128] K. J. Shields, M. J. Beckman, G. L. Bowlin, and J. S. Wayne, “Mechanical properties and cellular proliferation of electrospun collagen type II.,” *Tissue Eng.*, vol. 10, no. 9–10, pp. 1510–7, 2004.
- [129] M. Mekhail, K. K. H. Wong, D. T. Padavan, Y. Wu, D. B. O’Gorman, and W. Wan, “Genipin-Cross-linked Electrospun Collagen Fibers.,” *J. Biomater. Sci.*

Polym. Ed., vol. 22, no. 17, pp. 2241–2259, Nov. 2010.

- [130] Y. Z. Zhang, J. Venugopal, Z.-M. Huang, C. T. Lim, and S. Ramakrishna, “Characterization of the surface biocompatibility of the electrospun PCL-collagen nanofibers using fibroblasts,” *Biomacromolecules*, vol. 6, no. 5, pp. 2583–9, 2005.
- [131] Y.-J. Hwang, J. Larsen, T. B. Krasieva, and J. G. Lyubovitsky, “Effect of Genipin Crosslinking on the Optical Spectral Properties and Structures of Collagen Hydrogels,” *ACS Appl. Mater. Interfaces*, vol. 3, no. 7, pp. 2579–2584, Jul. 2011.
- [132] W. Zhao, X. Li, X. Liu, N. Zhang, and X. Wen, “Effects of substrate stiffness on adipogenic and osteogenic differentiation of human mesenchymal stem cells,” *Mater. Sci. Eng. C*, vol. 40, pp. 316–323, 2014.
- [133] G. Damodaran, R. Collighan, M. Griffin, and A. Pandit, “Tethering a laminin peptide to a crosslinked collagen scaffold for biofunctionality,” *J. Biomed. Mater. Res. A*, vol. 89, no. 4, pp. 1001–10, Jun. 2009.
- [134] G. M. Cunniffe and F. J. O’Brien, “Collagen scaffolds for orthopedic regenerative medicine,” *JOM*, vol. 63, no. 4, pp. 66–73, 2011.
- [135] S. Ricard-Blum, F. Ruggiero, and M. Van Der Rest, “The collagen superfamily,” *Top. Curr. Chem.*, vol. 247, pp. 35–84, 2005.
- [136] G. P. Huang *et al.*, “An investigation of common crosslinking agents on the stability of electrospun collagen scaffolds,” *J. Biomed. Mater. Res. A*, pp. 1–10, 2014.
- [137] K. Stenfeldt, C. Johansson, and S. Hellstrom, “The Collagen Structure of the Tympanic Membrane,” *Arch otolaryngol head neck surg*, vol. 132, pp. 293–298, 2006.
- [138] P. Fratzl, “Collagen: Structure and Mechanics, an Introduction,” P. Fratzl, Ed. Springer Science, 2008, pp. 1–13.

- [139] P. Fratzl and R. Weinkamer, "Nature's hierarchical materials," *Prog. Mater. Sci.*, vol. 52, no. 8, pp. 1263–1334, 2007.
- [140] D. J. S. Hulmes, "Building Collagen Molecules, Fibrils, and Suprafibrillar Structures," *J. Struct. Biol.*, vol. 137, no. 1–2, pp. 2–10, 2002.
- [141] M. D. Shoulders and R. T. Raines, "Collagen Structure and Stability," *Annu. Rev. Biochem.*, vol. 78, no. 1, pp. 929–958, 2009.
- [142] D. J. S. Hulmes, "Collagen Diversity, Synthesis and Assembly," in *Collagen*, Boston, MA: Springer US, 2008, pp. 15–47.
- [143] T. Koide and K. Nagata, "Collagen biosynthesis," *Top. Curr. Chem.*, vol. 247, pp. 85–114, 2005.
- [144] J. Glowacki and S. Mizuno, "Collagen scaffolds for tissue engineering," *Biopolymers*, vol. 89, no. 5, pp. 338–44, May 2008.
- [145] M. Sandri, A. Tampieri, L. Salvatore, A. Sannino, J. H. L. Ghiron, and G. Condorelli, "Collagen based scaffold for biomedical applications," *J. Biotechnol.*, vol. 150, pp. 29–29, Nov. 2010.
- [146] S. Meghezi, F. Couet, P. Chevallier, and D. Mantovani, "Effects of a pseudophysiological environment on the elastic and viscoelastic properties of collagen gels," *Int. J. Biomater.*, vol. 2012, 2012.
- [147] A. K. Lynn, I. V. Yannas, and W. Bonfield, "Antigenicity and immunogenicity of collagen," *J. Biomed. Mater. Res. - Part B Appl. Biomater.*, vol. 71, no. 2, pp. 343–354, 2004.
- [148] D. E. Birk and P. Bruckner, "Collagen suprastructures," *Top. Curr. Chem.*, vol. 247, pp. 185–205, 2005.
- [149] C. R. Carlisle, C. Coulais, and M. Guthold, "The mechanical stress-strain properties of single electrospun collagen type I nanofibers," *Acta Biomater.*, vol. 6,

no. 8, pp. 2997–3003, 2010.

- [150] A. Elamparithi, A. M. Punnoose, and S. Kuruvilla, “Electrospun type 1 collagen matrices preserving native ultrastructure using benign binary solvent for cardiac tissue engineering,” *Artif. cells, nanomedicine, Biotechnol.*, vol. 1401, no. January 2016, pp. 1–8, 2015.
- [151] M. G. Haugh, C. M. Murphy, R. C. McKiernan, C. Altenbuchner, and F. J. O’Brien, “Crosslinking and mechanical properties significantly influence cell attachment, proliferation, and migration within collagen glycosaminoglycan scaffolds,” *Tissue Eng. Part A*, vol. 17, no. 9–10, pp. 1201–8, May 2011.
- [152] M. G. Haugh, M. J. Jaasma, and F. J. O’Brien, “The effect of dehydrothermal treatment on the mechanical and structural properties of collagen-GAG scaffolds,” *J. Biomed. Mater. Res. A*, vol. 89, no. 2, pp. 363–9, 2009.
- [153] K. Weadock, E. Miller, L. Bellincampi, J. Zawadzsky, and M. Dunn, “Physical crosslinking of collagen fibers: comparison of ultraviolet irradiation and dehydrothermal treatment,” *J. Biomed. Mater. Res.*, vol. 29, pp. 1373–1379, 1995.
- [154] C. R. Rowland, D. P. Lennon, A. I. Caplan, and F. Guilak, “The effects of crosslinking of scaffolds engineered from cartilage ECM on the chondrogenic differentiation of MSCs,” *Biomaterials*, vol. 34, no. 23, pp. 5802–12, Jul. 2013.
- [155] L. Salvatore, M. Madaghiele, C. Parisi, F. Gatti, and A. Sannino, “Crosslinking of micropatterned collagen-based nerve guides to modulate the expected half-life,” *J. Biomed. Mater. Res. - Part A*, vol. 102, no. 12, pp. 4406–4414, 2014.
- [156] E. Khor, “Methods for the treatment of collagenous tissues for bioprostheses,” *Biomaterials*, vol. 18, pp. 95–105, 1997.
- [157] S. Itoh *et al.*, “Evaluation of cross-linking procedures of collagen tubes used in peripheral nerve repair,” *Biomaterials*, vol. 23, pp. 4475–4481, 2002.
- [158] A. Hsieh, T. Zahir, Y. Lapitsky, B. Amsden, W. Wan, and M. S. Shoichet,

“Hydrogel/electrospun fiber composites influence neural stem/progenitor cell fate,” *Soft Matter*, vol. 6, no. 10, p. 2227, 2010.

- [159] B. P. Chan *et al.*, “Photochemical cross-linking for collagen-based scaffolds: a study on optical properties, mechanical properties, stability, and hemocompatibility,” *Tissue Eng.*, vol. 13, no. 1, pp. 73–85, 2007.
- [160] A. Tirella, T. Liberto, and A. Ahluwalia, “Riboflavin and collagen: New crosslinking methods to tailor the stiffness of hydrogels,” *Mater. Lett.*, vol. 74, pp. 58–61, May 2012.
- [161] S. A. Pot, N. S. Gallhöfer, F. L. Matheis, K. Voelter-Ratson, F. Hafezi, and B. M. Spiess, “Corneal collagen cross-linking as treatment for infectious and noninfectious corneal melting in cats and dogs: results of a prospective, nonrandomized, controlled trial,” *Vet. Ophthalmol.*, vol. 17, no. 4, pp. 250–260, 2014.
- [162] D. Cherfan *et al.*, “Collagen Cross-Linking Using Rose Bengal and Green Light to Increase Corneal Stiffness,” *Investig. Ophthalmology Vis. Sci.*, vol. 54, no. 5, p. 3426, 2013.
- [163] V. Au and S. a Madison, “Effects of singlet oxygen on the extracellular matrix protein collagen: oxidation of the collagen crosslink histidinohydroxylysine and histidine,” *Arch. Biochem. Biophys.*, vol. 384, no. 1, pp. 133–42, 2000.
- [164] C.-C. Chang, Y.-T. Yang, J.-C. Yang, H.-D. Wu, and T. Tsai, “Absorption and emission spectral shifts of rose bengal associated with DMPC liposomes,” *Dye. Pigment.*, vol. 79, no. 2, pp. 170–175, 2008.
- [165] S. Mckerrall, P. Singlet, and O. Reactions, “Singlet Oxygen in Organic Synthesis Singlet Oxygen in Organic Synthesis,” *Reactions*, pp. 1–9, 2008.
- [166] M. C. DeRosa and R. J. Crutchley, “Photosensitized singlet oxygen and its applications,” *Coord. Chem. Rev.*, vol. 233–234, pp. 351–371, 2002.

- [167] H. Dong and T. Bell, "State-of-the-art overview: ion beam surface modification of polymers towards improving tribological properties," *Surf. Coatings Technol.*, vol. 111, no. 1, pp. 29–40, 1999.
- [168] R. J. Pelham and Y. -l. Wang, "Cell locomotion and focal adhesions are regulated by substrate flexibility," *Proc. Natl. Acad. Sci.*, vol. 94, no. 25, pp. 13661–13665, Dec. 1997.
- [169] E. Gentleman, A. N. Lay, D. a. Dickerson, E. a. Nauman, G. a. Livesay, and K. C. Dee, "Mechanical characterization of collagen fibers and scaffolds for tissue engineering," *Biomaterials*, vol. 24, no. 21, pp. 3805–3813, Sep. 2003.
- [170] J. Yao, C. Bastiaansen, and T. Peijs, "High Strength and High Modulus Electrospun Nanofibers," *Fibers*, vol. 2, no. 2, pp. 158–186, 2014.
- [171] T. Courtney, M. S. Sacks, J. Stankus, J. Guan, and W. R. Wagner, "Design and analysis of tissue engineering scaffolds that mimic soft tissue mechanical anisotropy," *Biomaterials*, vol. 27, no. 19, pp. 3631–3638, 2006.
- [172] C. R. Carlisle, C. Coulais, M. Namboothiry, D. L. Carroll, R. R. Hantgan, and M. Guthold, "The mechanical properties of individual, electrospun fibrinogen fibers," *Biomaterials*, vol. 30, no. 6, pp. 1205–1213, 2009.
- [173] N. J. Amoroso, A. D'Amore, Y. Hong, W. R. Wagner, and M. S. Sacks, "Elastomeric Electrospun Polyurethane Scaffolds: The Interrelationship Between Fabrication Conditions, Fiber Topology, and Mechanical Properties," *Adv. Mater.*, vol. 23, no. 1, pp. 106–111, Jan. 2011.
- [174] M. S. Sacks, "Biaxial mechanical evaluation of planar biological materials," *J. Elast.*, vol. 61, no. 1–3, pp. 199–246, 2000.
- [175] H.-W. Tong, "Electrospinning of Fibrous PHBV Tissue Engineering Scaffolds: Fiber Diameter Control, Fiber Alignment and Mechanical Properties," *Polym. Mater. Sci. Eng.*, vol. 85, p. 51, 2001.

- [176] C. Xiang and M. Frey, "Increasing Mechanical Properties of 2-D-Structured Electrospun Nylon 6 Non-Woven Fiber Mats," *Materials (Basel)*, vol. 9, no. 4, p. 270, Apr. 2016.
- [177] J. Xiao *et al.*, "Kafirin Protein Based Electrospun Fibers with Tunable Mechanical Property, Wettability, and Release Profile," *J. Agric. Food Chem.*, vol. 64, no. 16, pp. 3226–3233, 2016.
- [178] J. S. Jeong, J. S. Moon, S. Y. Jeon, J. H. Park, P. S. Alegaonkar, and J. B. Yoo, "Mechanical properties of electrospun PVA/MWNTs composite nanofibers," *Thin Solid Films*, vol. 515, no. 12, pp. 5136–5141, 2007.
- [179] E. P. S. Tan, S. Y. Ng, and C. T. Lim, "Tensile testing of a single ultrafine polymeric fiber," *Biomaterials*, vol. 26, no. 13, pp. 1453–1456, 2005.
- [180] S. C. Wong, A. Baji, and S. Leng, "Effect of fiber diameter on tensile properties of electrospun poly(ϵ -caprolactone)," *Polymer (Guildf)*, vol. 49, no. 21, pp. 4713–4722, 2008.
- [181] Z. Zhang, Y. Yang, and H. Hamada, "The effects of open holes on the fracture behaviors and mechanical properties of glass fiber mat composites," *Sci. Eng. Compos. Mater.*, vol. 22, no. 5, pp. 555–564, 2015.
- [182] E. P. S. Tan and C. T. Lim, *Nanomechanics of Materials and Structures*. Berlin/Heidelberg: Springer-Verlag, 2006.
- [183] L. Sun, R. P. S. Han, J. Wang, and C. T. Lim, "Modeling the size-dependent elastic properties of polymeric nanofibers," *Nanotechnology*, vol. 19, no. 45, p. 455706, 2008.
- [184] A. Arinstein and E. Zussman, "Electrospun polymer nanofibers: Mechanical and thermodynamic perspectives," *J. Polym. Sci. Part B Polym. Phys.*, vol. 49, no. 10, pp. 691–707, 2011.
- [185] K. K. H. Wong, M. Zinke-Allmang, J. L. Hutter, S. Hrapovic, J. H. T. Luong, and

- W. Wan, "The effect of carbon nanotube aspect ratio and loading on the elastic modulus of electrospun poly(vinyl alcohol)-carbon nanotube hybrid fibers," *Carbon N. Y.*, vol. 47, no. 11, pp. 2571–2578, 2009.
- [186] E. P. S. Tan, C. N. Goh, C. H. Sow, and C. T. Lim, "Tensile test of a single nanofiber using an atomic force microscope tip," *Appl. Phys. Lett.*, vol. 86, no. 7, pp. 1–3, 2005.
- [187] J. Domke and M. Radmacher, "Measuring the elastic properties of thin polymer films with the atomic force microscope," *Langmuir*, vol. 14, no. 12, pp. 3320–3325, 1998.
- [188] M. Wang, H. J. Jin, D. L. Kaplan, and G. C. Rutledge, "Mechanical Properties of Electrospun Silk Fibers," *Macromolecules*, vol. 37, no. 18, pp. 6856–6864, 2004.
- [189] L. M. Bellan, J. Kameoka, and H. G. Craighead, "Measurement of the Young's moduli of individual polyethylene oxide and glass nanofibres," *Nanotechnology*, vol. 16, no. 8, p. 1095, 2005.
- [190] B. Wen, J. E. Sader, and J. J. Boland, "Mechanical properties of ZnO nanowires," *Phys. Rev. Lett.*, vol. 101, no. 17, pp. 2–5, 2008.
- [191] S. D. Hudson, V. Zhurov, V. Grbić, M. Grbić, and J. L. Hutter, "Measurement of the elastic modulus of spider mite silk fibers using atomic force microscopy," *J. Appl. Phys.*, vol. 113, no. 15, p. 154307, 2013.
- [192] L. Yang, K. O. van der Werf, C. F. C. Fitié, M. L. Bennink, P. J. Dijkstra, and J. Feijen, "Mechanical Properties of Native and Cross-linked Type I Collagen Fibrils," *Biophys. J.*, vol. 94, no. 6, pp. 2204–2211, 2008.
- [193] G. Guhados, W. Wan, and J. L. Hutter, "Measurement of the Elastic Modulus of Single Bacterial Cellulose Fibers Using Atomic Force Microscopy," *Langmuir*, vol. 21, no. 14, pp. 6642–6646, Jul. 2005.
- [194] J. P. Salvétat *et al.*, "Elastic and Shear Moduli of Single-Walled Carbon Nanotube

- Ropes,” *Phys. Rev. Lett.*, vol. 82, no. 5, pp. 944–947, 1999.
- [195] K. K. H. Wong, M. Zinke-Allmang, and W. Wan, “Effect of annealing on aqueous stability and elastic modulus of electrospun poly(vinyl alcohol) fibers,” *J. Mater. Sci.*, vol. 45, no. 9, pp. 2456–2465, Jan. 2010.
- [196] S. Y. Chew, T. Hufnagel, C. T. Lim, and K. W. Leong, “Mechanical properties of single electrospun drug-encapsulated nanofibres,” *Nanotechnology*, vol. 15, no. 5, pp. 3880–3891, 2006.
- [197] N. Wu, L. Chen, Q. Wei, Q. Liu, and J. Li, “Nanoscale three-point bending of single polymer/inorganic composite nanofiber,” *J. Text. Inst.*, vol. 103, no. 2, pp. 154–158, 2012.
- [198] B. N. J. Persson, “Contact mechanics for randomly rough surfaces,” *Surf. Sci. Rep.*, vol. 61, no. 4, pp. 201–227, 2006.
- [199] S. R. Baker, S. Banerjee, K. Bonin, and M. Guthold, “Determining the mechanical properties of electrospun polycaprolactone (PCL) nanofibers using AFM and a novel fiber anchoring technique,” *Mater. Sci. Eng. C*, vol. 59, pp. 203–212, 2016.
- [200] S. H. Lee, C. Tekmen, and W. M. Sigmund, “Three-point bending of electrospun TiO₂ nanofibers,” *Mater. Sci. Eng. A*, vol. 398, no. 1–2, pp. 77–81, 2005.
- [201] J. L. Duvail *et al.*, “Physical properties of conducting polymer nanofibers,” *Synth. Met.*, vol. 135–136, pp. 329–330, Apr. 2003.
- [202] G. Guhados, W. Wan, X. Sun, and J. L. Hutter, “Simultaneous measurement of Young’s and shear moduli of multiwalled carbon nanotubes using atomic force microscopy,” *J. Appl. Phys.*, vol. 101, no. 3, p. 033514, Feb. 2007.
- [203] K. Watanabe, T. Nakamura, B.-S. Kim, and I.-S. Kim, “Effect of organic solvent on morphology and mechanical properties of electrospun syndiotactic polypropylene nanofibers,” *Polym. Bull.*, vol. 67, no. 9, pp. 2025–2033, 2011.

- [204] Z. Chen, B. Wei, X. Mo, C. T. Lim, S. Ramakrishna, and F. Cui, “Mechanical properties of electrospun collagen-chitosan complex single fibers and membrane,” *Mater. Sci. Eng. C*, vol. 29, no. 8, pp. 2428–2435, 2009.
- [205] E. P. S. Tan and C. T. Lim, “Nanoindentation study of nanofibers,” *Appl. Phys. Lett.*, vol. 87, no. 12, p. 123106, Sep. 2005.
- [206] J. G. Park, S. H. Lee, B. Kim, and Y. W. Park, “Electrical resistivity of polypyrrole nanotube measured by conductive scanning probe microscope: The role of contact force,” *Appl. Phys. Lett.*, vol. 81, no. 24, pp. 4625–4627, Dec. 2002.
- [207] A. Camposeo *et al.*, “Local mechanical properties of electrospun fibers correlate to their internal nanostructure,” *Nano Lett.*, vol. 13, no. 11, pp. 5056–5062, 2013.
- [208] R. Inai, M. Kotaki, and S. Ramakrishna, “Structure and properties of electrospun PLLA single nanofibres,” *Nanotechnology*, vol. 16, no. 2, pp. 208–213, 2005.
- [209] L. R. Xu, “Mechanical Property Characterization of a Polymeric Nanocomposite Reinforced by Graphitic Nanofibers with Reactive Linkers,” *J. Compos. Mater.*, vol. 38, no. 18, pp. 1563–1582, 2004.
- [210] S. Boussaad and N. J. Tao, “Polymer wire chemical sensor using a microfabricated tuning fork,” *Nano Lett.*, vol. 3, no. 8, pp. 1173–1176, 2003.
- [211] S. Cuenot, C. Frétiigny, S. Demoustier-Champagne, and B. Nysten, “Measurement of elastic modulus of nanotubes by resonant contact atomic force microscopy,” *J. Appl. Phys.*, vol. 93, no. 9, pp. 5650–5655, Apr. 2003.
- [212] S. Cuenot, C. Frétiigny, S. Demoustier-Champagne, and B. Nysten, “Surface tension effect on the mechanical properties of nanomaterials measured by atomic force microscopy,” *Phys. Rev. B*, vol. 69, no. 16, p. 165410, Apr. 2004.
- [213] L. Vi, A. Njarlangattil, Y. Wu, B. S. Gan, and D. B. O’Gorman, “Type-1 Collagen differentially alters β -catenin accumulation in primary Dupuytren’s Disease cord and adjacent palmar fascia cells,” *BMC Musculoskelet. Disord.*, vol. 10, no. 1, p.

72, Dec. 2009.

- [214] M. K. Shin, S. I. Kim, S. J. Kim, S.-K. Kim, H. Lee, and G. M. Spinks, “Size-dependent elastic modulus of single electroactive polymer nanofibers,” *Appl. Phys. Lett.*, vol. 89, no. 23, p. 231929, Dec. 2006.
- [215] J. M. Ferreira, C. Capela, J. Manaia, and J. D. Costa, “Mechanical properties of woven mat jute/epoxy composites,” *Mater. Res.*, vol. 19, no. 3, pp. 702–710, 2016.
- [216] A. Heidelberg *et al.*, “A generalized description of the elastic properties of nanowires,” *Nano Lett.*, vol. 6, no. 6, pp. 1101–1106, 2006.
- [217] H. Pan, L. Li, L. Hu, and X. Cui, “Continuous aligned polymer fibers produced by a modified electrospinning method,” *Polymer (Guildf.)*, vol. 47, no. 14, pp. 4901–4904, Jun. 2006.
- [218] J. Liu, S. K. Agrawal, H. M. Ladak, and W. Wan, “Fiber Arrangement in the Rat Tympanic Membrane,” *Anat. Rec.*, vol. 299, no. 11, pp. 1531–1539, Nov. 2016.
- [219] D. Papkov, Y. Zou, M. N. Andalib, A. Goponenko, S. Z. D. Cheng, and Y. A. Dzenis, “Simultaneously strong and tough ultrafine continuous nanofibers,” *ACS Nano*, vol. 7, no. 4, pp. 3324–3331, 2013.
- [220] A. Arinstein, M. Burman, O. Gendelman, and E. Zussman, “Effect of supramolecular structure on polymer nanofibre elasticity,” *Nat. Nanotechnol.*, vol. 2, no. 1, pp. 59–62, 2007.
- [221] D. Zhang, I. Y. Shadrin, J. Lam, H.-Q. Xian, H. R. Snodgrass, and N. Bursac, “Tissue-engineered cardiac patch for advanced functional maturation of human ESC-derived cardiomyocytes,” *Biomaterials*, vol. 34, no. 23, pp. 5813–20, Jul. 2013.
- [222] J. D. Kretlow and A. G. Mikos, “Review: mineralization of synthetic polymer scaffolds for bone tissue engineering,” *Tissue Eng.*, vol. 13, no. 5, pp. 927–38, May 2007.

- [223] J. Lannutti, D. Reneker, T. Ma, D. Tomasko, and D. Farson, “Electrospinning for tissue engineering scaffolds,” *Mater. Sci. Eng. C*, vol. 27, no. 3, pp. 504–509, 2007.
- [224] H. Jiang, G. Campbell, D. Boughner, W. K. Wan, and M. Quantz, “Design and manufacture of a polyvinyl alcohol (PVA) cryogel tri-leaflet heart valve prosthesis,” *Med. Eng. Phys.*, vol. 26, no. 4, pp. 269–277, 2004.
- [225] W. K. Wan, L. Yang, and D. T. Padavan, “Use of degradable and nondegradable nanomaterials for controlled release,” *Nanomedicine (Lond)*, vol. 2, no. 4, pp. 483–509, Aug. 2007.
- [226] H. S. Yoo, T. G. Kim, and T. G. Park, “Surface-functionalized electrospun nanofibers for tissue engineering and drug delivery,” *Adv. Drug Deliv. Rev.*, vol. 61, no. 12, pp. 1033–1042, Oct. 2009.
- [227] A. S. Abhilash, B. M. Baker, B. Trappmann, C. S. Chen, and V. B. Shenoy, “Remodeling of fibrous extracellular matrices by contractile cells: Predictions from discrete fiber network simulations,” *Biophys. J.*, vol. 107, no. 8, pp. 1829–1840, 2014.
- [228] L. Ma, “Collagen/chitosan porous scaffolds with improved biostability for skin tissue engineering,” *Biomaterials*, vol. 24, no. 26, pp. 4833–4841, Nov. 2003.
- [229] J. S. Graham, A. N. Vomund, C. L. Phillips, and M. Grandbois, “Structural changes in human type I collagen fibrils investigated by force spectroscopy,” *Exp. Cell Res.*, vol. 299, no. 2, pp. 335–342, 2004.
- [230] N. Rajan, J. Habermehl, M.-F. Coté, C. J. Doillon, and D. Mantovani, “Preparation of ready-to-use, storable and reconstituted type I collagen from rat tail tendon for tissue engineering applications,” *Nat. Protoc.*, vol. 1, no. 6, pp. 2753–2758, 2006.
- [231] J. Currey, “Collagen and the mechanical properties of bone and calcified cartilage,” *Collagen Struct. Mech.*, no. Chapter 15, pp. 397–420, 2008.

- [232] C. Hadamitzky *et al.*, “Aligned nanofibrillar collagen scaffolds – Guiding lymphangiogenesis for treatment of acquired lymphedema,” *Biomaterials*, vol. 102, pp. 259–267, 2016.
- [233] C. H. Lee *et al.*, “Nanofiber alignment and direction of mechanical strain affect the ECM production of human ACL fibroblast,” *Biomaterials*, vol. 26, no. 11, pp. 1261–1270, 2005.
- [234] A. Agrawal *et al.*, “Smooth Muscle Cell Alignment and Phenotype Control by Melt Spun Polycaprolactone Fibers for Seeding of Tissue Engineered Blood Vessels,” *Int. J. Biomater.*, vol. 2015, pp. 1–8, 2015.
- [235] E. Schnell *et al.*, “Guidance of glial cell migration and axonal growth on electrospun nanofibers of poly- ϵ -caprolactone and a collagen/poly- ϵ -caprolactone blend,” *Biomaterials*, vol. 28, no. 19, pp. 3012–3025, 2007.
- [236] P. B. Warren, P. Huebner, J. T. Spang, R. A. Shirwaiker, and M. B. Fisher, “Engineering 3D-Bioprinted scaffolds to induce aligned extracellular matrix deposition for musculoskeletal soft tissue replacement,” *Connect. Tissue Res.*, vol. 58, no. 3–4, pp. 342–354, 2017.
- [237] E. A. Sander, V. H. Barocas, and R. T. Tranquillo, “Initial fiber alignment pattern alters extracellular matrix synthesis in fibroblast-populated fibrin gel cruciforms and correlates with predicted tension,” *Ann. Biomed. Eng.*, vol. 39, no. 2, pp. 714–729, 2011.
- [238] I. C. Liao, S. Y. Chew, and K. W. Leong, “Aligned core-shell nanofibers delivering bioactive proteins,” *Nanomedicine (Lond.)*, vol. 1, no. 4, pp. 465–71, Dec. 2006.
- [239] W. C. Hayes, L. M. Keer, G. Herrmann, and L. F. Mockros, “A Mathematical Analysis for Indentation Test of Articular Cartilage,” *J Biomechanics*, vol. 5, pp. 541–551, 1972.
- [240] N. Sorkin and D. Varssano, “Corneal collagen crosslinking: A systematic review,”

Ophthalmologica, vol. 232, pp. 10–27, 2014.

- [241] H. E. Canavan, D. J. Graham, X. Cheng, B. D. Ratner, and D. G. Castner, “Comparison of native extracellular matrix with adsorbed protein films using secondary ion mass spectrometry,” *Langmuir*, vol. 23, no. 1, pp. 50–56, 2007.
- [242] I. L. Kim, S. Khetan, B. M. Baker, C. S. Chen, and J. A. Burdick, “Fibrous hyaluronic acid hydrogels that direct MSC chondrogenesis through mechanical and adhesive cues,” *Biomaterials*, vol. 34, no. 22, pp. 5571–80, Jul. 2013.
- [243] Y. Su *et al.*, “Controlled release of bone morphogenetic protein 2 and dexamethasone loaded in core-shell PLLACL-collagen fibers for use in bone tissue engineering,” *Acta Biomater.*, vol. 8, no. 2, pp. 763–771, Feb. 2012.
- [244] S. Agarwal, J. H. Wendorff, and A. Greiner, “Progress in the field of electrospinning for tissue engineering applications,” *Adv. Mater.*, vol. 21, pp. 3343–3351, 2009.
- [245] J. A. Uquillas, V. Kishore, and O. Akkus, “Effects of phosphate-buffered saline concentration and incubation time on the mechanical and structural properties of electrochemically aligned collagen threads,” *Biomed. Mater.*, vol. 6, no. 3, p. 035008, Jun. 2011.
- [246] S. J. Eppell, B. N. Smith, H. Kahn, and R. Ballarini, “Nano measurements with micro-devices: mechanical properties of hydrated collagen fibrils,” *J. R. Soc. Interface*, vol. 3, no. 6, pp. 117–121, 2006.
- [247] Z. H. Sun, X. X. Wang, A. K. Soh, H. A. Wu, and Y. Wang, “Bending of nanoscale structures: Inconsistency between atomistic simulation and strain gradient elasticity solution,” *Comput. Mater. Sci.*, vol. 40, no. 1, pp. 108–113, 2007.
- [248] R. Sengupta *et al.*, “A Short Review on Rubber / Clay Nanocomposites With Emphasis on Mechanical Properties,” *Engineering*, vol. 47, pp. 21–25, 2007.

- [249] S. Cuenot, S. Demoustier-Champagne, and B. Nysten, “Elastic modulus of polypyrrole nanotubes,” *Phys. Rev. Lett.*, vol. 85, no. 8, pp. 1690–1693, 2000.
- [250] B. Jiang, C. Liu, C. Zhang, B. Wang, and Z. Wang, “The effect of non-symmetric distribution of fiber orientation and aspect ratio on elastic properties of composites,” *Compos. Part B Eng.*, vol. 38, no. 1, pp. 24–34, 2007.
- [251] J. A. J. Van Der Rijt, K. O. Van Der Werf, M. L. Bennink, P. J. Dijkstra, and J. Feijen, “Micromechanical testing of individual collagen fibrils,” *Macromol. Biosci.*, vol. 6, no. 9, pp. 699–702, 2006.
- [252] J. Albuschies and V. Vogel, “The role of filopodia in the recognition of nanotopographies,” *Sci. Rep.*, vol. 3, 2013.
- [253] S. W. Lee, S. Y. Kim, I. C. Rhyu, W. Y. Chung, R. Leesungbok, and K. W. Lee, “Influence of microgroove dimension on cell behavior of human gingival fibroblasts cultured on titanium substrata,” *Clin. Oral Implants Res.*, vol. 20, no. 1, pp. 56–66, 2009.
- [254] Michael A. Partridge and Eugene E. Marcantonio, “Initiation of Attachment and Generation of Mature Focal Adhesions by Integrin-containing Filopodia in Cell Spreading,” *Mol. Biol. Cell*, vol. 17, no. December, pp. 4237–4248, 2006.
- [255] Y. Yang *et al.*, “Neurotrophin releasing single and multiple lumen nerve conduits,” *J. Control. Release*, vol. 104, no. 3, pp. 433–446, 2005.

Appendices

Appendix A Rat tail collagen preparation procedure

1. Put frozen rat tails in 70% ethanol to thaw for about an hour
2. With a scalpel, cur the tip of the tail to expose the white collagen fibers, using forceps pull the fibers from the tail and place them in a plastic petri dish
3. Continue cutting the tail in small increments and pulling out the fibers
4. Clean the fibers free of contaminating tissue and place them in another clean container
5. Collagen fibers can be stored at -20 °C or proceed to collagen solution
6. Weigh out about 4g/L collagen fibers (equivalent to about 5 tails) and soak in 200 mL 70 % ethanol for 30 mins (leave forceps inside the beaker as well).
7. Prepare acetic acid solution (1mL of concentrated acetic acid and 1L of dH₂O) and filter sterilize with bottle top filter
8. Add 900 ml of the bottle filtered solution to collagen fibers in an autoclaved flask with a stir bar and dissolve the collagen at 4 °C for 7 days
9. Centrifuge the solution at 11,000 RPM (10 000 xg) overnight at 4 °C.
10. Collect the supernatant into a sterile bottle and store at 4 °C
11. Lyophilize the solution to obtain dry collagen powder

Appendix B Deflection due to tension

The force vs. fiber deflection curves obtained near the center of the suspended fibers were also fitted using models developed by Hudson et al. [191]. This model allows the possibility of including a pre-existing tension due to the fiber deposition process. Fits to the entire range of data can only be performed for fibers that experience only elastic deformation where the yield point was not reached. The Young's modulus was obtained using the model of Hudson et al. to fit force vs. displacement data with initial tension and Young's modulus as free parameters. A few points near the center of fiber were used for analysis as the model was developed only for loads applied at the center of the fiber.

For some of the data points with small fiber diameter and higher modulus, individual force curves are non-linear (Figure A). This nonlinearity is not predicted by the pure bending model. The pure bending model assumes that the lengths of the fibers do not change during the measurements. This may not be a good approximation for small diameter fibers, which may significantly deform during measurements. The model of Hudson et al. was used to consider the possibility of pre-existing tension in the fibers, which might be expected from electrospinning and deposition process. From Figure A, it is seen that the model of Hudson et al. (b) fits the data for force as a function of fiber deflection much better than the Heidelberg model with no initial force (a). This is only the case for a few fibers, for most fibers, the deflection is small and the nonlinearity in force vs. deflection curves was not observed. For the fiber shows in Figure A, the Young's modulus of the fiber was determined to be 118 ± 7.23 MPa using the pure bending model and reduced to $42.7\text{MPa} \pm 8.12\text{MPa}$ using Hudson model. The difference indicates the importance of pre-tension in fiber stiffness calculation for small fibers.

Since the difference of Young's modulus obtained with pure bending model were only observed in fibers with small diameters (e.g. 100-150 nm for as spun fibers, 250-300 nm for photoinitiator incorporated fibers and 50-100nm for genipin crosslinked fibers), this difference can be attributed to the possibility of pre-existing tension in the fibers, which might be expected due to the nature of the electrospinning and fiber deposition process.

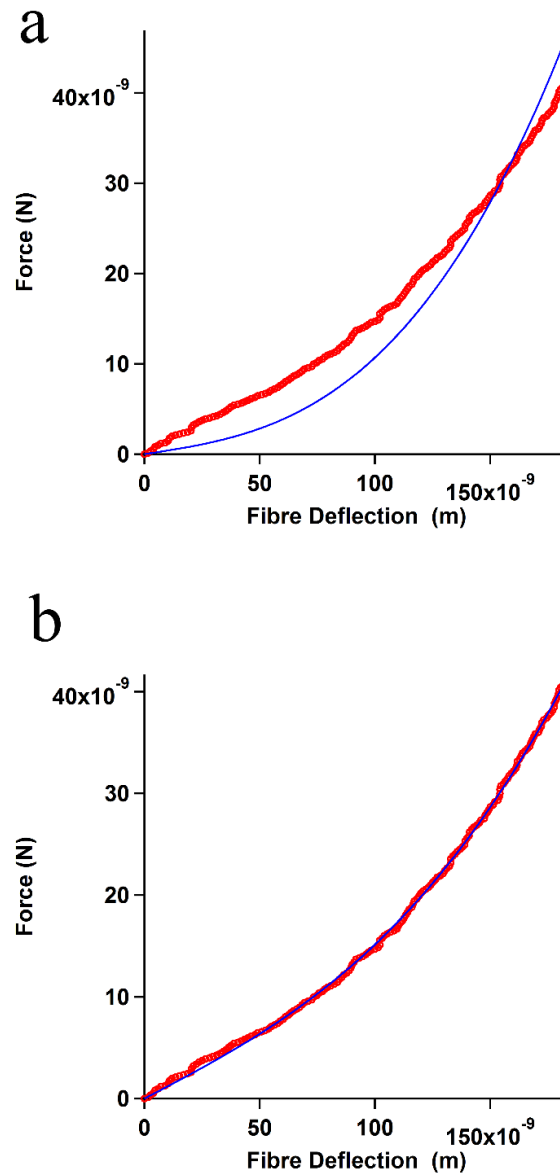
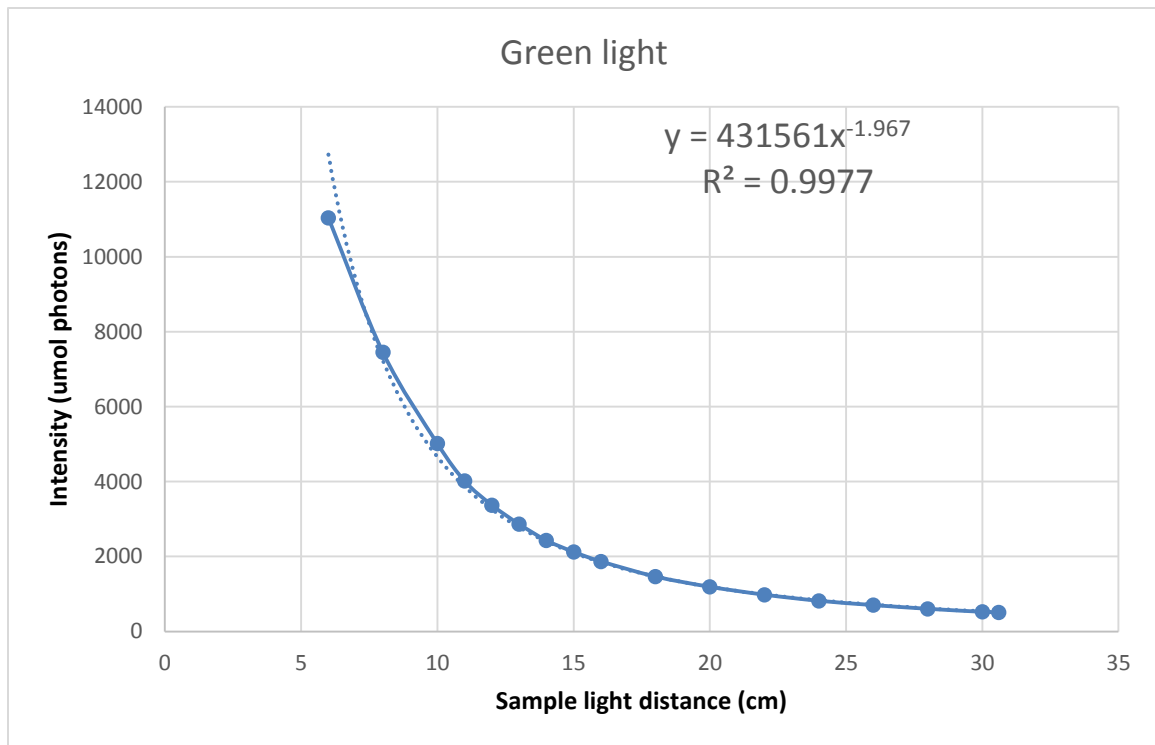
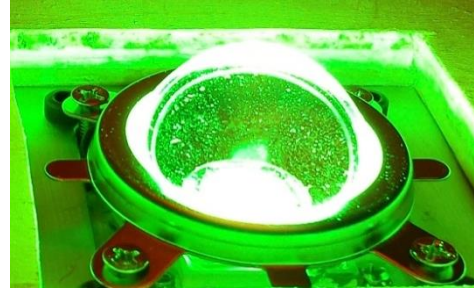
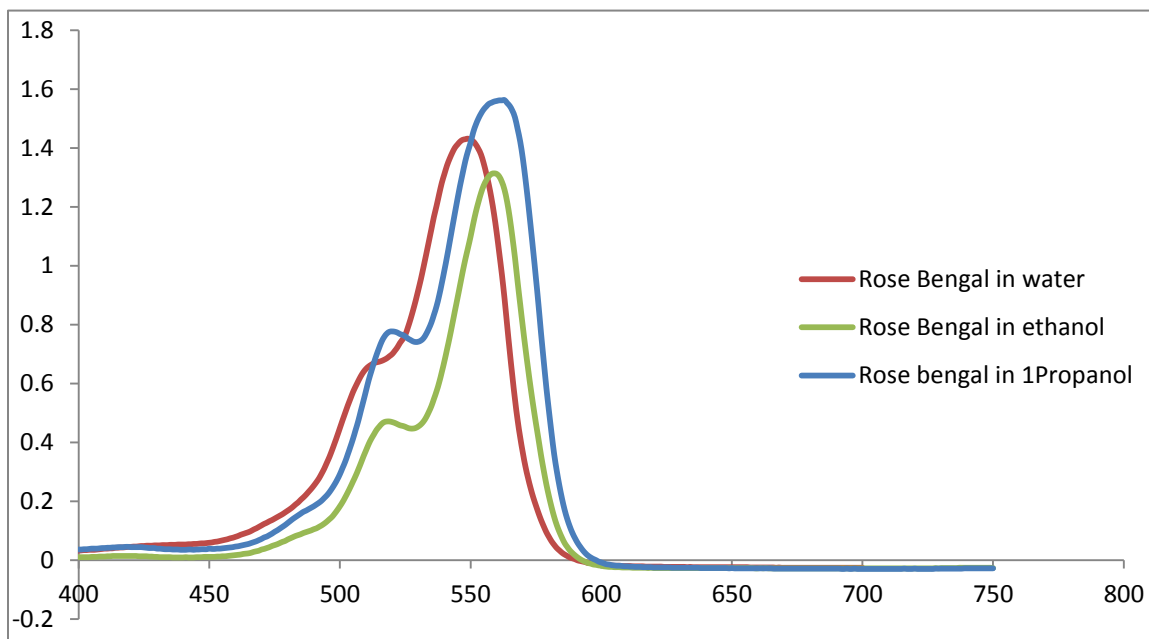


Figure A. Force as a function of fiber deflection for a fiber deformed within its elastic range. (a) The solid curve illustrates the model of Hudson et al. without pre-tension incorporated into fitting parameters. (b) the solid curve illustrates the model of Hudson et al. with pre-tension incorporated.

Appendix C green light light distance and intensity chart



Appendix D Rose Bengal UV-Vis spectra in different solvent system



Solvent	Peak	FWHM
Water	548nm	520-565nm
Ethanol	559nm	539-572nm
Isopropanol	562nm	543-575nm

Curriculum Vitae

Name: Ying (Betty) Li

Post-secondary Education and Degrees: University of Toronto
Toronto, Ontario, Canada
2007-2011, BAsC in Engineering Science
Major in NanoEngineering

The University of Western Ontario
London, Ontario, Canada
2011-2013, MESc in Chemical and Biochemical Engineering

The University of Western Ontario
London, Ontario, Canada
2013-2018 Ph.D. in Biomedical Engineering

Honours and Awards: Ontario Graduate Scholarships (OGS) and QEII Graduate Scholarships in Science and Technology (QEII-GSST)
2015-2016, 2016-2017

Related Work Experience Teaching Assistant
The University of Western Ontario
2011-2018

Publications:

Y. Li, W. Wan. (September 2017). Exploring polymer nanofiber mechanics. A review of the methods for determining their properties. IEEE Nanotechnology Magazine. DOI: 10.1109/MNANO.2017.2708819

Y. Li, J. Liu, J.R. de Bruyn, and W. Wan. (November 2014). Optimization of the electrospinning process for core-shell fiber preparation. Journal of Biomaterials and Tissue Engineering. 4, 973-980